UNIVERSIDADE DE SANTIAGO DE COMPOSTELA
FACULTADE DE FÍSICA
DEPARTAMENTO DE FÍSICA DA MATERIA CONDENSADA
Laboratorio de Baixas Temperaturas e Superconductividade (LBTS)

PhD THESIS

Unconventional effects in the magnetization and magnetoconductivity of iron based superconductors near T_c as probed by thermal fluctuation spectroscopy

Author:
Alberto Ramos Álvarez

PhD supervisors:
Jesús Manuel Mosqueira Rey
Félix Vidal Costa

September 25, 2015


USC
UNIVERSIDADE
DE SANTIAGO
DE COMPOSTELA

Dr. Jesús Manuel Mosqueira Rey
Profesor titular do Departamento de Física da Materia Condensada

Dr. Félix Vidal Costa
Catedrático Emérito do Departamento de Física da Materia Condensada

Como Directores da Tese de Doutoramento titulada

"Unconventional effects in the magnetization and magnetoconductivity of iron based superconductors near T_c as probed by thermal fluctuation spectroscopy"

Presentada por **D. Alberto Ramos Álvarez**
Alumno do Programa de Doutoramento Ciencia de Materiais

Autorizan a presentación da tese indicada, considerando que reúne os requisitos esixidos no artigo 34 do regulamento de Estudos de Doutoramento, e que como Directores da mesma non incurren nas causas de abstención establecidas na lei 30/1992.

Santiago de Compostela, 25 Setembro de 2015

Asdo. **Jesús M. Mosqueira Rey** Asdo. **Félix Vidal Costa**


USC
UNIVERSIDADE
DE SANTIAGO
DE COMPOSTELA

A mis padres, mi hermano y
a dos grandes amigos con los
que tan buenos momentos he
pasado en Santiago, Javier y
Mario


USC
UNIVERSIDADE
DE SANTIAGO
DE COMPOSTELA

Acknowledgments

At the end of my thesis period, I would like to thank some people and institutions for their support and help.

First, I appreciate enormously the assistance provided by Dr. Jesús Mosqueira. Under his supervision, I have learnt all I know about superconductivity. Thanks to his inestimable help, I acquired all the knowledge and patience required to work as an experimental physicist. I acknowledge Professor Félix Vidal, who has also supervised this PhD thesis, for his guidance in the research issues leading to this work. His scientific knowledge and his advice was very helpful at any time to take decisions. Someday I hope acquire his talent to make perfect works.

Second, but no less important, I would also like to acknowledge the rest of the group, especially to Dr. Manuel V. Ramallo for his help with the theoretical questions and his advice to perform the experimental data analysis. The other group members, Carlos, Carolina, Antonio and Jesús were friendly with me when I needed help. I will not forget the great help provided by the technicians of our lab: Juan Turnes and Magdalena Echezarreta and the good work done by Juan José Ponte with the measurement performed in the PPMS. Of course, I would like to acknowledge to my co-workers Juan Doval, Ramón Iglesias, Noelia Cotón, Javier Dancausa, Diego Vidal, Daniel Sóñora and José Castaño, with their companionship everything was more fun.

On the other hand, I would like to thank Professor Konstantin Arutyunov, who has overseen my work during my doctoral stay in Finland. With him, I have learned other topics of superconductivity which have been very helpful in my scientific education.

This work has been possible thanks to the high quality superconducting samples sent by the Professor Huiqian Luo from Institute of Physics and National Laboratory for Condensed Matter Physics in Beijing.

The works leading to this PhD thesis and all the related published papers were supported by the Ministerio de Ciencia e Innovación under projects FIS2007-63709, FIS2010-19807 and by the Xunta de Galicia under projects 2010/XA043, 10TMT1206012PR and under grant GPC2014/038. I also acknowledge the financial support of MICINN during four years trough a FPI grant n° BES-2011-046820. Additional funds for conferences and meetings were supplied by European Union under the ENERMAT and COST projects.

Contents


USC
UNIVERSIDADE
DE SANTIAGO
DE COMPOSTELA

General introduction and scope of this thesis

The great interest drawn since the discovery of the iron-based superconductors, [1, 2] FeSCs, has lead to the beginning of a new era in superconductivity research. This interest is in part motivated by the fact that in these compounds there is a coexistence of superconductivity and magnetism, as well as a multiband electronic structure, providing a large variety of new effects. Moreover, the comparison with the cuprates could help us to understand the mechanism of high temperature superconductivity, and to find out the way of increasing the critical temperature, T_c. The FeSCs are also attractive due to the quasi-isotropic critical current as compared with cuprate superconductors, and the higher upper critical field relative to the low-T_c superconductors.[3–5] These properties indicate that the FeSCs have a great potential for future electrical transport and high-field applications.[6]

The central aim of this work is the experimental study of some unconventional effects presented on the magnetization and on the magnetoconductivity of iron-based superconductors, mainly from the '122' family. For that purpose, it has been measured the superconducting fluctuation effects around T_c on both observables. Such a procedure, that has been nicknamed *superconducting fluctuation spectroscopy*,[7] allows us to obtain fundamental parameters such as the upper critical field, the superconducting coherence lengths, the anisotropy, and also the effective dimensionality of the material under study.[8] The superconducting fluctuation spectroscopy is a technique particularly useful for the high-temperature superconductors (cuprates or FeSCs), due to their high critical temperatures and their layered nature, which enhance the fluctuation effects around T_c. Nevertheless, before the systematic application of this technique, one must probe which theoretical approaches are well adapted to analyze these fluctuation effects in a extended region above T_c. In our case, we will probe the so-called Gaussian-Ginzburg-Landau (GGL) approach. This is going to be a first crucial step of the different analysis presented in this PhD thesis.

This thesis is structured as follows:

In *chapter 0*, a summary about iron-based superconductors is presented in order to show a general view about these compounds, comparing these materials with the cuprates. After that, a theoretical background for the superconducting fluctuations around the superconducting transition temperature, in the framework of the Gaussian Ginzburg-Landau approach (GGL), is presented. This one includes the GGL equations for the diamagnetism and magnetoconductivity induced by superconducting fluctuations, extended to high reduced temperatures by introducing the so-called *total energy cutoff*.[9] These extended GGL equations take also into account the presence of a magnetic field applied at different orientations. The applicability limits of these equations are also established.

In *chapter 1*, the fluctuation effects on the magnetization above T_c is studied on the iron-based superconductor $\mathrm{Ba(Fe_{1-x}Ni_x)_2As_2}$ with different doping levels, x, from the optimal doping to the highly overdoped region. These measurements allowed us to determine the x-dependence of the superconducting parameters. In particular, it is shown a large increase of the superconducting anisotropy factor with x, in good agreement with the conclusions previously pointed out in Ref. [10].

In *chapter 2*, measurements of the magnetization and the magnetoconductivity on the isovalently substituted $BaFe_2(As_{1-x}P_x)_2$ are presented. The corresponding experimental data allowed us to determine the superconducting parameters of this material. Significant differences are found between the out-of-plane coherence length values resulting from electrical transport and magnetization measurements. According to recent theoretical approaches, these differences may be attributed to the multiband superconducting nature of this compound.[11] Furthermore, the analysis of the magnetization in the low-field region around the transition temperature seems to discard the presence of appreciable phase fluctuations, claimed to be important in other high-T_c superconductors. [12]

In *chapter 3*, measurements of the magnetoconductivity on $BaFe_2(As_{1-x}P_x)_2$ single crystal with the applied magnetic field at different orientations with respect to the FeAs layers are presented. These data allowed us to obtain the angular dependence of the upper critical field. For the first time in this compound, it is reported a slight deviation from the behavior predicted by the anisotropic Ginzburg-Landau theory when the relative angle is close to 90°.

Finally, in *chapter 4*, just as an example of how sensitive is the fluctuation spectroscopy to inadequate analysis procedures, it is briefly commented the proposals givens in Ref. [13] about the two-dimensional nature of the iron-based superconductor LiFeAs. It is shown that these seemingly anomalous results [13] may be just a consequence of the inadequate procedure used to remove the normal-state (background) contributions.


USC
UNIVERSIDADE
DE SANTIAGO
DE COMPOSTELA

Chapter 0

Brief review on iron-based superconductors and introduction to the theoretical aspects of superconducting fluctuation spectroscopy

1 Iron based superconductors

There are many types of FeSCs with different structures and compositions but all of them share a common building block consisting of a square planar sheet of Fe, which is tetrahedrally coordinated by neighboring pnictogen or chalcogen atoms as shown in Fig. 1. The electronic structure is similar between them, with a Fermi level with electrons coming from $3d$ Fe orbitals. In spite of their layered nature, the FeSCs show a low anisotropy in contrast with the cuprate superconductors. Moreover, these materials present higher superconducting transition temperatures and lower coherence lengths as compared with the conventional low-temperature superconductors. These features make that measurements of the temperature dependence of observables such as the conductivity or the magnetization present an important rounding close to the critical temperature, due to the superconducting fluctuations. This rounding, which changes with the application of a magnetic field, complicates the direct determination from the superconducting phase transition of parameters such as the upper critical field. Another aspect of the FeSCs is that in most cases, the Fe-layers spacing is lower than the Ginzburg-Landau transverse coherence length, which would suggest a three dimensional behavior of the superconducting fluctuations. On the other hand, the topology of the Fermi surface of the FeSCs is important to know the origin of their magnetic properties, which are strongly related to the superconductivity phase. For example, T_c is maximized at the point where the static magnetic ordering disappears completely. In most cases the Fermi-surface topology of the parent compounds consists of five sheets, resulting from five conduction bands which change rapidly with the doping level, leading to unusual superconducting and normal state properties (see e.g. Fig. 2).

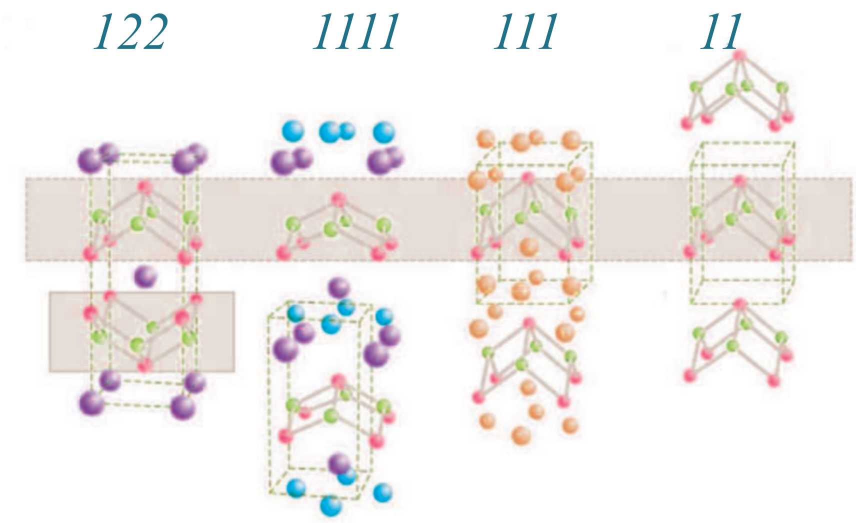

Figure 1: Several examples of crystal structures of some iron-based superconductors. The numbers at the top denote the chemical formula of the compound underneath. The common structural unit of all iron-based compounds is the Fe-As or Fe-Se tetrahedral layer (gray areas).

Three of the five sheets are hole-type and the other two are electron-type. The cylinders at the Γ and M points are nearly nested. This fact can lead in general to enhanced spin fluctuations and if these ones are strong, they can promote a Spin-Density-Wave (SDW) ordering. The main effect of doping is suggested to be a reduction in the degree of nesting of the Fermi surface.

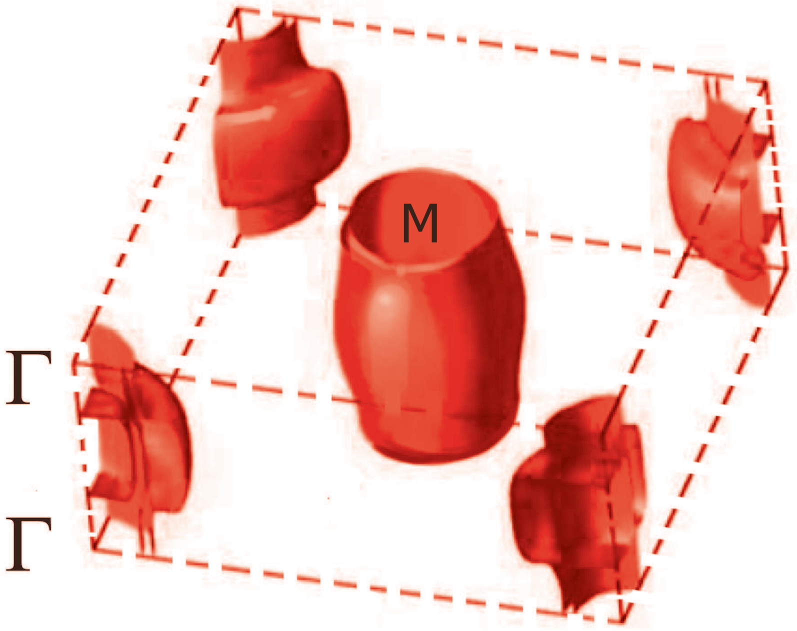

Figure 2: Example of LaFeAsO Fermi surface in non-magnetic phase calculated in Ref. [14]. This surface is similar in the $BaFe_2As_2$ and LiFeAs compounds.

In Fig. 3 it is shown an example of a generic phase diagram of a FeSC under chemical doping. A gradual increasing of the amount of dopants suppresses the structural and magnetic phase transitions, and eventually superconductivity emerges. The superconducting transition temperature is maximized at a certain doping level, and slowly decreases upon further chemical doping.

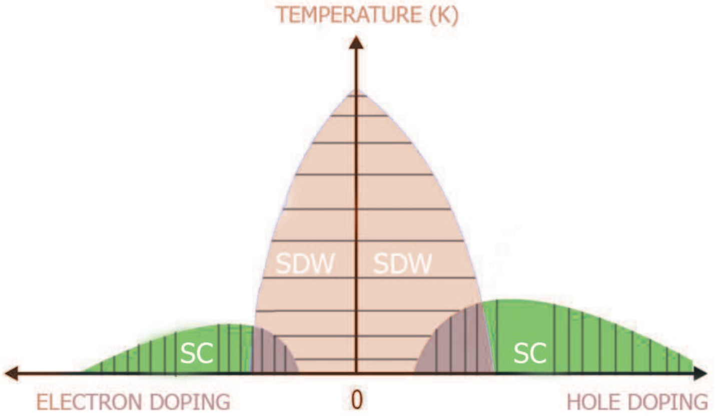

Figure 3: Example of a generic phase diagram of ‘122’ ferropnictides (see main text) versus chemical doping.

1.1 Main families of iron-based superconductors

Iron-based superconductors are arranged in four prototypical families, which are usually denoted by their stoichiometric ratios of chemical constituents: ‘1111’, ‘111’, ‘11’ and ‘122’, and further variations such as ‘42622’-type iron pnictides [15, 16] and ‘122’-type iron chalcogenidies [17, 18]:

1111-*type family* This group includes approximately 300 compounds. Starting from $LaFeAsO_{1-x}F_x$, this family keeps the records of T_c. The elements of this family have layers of FeP or FeAs stacked along the *c*-axis. It is noticeable that when pressure is applied to $LaFeAs_{0.89}OF_{0.11}$, the critical temperature increases, reaching a value of 43 K under 4GPa of pressure.[19] The higher value reported in this family is around 55 K in $SmFeAsO_{1-x}F_x$.[20] Finally, it is important to note that when superconducting phase transition begins in the doped superconducting compounds of this group, the static antiferromagnetic order disappears along with a lattice distortion. This fact suggests that the physical properties of this class of superconductors may have important similarities with the cuprates.

111-*type family* The main representative material of this group is LiFeAs.[21] This compound is stoichiometric, with a critical temperature about 18 K. Furthermore, it is non-magnetic, hence the observed band structure is free of SDW ordering. This family is highly reactive with air, being consequently a challenge to study. Another member of this family, NaFeAs, is less reactive with the environment than LiFeAs.[22]

11-*type family* These materials are iron chalcogenides with the simplest electronic structure. Some of them are FeSe with a T_c = 18 K [23] or $FeTe_{1-x}Se_x$ [24], with a T_c =14 K, at $x = 0.5$.

122-*type family* This family consists of a variety of different compounds with wide ranges of doping in both, hole and electron sides that form a rich phase diagram, where the superconductivity and magnetism compete or coexist. The parent compounds of 122 systems, AFe_2As_2 (A =Ca, Sr, Ba), have no superconductivity, but show metallic behavior in the temperature-dependent resistivity.[25, 26] However, the electrical resistivity value at room temperature is two orders of magnitude higher than in pure metals. For this reason, these elements are called poor metals. These metallic properties contrast with those ones present in the well-known cooper-oxide high-T_c superconductors, where the undoped compounds are Mott insulators.[27] The most studied materials in this group come from the parent compound $BaFe_2As_2$, which is a compensated metal, i.e., the total volume of two electron Fermi surface pockets is equal to its three hole Fermi surface pockets.[28] The first discovery of superconductivity in 122 system was the potassium-doped $Ba_{1-x}K_xFe_2As_2$ with a critical temperature of 38 K,[25] although there are others ways to introduce dopants and to get the appearance of superconductivity, as listed in Table 1.

Compound	Optimal doping level (x)	Type of charge carriers
$Ba_{1-x}K_xFe_2As_2$	0.32	hole
$Ba(Fe_{1-x}Co_x)_2As_2$	0.125	electron
$Ba(Fe_{1-x}Ni_x)_2As_2$	0.05	electron
$Ba(Fe_{1-x}Rh_x)_2As_2$	0.057	electron
$Ba(Fe_{1-x}Pd_x)_2As_2$	0.053	electron
$Ba(Fe_{1-x}Ru_x)_2As_2$	0.35	isovalent
$BaFe_2(As_{1-x}P_x)_2$	0.33	isovalent

Table 1: Several 122-ferropnictides indicating the optimal doping level and the type of charge carriers.

1.2 Comparison with cuprate superconductors

High-T_c cuprates are known for their high critical temperature and their unusual normal state properties. Let us compare these materials with the iron-based superconductors: *i)* In the first place, these compounds share a layered crystal structure that play an important role for most of physical properties. *ii)* Like in cuprates, the parent compounds of FeSCs possess an antiferromagnetic ordering accompanied by an orthorhombic structural distortion. *iii)* As in common high-T_c superconductors, the superconductivity emerges under charge doping above a certain doping level, and the static magnetic order becomes suppressed gradually. On the other side, there are some differences from cuprates as: *i)* while the parent compounds of cuprates exhibit Mott-insulting behavior, the parent compounds of FeSCs behave as poor metals. *ii)* If a pressure is applied, the superconductivity may appear in the FeSCs parent compunds without introducing chemical substitution, whereas in cuprates, the application of pressure enhances T_c if the superconducting phase already exist.

2 Introduction to the theoretical aspects of superconducting fluctuation spectroscopy

The fluctuation effects have been recently used in a number of works to characterize the superconducting properties of Fe-based superconductors through observables like the electrical conductivity, magnetization, or specific heat.[3, 10, 13, 29–47] In the same sense, in this thesis, superconducting fluctuations are used to determine some relevant parameters of the iron-based superconductors. To this end, in this section a summary about the theory used to analyze our experimental results is developed. Equations associated with the diamagnetism induced by superconducting fluctuations, and the superconducting fluctuations in the magnetoconductivity above T_c presented in this section were reported by others authors in Refs. [10, 48]

2.1 Ginzburg-Landau model for the thermal superconducting fluctuations above T_c

Ginzburg and Landau (GL) formulated their phenomenological theory of superconductivity taking into account some general consideration [49]: i) The assumption that the free energy functional, F, may be expressed as a power expansion of the order parameter (ψ) and its spacial derivatives ($\nabla\psi$) and ii) the identification of such an order parameter with the superconducting carriers. Let us write here the standard GL-functional for the free energy (relative to the free energy of the normal state, F_N, of a bulk isotropic 3D superconductor at $\mu_0 H = 0$ T [50–52]. We will neglect powers in $|\psi|$ higher than two, this corresponds to the so-called Gaussian-Ginzburg-Landau (GGL) approximation:

$$\Delta F[\psi] = F[\psi] - F_N = \int d^3\vec{r}\left\{a_0\varepsilon|\psi|^2 + a_0\xi^2(0)|\nabla\psi|^2\right\} \tag{1}$$

In this equation $\varepsilon \equiv \ln(\frac{T}{T_c})$ is the reduced temperature and a_0 is a so-called GL-normalization constant that may be related with the Ginzburg-Landau superconducting coherence length amplitude $\xi(0)$ [50, 51] through

$$a_0 = \frac{\hbar^2}{2m^*\xi^2(0)}$$

where $\hbar$ is the reduced Planck constant and m^* is the effective mass of the Cooper pairs. Let us now perform a standard Fourier-like expansion in plane waves of the order parameter:

$$\psi = \sum_{\vec{k}} \psi_{\vec{k}}\ e^{i\vec{k}\vec{r}}$$

here $\psi_{\vec{k}}$ is called the superconducting fluctuation mode with wavevector $\vec{k}$. Then, using that the plane waves are a set of orthogonal function we obtain from Eq. 1:

$$\Delta F = \sum_{\vec{k}} E_{\vec{k}}\ |\psi_{\vec{k}}|^2$$

where it has been assumed the mean-field reduced-temperature dependence of the superconducting coherence length, $\xi(\varepsilon) = \xi(0)\varepsilon^{-1/2}$ and therefore the coefficient $E_{\vec{k}}$ may be written as:

$$E_{\vec{k}} = \frac{\hbar^2 k^2}{2m^*} + \frac{\hbar^2}{2m^*\xi^2(\varepsilon)} \tag{2}$$

Now, it is clearly shown that the energy of each fluctuating mode comes from two different contributions: i) The first addend in the right-hand side of this equation may be easily understood as a kinetic energy of the fluctuations. ii) To understand the origin of the second addend it is only necessary to apply Heissenberg's uncertainty principle $\Delta x\ \Delta p \sim \hbar$. Then, by using $\Delta x = \xi(\varepsilon)$ and $\Delta p = \sqrt{2m^*\Delta E}$ we get that a Cooper pair has associated a confinement energy given by $\frac{\hbar^2}{2m^*\xi^2(\varepsilon)}$ that coincides with the second addend of the equation.

Once the GGL-functional has been expressed in momentum space, we may obtain the effective free energy due to fluctuations $\langle\Delta F\rangle$, by just taking into account that it corresponds to the standard thermal average $\Delta F[\psi]$ over all the possible configurations of the system. Such an average may be done by solving the following integration [52, 53]:

$$\langle\Delta F\rangle = -k_BT\int d\psi\ \exp\left(-\frac{\Delta F[\psi]}{k_BT}\right) \tag{3}$$

being k_B the Boltzmann constant. If we introduce now Eq. 1 in Eq. 3 taking into account the Fourier-like expansion made before and transforming the $\vec{k}$-summation in $\vec{k}$-integrals (by assuming henceforth volume unity), this equation may be rewritten as,

$$\langle\Delta F\rangle = \frac{k_BT}{8\pi^3}\int\!\!\int\!\!\int dk_xdk_ydk_z\left[\ln(k^2\xi^2(0)+\varepsilon) - \ln\frac{\pi k_BT}{a_0}\right] \tag{4}$$

It is easy to see that the result of the above equation equals infinity at all reduced-temperature. The origin of such a divergence is due to the fact that the GGL-approach assumes that both $|\psi|$ and $|\nabla\psi|$ are small. Thus, this implies that GGL does not estimate correctly the energy of the modes which have high $\nabla\psi$ (i.e. high-$\vec{k}$). In absence of an applied magnetic field this happens at high reduced-temperatures where the model increases with ε the statistical weight of the $\vec{k}$-modes. Indeed, the result for the calculated observable will become worse as we go far from T_c.

Let us calculate the effects of a external magnetic field (parallel to the z-axis for convenience) performing in Eq. 1 the following gauge-invariant transformation [50–52]

$$\nabla \to \nabla - \frac{2ie}{\hbar}\vec{A}$$

where e is the electron charge and $\vec{A}$ is the magnetic vector potential. Now, following the Ref. [52, 53] the change $\vec{k_\perp^2} \equiv k_x^2 + k_y^2$ may be done, which can be identified by

$$\frac{\hbar^2 k_\perp^2}{2m^*} \to \hbar \frac{2e\mu_0 H}{m^*}(1/2+n)$$

where $n = 0, 1, 2...$ is the Landau-level index. As a consequence, the integrals with respect to k_x and k_y are transformed into a sum over the Landau-level index. Applying this result in Eq. 4. We could get the well-know expression for the GGL-free energy of a 3D bulk superconductor in presence of a magnetic field [52, 53]:

$$\begin{aligned} \langle \Delta F(\varepsilon, h)\rangle &= \frac{k_B T}{8\pi^2 \xi^2(0)} 2h \sum_n \int dk_z \left[\ln\left(n + \frac{\varepsilon + h + k_z^2 \xi^2(0)}{2h}\right)\right. \\ &+ \left. \ln(2h) - \ln\left(\frac{\pi k_B T}{a_0}\right)\right] \end{aligned} \tag{5}$$

Note that from the change $k_\perp^2 \to \frac{4e\mu_0 H}{\hbar}(n+1/2)$ made before it is possible to estimate the H-region in which the short-wavelength regime will appear. For that, let us just multiply this change by $\xi^2(0)$ and using that the upper critical field is $\mu_0 H_{c2}(0) = \frac{\phi_0}{2\pi\xi^2(0)}$ being $\phi_0 = \frac{\pi\hbar}{e}$ the magnetic flux quantum, we obtain:

$$\xi^2(0) k_\perp^2 \to h(2n+1)$$

where $h = \frac{H}{H_{c2}}$. This last result shows that if a mode fluctuation has a $\vec{k}$-momentum of the order of $\xi^{-1}(0)$ associated with the lowest Landau-level $n = 0$ then, in a first approach, we may roughly estimate that the short-wavelength regime appear when $H \simeq H_{c2}$.

Although Eq. 5 is general, most expressions about fluctuation-induced observable that may be found in the literature are obtained in the so-called zero magnetic field regime, i.e. assuming in this equation that $h \ll \varepsilon$.[50, 51] This approach was first used by H. Schmidt [54] and, independently by A. Schmid [53]. The finite field effects were first considered by Prange [55] when studying the fluctuation-induced diamagnetism in a bulk isotropic 3D superconductor.

2.2 The total energy cutoff: A quantum constraint for superconducting fluctuations well above T_c

The proposed theory has certain limits of validity. The most popular of these limits is given by the so-called Levanyuk-Ginzburg criterion for the maximum approach from lowest temperature to the critical temperature[56, 57]: lower than a given value, T_{LG}, the thermal fluctuations associated with the transition become so important that it is no longer valid to perform a power expansion of F in the amplitude of ψ. Here another important limit of validity of the GGL approach for $T > T_c$ is presented.

Another constraint for superconducting fluctuations above the critical temperature, more fundamental and independent of any theoretical description about fluctuations, is associated with the limit imposed by the uncertainty principle on the shrinkage of the superconducting wave function when the temperature increases well above T_c. This quantum constraint was explicitly recognized by the first time by Vidal and coworkers.[9] On the grounds of the GGL description, this constraint must be added to the conventional momentum cutoff, and the corresponding condition was nicknamed "total energy cutoff".

The above indicated quantum constraint of the superconducting fluctuations may be easily introducing by taking into account that the superconducting coherence length is the characteristic distance over which the order parameter may vary, at any temperature above T_c, $\xi(T)$ must verify [9]:

$$\xi(T) \geq \xi_0$$

where ξ_0 is the minimum size of a Cooper pair.[58] This last equation restricts the confinement energy of the Cooper pairs to be always smaller than the ones at $T = 0$ K. So, at finite temperatures the coherent interactions must compensate, in addition to the kinetic energy associated with the thermal agitation, the quantum confinement energy. In other words, instead to the classical moment cutoff procedure, which only penalize the short wavelength fluctuation and that is temperature independent,[59–63] the total energy cutoff takes also into account the Heisenberg localization energy. This last constraint eliminates all fluctuation modes at reduces temperature equal or above some *supercritical* temperature, T^c, defined by $\xi(T^c) = \xi_0$.[9] The total energy cutoff may then expressed as [9, 64–66]:

$$\xi^{-2}(\varepsilon) + k^2 \leq \xi_0^{-2}$$

where ξ_0 may be expressed for convenience in the calculations of the different fluctuation-induced observables through the GL coherence length $\xi(c) \simeq \xi_0 \Rightarrow \xi_0^{-2} = c\xi(0)^{-2}$.Then we obtain:

$$\xi^{-2}(\varepsilon) + k^2 \leq c\xi(0)^{-2} \tag{6}$$

Eq. 6 was proposed in Refs. [48, 64, 65, 67, 68], prior to the establishment of the physical origin of the total-energy cutoff explained in Ref. [9].

With this condition the sum over n and the integral over k_z on the fluctuation part of the free energy are restricted up $n_{max} = \frac{c-\epsilon}{2h} - 1$ and $|k_z^{max}| = \sqrt{c-\epsilon}/\xi_c(0)$, and Eq. 5 is transformed in:

$$\begin{aligned} \langle \Delta F(\varepsilon, h)\rangle &= \frac{k_B T\sqrt{2h}}{4\pi^2\xi^3(0)} \int_0^{\sqrt{(c-\varepsilon)/2h}} dx \left\{ 2h \left[\ln\Gamma\left(\frac{h+c}{2h} + x^2\right) \right.\right. \\ &- \left.\left. \ln\Gamma\left(\frac{\varepsilon+h}{2h} + x^2\right)\right] + (c-\varepsilon)\ln(2h) \right\} \end{aligned} \tag{7}$$

where Γ is the Gamma function. Let us stress that the cutoff regularization not only allows us to very easily obtain explicit expressions of $< \Delta F >$ but, in addiction, Eq. 7 include the effective free energy without cutoff as a particular case, which corresponds to $h, \varepsilon \ll c$.

2.3 Fluctuation-induced magnetization in a bulk anisotropic 3D superconductor

The associated fluctuation-induced magnetization may be defined as [51]:

$$M_{fl}(T,H) = M(T,H) - M_B(T,H)$$

where M and M_B are respectively the as-measured and the normal state behaviour of the magnetization. On the other side the resulting M_{fl} under a total energy cutoff for an arbitrary applied field may be obtained as:

$$M_{fl}(\varepsilon,h) = -\frac{1}{\mu_0 H_{c2}} \frac{\partial \langle \Delta F(\varepsilon,h) \rangle}{\partial h}$$

Then using Eq. 7 into the last expression, it is obtained [48]:

$$\begin{aligned} M_{fl}(\varepsilon,h) = & - \frac{k_B T}{\pi \phi_0 \xi(0)} \sqrt{2h} \int_0^{\sqrt{(c-\varepsilon)/2h}} dx \left[\frac{c-\varepsilon}{2h} \right. \\ & - \left(\frac{c}{2h} + x^2 \right) \psi \left(\frac{1}{2} + \frac{c}{2h} + x^2 \right) \\ & + \ln\Gamma \left(\frac{1}{2} + \frac{c}{2h} + x^2 \right) \left(\frac{\varepsilon}{2h} + x^2 \right) \psi \left(\frac{1}{2} + \frac{\varepsilon}{2h} + x^2 \right) \\ & - \left. \ln\Gamma \left(\frac{1}{2} + \frac{\varepsilon}{2h} + x^2 \right) \right] \qquad (8) \end{aligned}$$

where here ψ is the digamma function. Note that Eq. 8 also includes the Prange-regime without cutoff as a particular case, that corresponds to ε, $h \ll c$.

However, in view of the moderate anisotropy observed in our experiments (see below), the results will be analyzed in the framework of the three-dimensional Ginzburg-Landau approach for anisotropic superconductors (3D-aGL). This theory predicts that the fluctuation-induced magnetization for magnetic fields applied perpendicular or parallel to the crystal ab layers may be obtained from the result for

3D isotropic materials, M_{fl}, through :

$$M_{fl}^{\perp}(H) = \gamma M_{fl}(H) \tag{9}$$

and

$$M_{fl}^{\parallel}(H) = M_{fl}\left(\frac{H}{\gamma}\right) \tag{10}$$

where γ is the superconducting anisotropy factor. This transformation was introduced by Klemm and Clem [69] and generalized by Blatter [70] and by Hao and Clem [71] to different observables and different regions in the $H-T$ phase diagram.

2.4 Fluctuation-induced in-plane magnetoconductivity $\Delta\sigma_{ab}$

To conclude this chapter, we present below the calculations of the theory for $\Delta\sigma_{ab}$ for 3D superconductors under the total-energy cutoff.

On the grounds of the GGL-approach, the paraconductivity $\Delta\sigma$ can be obtained as:

$$\Delta\sigma = \sum_{\vec{k}} \frac{4e^2 \left\langle |\psi_{\vec{k}}|^2 \right\rangle \tau_{\vec{k}}}{m^*} \tag{11}$$

In this equation $\left\langle |\psi_{\vec{k}}|^2 \right\rangle$ is the thermal average of the squared amplitude of the fluctuation mode with wavevector $\vec{k}$. It is actually given by the ratio between the thermal activation energy k_BT and its total energy $E_{\vec{k}}$ defined in Eq. 2 and it represents the superfluid density with wavevector $\vec{k}$:

$$n_{\vec{k}} = \left\langle |\psi_{\vec{k}}|^2 \right\rangle = \frac{k_BT}{E_{\vec{k}}} = \frac{2m^*\xi^2(0)}{\hbar^2}\frac{k_BT}{\varepsilon + k^2\xi^2(0)}$$

The parameter $\tau_{\vec{k}}$ is the relaxation time of each fluctuation $\vec{k}$-mode and it is given by $\tau_{\vec{k}} = \frac{\pi\hbar}{32k_BTE_{\vec{k}}}$.[72, 73] Then substituting into Eq. 11 and transforming the $\vec{k}$-summations into $\vec{k}$-integrals, it may be rewritten as:

$$\Delta\sigma = \frac{e^2\xi^2(0)}{32\pi^2\hbar}\int\int\int \frac{dk_x dk_y dk_z}{(\epsilon + \xi^2(0)k^2)^2} \tag{12}$$

Eq. 12 has been derived in the framework of a general model for a 3D isotropic superconductor. However, in view of the ratio between the superconducting coherence length amplitudes in our compounds (see below), the 3D anisotropic scenario seems to be more appropriate. In this last dimensional case, the scale variation of the order parameter in each spatial direction is determined by the corresponding superconducting coherence length. Thus, considering that the x and y directions lie on the ab-plane and that z corresponds to the crystallographic c-axis, Eq. 12 can be adapted to anisotropic 3D superconductors by applying $\xi^2(0)k^2 \rightarrow \xi^2_{ab}(0)k^2_x + \xi^2_{ab}k^2_y + \xi^2_c k^2_z$ (here $\xi_{ab}(0)$ is the in-plane superconducting coherence length amplitude). Using polar coordinates for the xy-plane this leads to

$$\Delta\sigma_{ab} = \frac{e^2\xi^2_{ab}(0)}{16\pi\hbar}\int\int \frac{k_{xy}dk_{xy}dk_z}{[\epsilon + \xi^2_{ab}(0)k^2_{xy} + \xi^2_c(0)k^2_z]^2}. \qquad (13)$$

If an external magnetic field H is applied parallel to the $c-$direction, the in-plane spectrum of the fluctuations becomes equivalent to that of a charged particle in a magnetic field.[52] Thus, k_{xy} in Eq. (13) must be replaced by $\frac{4e\mu_0 H}{\hbar}\left(n+\frac{1}{2}\right)$, where μ_0 is the vacuum magnetic permeability and $n = 0, 1\ldots$ is the Landau-level index. As a consequence, the integral with respect to k_{xy} is transformed into a sum over n through $\frac{1}{2\pi}\int k_{xy}\mathrm{d}k_{xy} \rightarrow \sum_n$. Besides, we must also include as a multiplier to Eq. (13) the so-called Landau degeneracy factor given by $\frac{e\mu_0 H}{\pi\hbar} = \frac{\mu_0 H}{\phi_0}$ (here ϕ_0 is the magnetic flux quantum). The resulting expression for $\Delta\sigma_{ab}$ is

$$\Delta\sigma_{ab} = \frac{e^2 h}{16\pi\hbar}\int \mathrm{d}k_z \sum_n [\epsilon + h(2n+1) + \xi^2_c(0)k^2_z]^{-2} \qquad (14)$$

where $h = H/H_{c2}(0)$ is the reduced magnetic field and $H_{c2}(0) = \phi_0/2\pi\mu_0\xi^2_{ab}(0)$ is the upper critical magnetic field perpendicular to the ab-planes, linearly extrapolated to $T = 0$ K.

To take into account the limit imposed by the uncertainty principle to the shrinkage of the superconducting wavefunction when ϵ or h

increase, an energy cutoff constraint explained above must be applied to Eq. (14).[9] This restricts the sum over n and the integration over k_z through $n_{max} = \frac{c-\epsilon}{2h} - 1$ and $|k_z^{max}| = \sqrt{c-\epsilon}/\xi_c(0)$ leading to

$$\Delta\sigma_{ab} = \frac{e^2}{32\hbar\pi\xi_c(0)}\sqrt{\frac{2}{h}}\int_0^{\sqrt{\frac{c-\varepsilon}{2h}}} \mathrm{d}x \left[\psi^1\left(\frac{\varepsilon+h}{2h}+x^2\right)\right.$$
$$\left. -\psi^1\left(\frac{c+h}{2h}+x^2\right)\right]. \tag{15}$$

In the zero magnetic field limit, *i.e.*, for $h \ll \epsilon, c$, this equation is transformed into

$$\Delta\sigma_{ab} = \frac{e^2}{16\hbar\pi\xi_c(0)}\left(\frac{\arctan\sqrt{\frac{c-\varepsilon}{\varepsilon}}}{\sqrt{\varepsilon}} - \frac{\arctan\sqrt{\frac{c-\varepsilon}{c}}}{\sqrt{c}}\right) \tag{16}$$

that corresponds to the paraconductivity under an energy cutoff. At low reduced temperatures and magnetic fields, $h, \epsilon \ll c$, the cutoff effects become unimportant. [9, 74] Accordingly, in this regime Eqs. (3.3) and (16) reduce to the c-independent expressions

$$\Delta\sigma_{ab} = \frac{e^2}{32\hbar\pi\xi_c(0)}\sqrt{\frac{2}{h}}\int_0^{\infty} \mathrm{d}x\, \psi^1\left(\frac{\varepsilon+h}{2h}+x^2\right) \tag{17}$$

and by simply imposing $\varepsilon \ll c$ the conventional Aslamazov-Larkin [75] expression for the paraconductivity in a $3D$ superconductor may be recovered

$$\Delta\sigma = \frac{e^2}{32\hbar\xi_c(0)}\varepsilon^{-1/2}$$

Note finally that Eqs. (3.3) or (16) lead to the $\Delta\sigma_{ab}$ vanishing at $\varepsilon = c$.


USC
UNIVERSIDADE
DE SANTIAGO
DE COMPOSTELA

Chapter 1

Large increase of the anisotropy factor in the overdoped region of $\mathrm{Ba(Fe_{1-x}Ni_x)_2As_2}$ as probed by fluctuation spectroscopy

Summary of this chapter *The diamagnetism induced by thermal fluctuations above the superconducting transition on the iron pnictide* $\mathrm{Ba(Fe_{1-x}Ni_x)_2As_2}$ *is studied with different doping levels,* x*. The measurements are performed with magnetic fields up to 7 T applied in the two main crystal directions. The experimental data provide double information: first, they confirm at a quantitative level the applicability to these materials the 3D-anisotropic Ginzburg-Landau approach. Then, they allow us to determine the doping-level dependence of the superconducting anisotropy factor,* γ*, in good agreement with the conclusions previously pointed out in Ref. [10]. The implications of the applicability of the model used to a multiband superconductor are discussed.*

1 Introduction

Nowadays, the properties of of Fe-based superconductors at the optimal doping were extensively studied and are already rather well understood. However, their behavior at doping levels far from the optimal one are much less investigated and some aspects remain still open. An important example is the large anisotropy observed in $\mathrm{Ba(Fe_{1-x}Ni_x)_2As_2}$ as follows from recent measurements of the fluctuation in-plane magnetoconductivity: in this compound the anisotropy factor (defined as the ratio between the in-plane and transverse coherence lengths) increases from $\gamma = 2$ at optimal doping ($x = 0.05$) up to around $\gamma = 15$ for $x = 0.10$. [10] To the best of our knowledge, such a γ value is the largest reported for an iron pnictide of the 122 family, and it is even larger than the one observed in some high-T_c cuprates (e.g., optimally doped $\mathrm{YBa_2Cu_3O_{7-\delta}}$). It is worth noting, however, that these results may be affected by large uncertainties (up to 30%) in the geometry of the crystals and of the electrical contacts and, therefore, further verification is desirable.

Here we present measurements of the fluctuation-induced magnetic susceptibility above T_c, χ_{fl}, in $\mathrm{Ba(Fe_{1-x}Ni_x)_2As_2}$ with different doping levels. The data were taken with magnetic fields applied in the two main crystallographic directions (parallel and perpendicular to the FeAs (ab) layers). The interest of these measurements is twofold. On the one side, the present work would allow to check the applicability of the phenomenological 3D-anisotropic Ginzburg-Landau (3D-aGL) approach to describe χ_{fl} in this region as a function of the doping level. But also of particular interest is the behavior at high reduced magnetic fields, at which multiband effects could be observable [11]. On the other side, χ_{fl} is highly dependent on the orientation of the applied magnetic field, and it will be very useful to accede experimentally to the anisotropy factor. In particular, the 3D-aGL approach predicts that in the zero-field limit $\chi_{\mathrm{fl}}^{\perp}/\chi_{\mathrm{fl}}^{\parallel} \approx \gamma^2$, where the superscripts $\perp$ and $\parallel$ correspond to $H \perp ab$ and $H \parallel ab$, respectively. Thus, the simultaneous measurement of both $\chi_{\mathrm{fl}}^{\perp}$ and $\chi_{\mathrm{fl}}^{\parallel}$ would allow to confirm the striking increase of γ upon overdoping observed in Ref. [10].

2 Experimental details and results

2.1 Crystals fabrication and characterization

The $Ba(Fe_{1-x}Ni_x)_2As_2$ samples used in this work are plate-like single crystals (see Table 1.1)provided by the professor Huiqian Luo (from Institute of Physics in Beijing (China)) with the crystal ab layers parallel to the largest faces. They were cleaved from larger crystals grown by the self-flux method. Their nominal Ni doping levels are $x = 0.05$, 0.075, 0.09 and 0.10, although the actual doping level was found to be a factor ~ 0.8 smaller (see Ref. [76], where all the details of the growth procedure and characterization may be found). In turn, we checked the excellent stoichiometric and structural quality of the crystal studied here by x-ray diffraction Fig. 1.1. In particular, the $(00l)$ linewidths were found to be slightly larger ($\Delta(2\theta) \sim 0.10°$ FWHM) than the corresponding instrumental linewidths, ($\Delta(2\theta) \sim 0.07°$ FWHM). This was attributed to a dispersion in the c-axis lattice parameter, and was used to roughly estimate the doping dispersion $\Delta x \sim 10^{-2}$ through the x dependence of the c-axis parameter presented in Ref. [76]

2.2 Superconducting transition temperatures and transition widths

The magnetization measurements were performed with a commercial SQUID magnetometer (Quantum Design, model MPMS-XL) with magnetic fields up to 7 T *see appendix A*. As commented above, the measurements were performed with both $H \parallel ab$ and $H \perp ab$. In the first case the crystals were glued with GE varnish to a quartz sample holder (0.3 cm in diameter, 22 cm in length) with two plastic rods at the ends which ensured an alignment better than 0.1°. For the measurements with $H \perp ab$ we made a groove (~ 0.3 mm wide) in

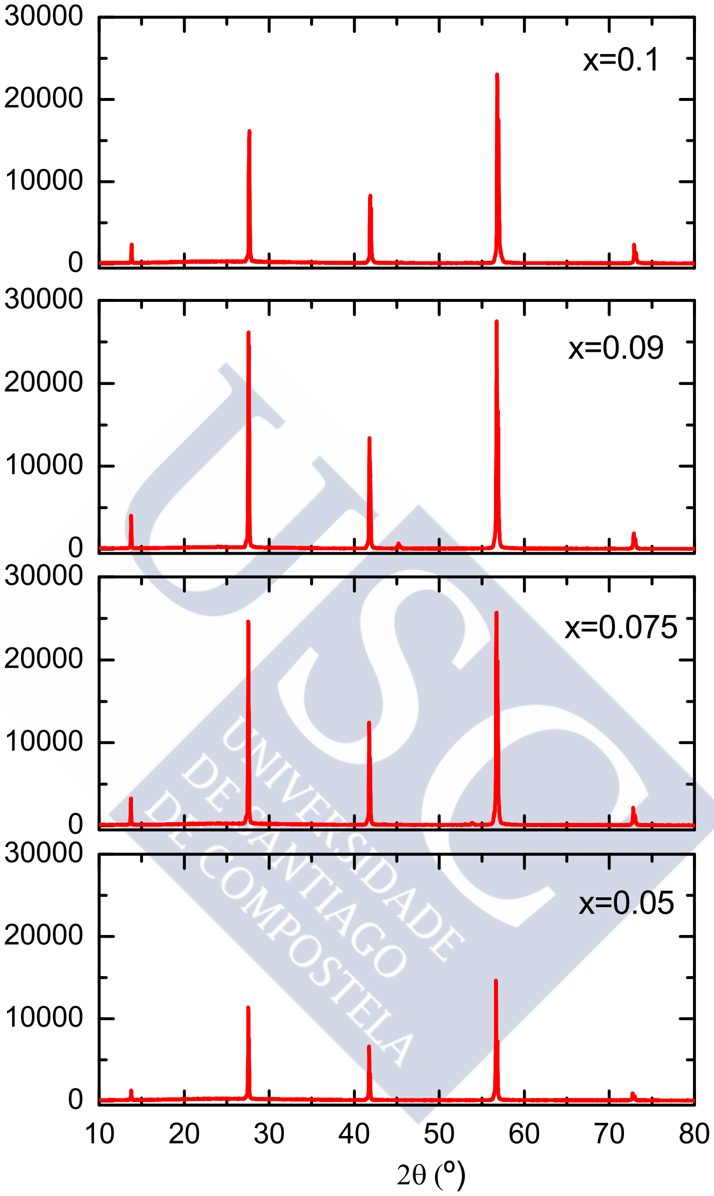

Figure 1.1: The x-ray diffraction patterns of $Ba(Fe_{1-x}Ni_x)_2As_2$ (x = 0.05, 0.0.75, 0.09, and 0.1) single crystals at room temperature.

the sample holder into which the crystals were glued also with GE varnish. The crystal alignment was checked by optical microscopy to be better than 5°. This allowed to determine the anisotropy factor from the anisotropy of the precursor diamagnetism with a $\sim 0.5\%$ uncertainty.[1]

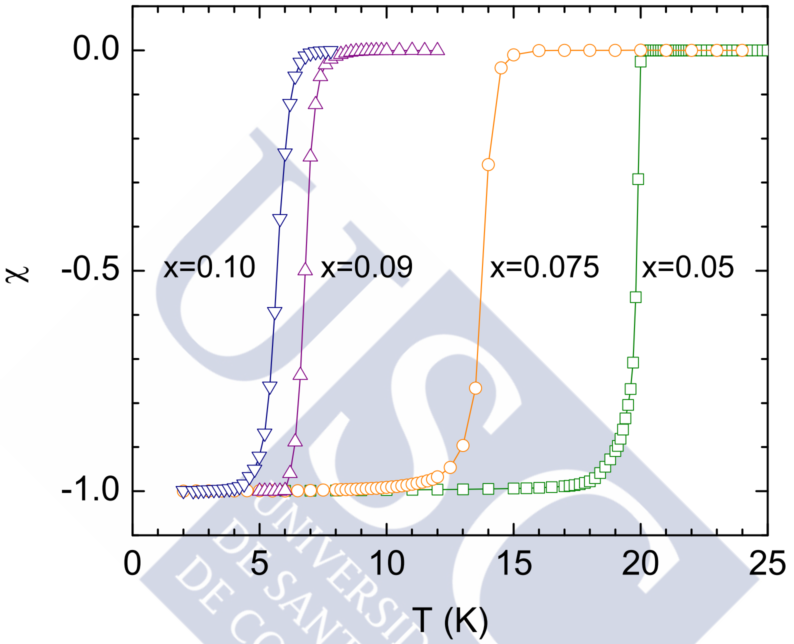

Figure 1.2: Temperature dependence of the ZFC magnetic susceptibility of the samples studied (already corrected for demagnetizing effects) obtained with a 0.5 mT perpendicular to the *ab*-layers. The x value represents the doping level.

In Fig. 1.2 it is presented the temperature dependence of the zero-field-cooled (ZFC) magnetic susceptibility for all crystals studied, measured with a 0.5 mT field applied perpendicular to the *ab* layers. The demagnetizing effect was corrected by using the demagnetizing

---

[1] According to the 3D-aGL approach in the low-field limit, if the crystal misalignment when measuring with $H \perp ab$ ($H \parallel ab$) is $\theta_\perp$ ($\theta_\parallel$), the measured $\chi^{\perp}_{\rm fl}/\chi^{\parallel}_{\rm fl}$ would be given by $\gamma^2_{\rm eff} = (\gamma^2\cos^2\theta_\perp + \sin^2\theta_\perp)/(\gamma^2\sin^2\theta_\parallel + \cos^2\theta_\parallel)$ (see, e.g., Ref. [77]). By using $\theta_\perp = 5°$, $\theta_\parallel = 0.1°$, and $\gamma \sim 2-15$ (see Ref. [10]), $\gamma_{\rm eff}$ would be within 0.5% the actual γ value.

x	$L_a \times L_b \times L_c$ (mm^3)	D	T_c (K)	ΔT_c (K)	T_{onset} (K)
0.05	$3.7 \times 1.45 \times 0.32$	0.77	20.0	0.3	27.0
0.075	$1.5 \times 1.20 \times 0.13$	0.82	14.2	0.6	18.2
0.09	$4.2 \times 1.85 \times 0.07$	0.90	7.2	0.8	10.2
0.10	$2.0 \times 1.80 \times 0.10$	0.92	6.3	0.6	8.9

Table 1.1: Some parameters of the crystals studied relevant for the analysis. See the main text for details.

factors D needed to attain the ideal value of -1 at low temperatures, which are within 5% the ones resulting from the crystals shape (see Table 1). From these curves, T_c was estimated by linearly extrapolating to $\chi = 0$ the higher-slope $\chi(T)$ data, and the transition width as $\Delta T_c = T_{c0} - T_c$, where T_{c0} is the highest temperature at which a diamagnetic signal is resolved in these low-field measurements. The results are also compiled in Table 1. As it may be seen ΔT_c is well below 1 K in most of the crystals, which will allow to study fluctuation effects in a wide temperature region above $T_c(H)$.

2.3 Fluctuation contribution to the magnetic susceptibility above T_c

To measure the weak magnetic moment due to superconducting fluctuations above T_c ($m \sim -10^{-5}$ emu in the samples used) we used the *Reciprocating Sample Option* (RSO). We averaged eight measurements consisting of 10 cycles at 1 Hz frequency, which lead to a resolution in the $\sim 10^{-8}$ emu range. In the present experiments we have used magnetic fields $\mu_0 H \geq 3$ T. This allowed us to analyze the data with the conventional GGL approach described below (at lower field amplitudes it has been reported that the fluctuation effects in these materials are strongly enhanced with respect to conventional GGL approaches, due to the possible presence of phase fluctuations [42] and/or T_c inhomogeneities [10]).

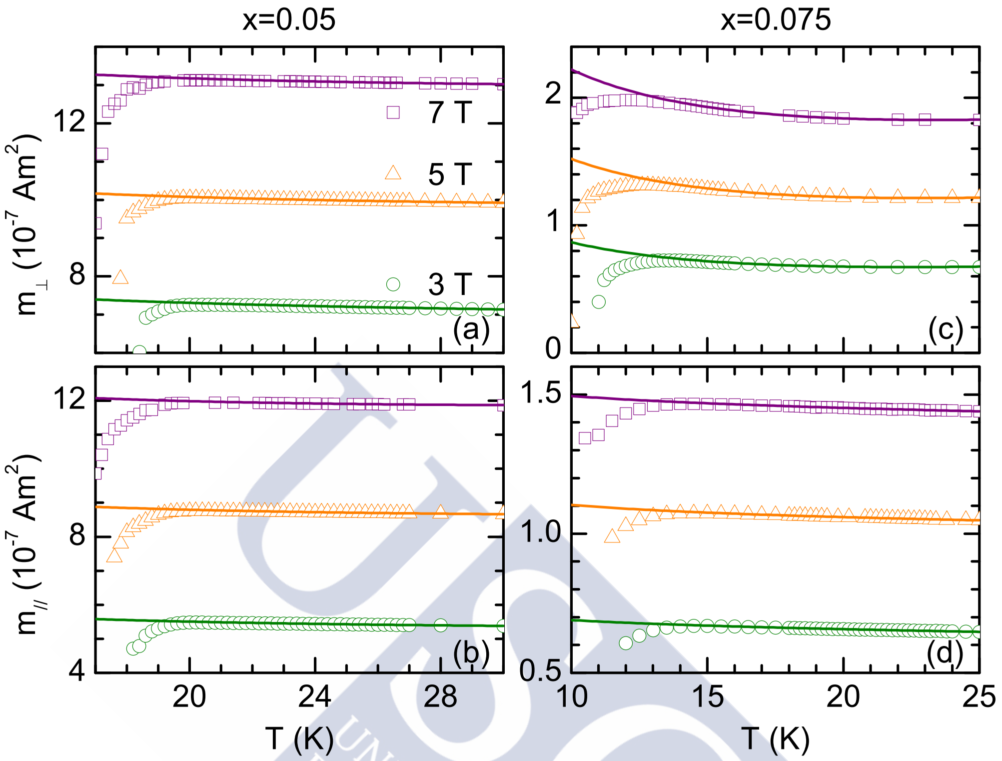

Figure 1.3: Example, for two of the studied samples, of the temperature dependence of the magnetic moment above T_c. Upper (lower) panels were obtained with $H \perp ab$ ($H \parallel ab$). The normal-state backgrounds (lines) were determined by fitting a Curie-like function (Eq. (1.2)) above $\sim 1.3T_c$, where fluctuation effects are negligible. For details see the main text.

Some examples of the as-measured $m(T)$ data around T_c are presented in Fig. 1.3, where the rounding associated to superconducting fluctuations may already be appreciated. For each applied field, the temperature dependence of the fluctuation magnetic moment was obtained through

$$m_{\rm fl}(T) = m(T) - m_B(T) \tag{1.1}$$

where $m_B(T)$ is the background contribution due to the samples normal state and to the sample holder. This last was determined by fitting a Curie-like function

$$m_B(T) = c_1 + c_2 T + \frac{c_3}{T} \tag{1.2}$$

to the raw data in a temperature interval from $\sim 1.3T_c$ up to above $\sim 1.8T_c$ (c_1, c_2 and c_3 are free parameters). The lower bound of this fitting region corresponds to a reduced temperature $\varepsilon \equiv \ln(T/T_c) \approx 0.3$, above which fluctuation effects in these materials are expected to be negligible [10, 47]. The resulting $m_B(T)$ contributions are presented as solid lines in Fig. 1.3.

The resulting fluctuation magnetic susceptibility, $\chi_{\mathrm{fl}}(T) = m_{\mathrm{fl}}(T)/HV$ (where V is the crystals volume estimated from their mass and from the theoretical density), is presented in Fig. 1.4 for all studied samples and for both $H \perp ab$ and $H \parallel ab$. Some qualitative aspects may be directly obtained from this figure: i) The rounded $\chi_{\mathrm{fl}}(T)$ behavior extends several Kelvin above T_c for all doping levels, up to an onset temperature $T_{onset} \approx 1.3T_c$ (see Table 1) which is well beyond the corresponding transition widths. This indicates that T_c inhomogeneities may play a negligible role. ii) The fluctuation magnetic susceptibility is anisotropic, being significantly larger in amplitude when $H \perp ab$. This anisotropy increases appreciably with the doping level, which is already consistent with the large increase of the anisotropy factor observed in Ref. [10] in the same compounds above the optimal doping. iii) The χ_{fl} amplitude decreases with the magnetic field (mainly when it is applied perpendicular to the ab layers, due to the anisotropy of the upper critical field). This indicates that the fields used in the experiments are large enough as to enter in the finite field (or Prange) fluctuation regime, where χ_{fl} strongly decreases with H [78]. The quantitative analysis of the data would then require using theoretical approaches valid beyond the zero-field (or Schmidt) limit.

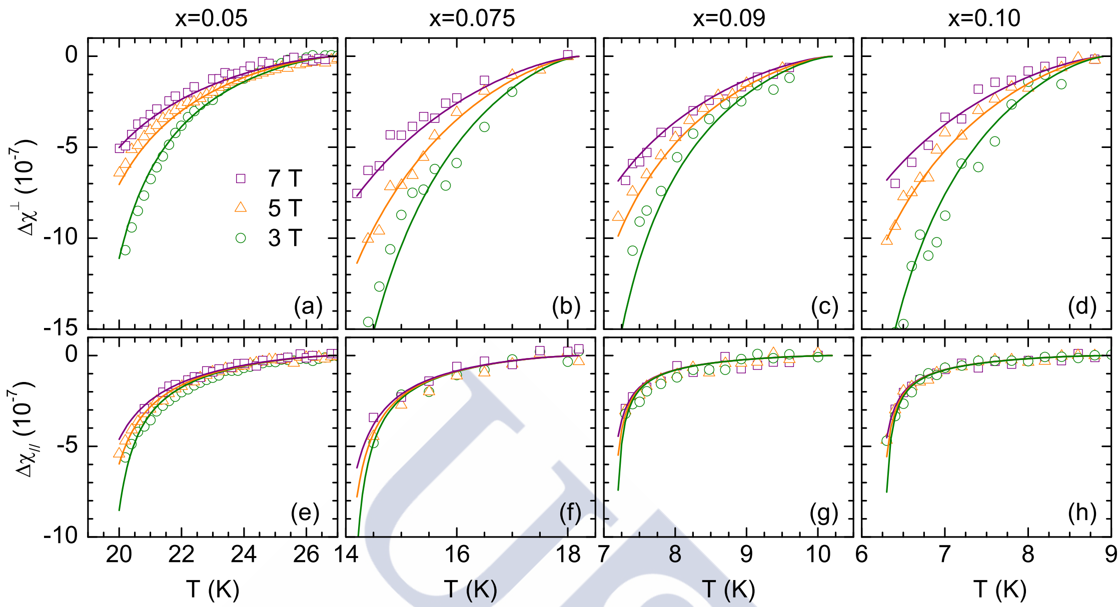

Figure 1.4: Temperature dependence just above T_c of the fluctuation magnetic susceptibility for all studied doping levels. Upper (lower) panels correspond to $H \perp ab$ ($H \parallel ab$). The lines in the upper panels are the best fits of the 3D-aGL approach for $H \perp ab$ (Eq. (1.7)) with $\xi_{ab}(0)$ and $\xi_c(0)$ as the only free parameters for each doping level. The lines in the lower panels were obtained *without free parameters*, by using in the 3D-aGL expression for $H \parallel ab$ (Eq. (1.8)) the same coherence lengths.

3 Brief summary of theory

In spite of the multiband nature of the compound under study, previous measurements of the fluctuation-induced conductivity and magnetoconductivity were successfully explained in terms of a GGL approach for single-band three-dimensional anisotropic superconductors (3D-aGL approach), and it will be our starting point. Below we will comment on the implications of the applicability of single-band approaches to these materials.

In terms of the 3D-aGL approach the fluctuation magnetization $M_{\rm fl}$ of an anisotropic superconductor (in presence of a field applied in the two main crystallographic directions) may be related to that of an isotropic superconductor through [69–71]

$$M_{\text{fl}}^{\perp}(T,H) = \gamma M_{\text{fl}}^{\text{iso}}(T,H) \tag{1.3}$$

for $H \perp ab$, and

$$M_{\text{fl}}^{\parallel}(T,H) = M_{\text{fl}}^{\text{iso}}(T,H/\gamma) \tag{1.4}$$

for $H \parallel ab$. In the low-field limit, i.e. for $H \ll H_{c2}(0)$, $M_{\text{fl}}^{\text{iso}}$ is given by Schmidt's classic result [53, 54],

$$M_{\text{fl}}^{\text{iso}}(T,H) = -\frac{\pi k_B T \mu_0 H \xi(0)}{6\phi_0^2}\varepsilon^{-1/2}, \tag{1.5}$$

where k_B is the Boltzmann constant, μ_0 is the vacuum magnetic permeability, ϕ_0 is the magnetic flux quantum, $\xi(0)$ is the coherence length, and $\varepsilon = \ln(T/T_c)$ is the reduced temperature. In this case, as $M_{\text{fl}}^{\text{iso}} \propto H$, the anisotropy factor could be obtained directly from the ratio

$$\frac{M_{\text{fl}}^{\perp}(T,H)}{M_{\text{fl}}^{\parallel}(T,H)} = \gamma^2. \tag{1.6}$$

As commented in the section 2.3 of this chapter, the H amplitudes used in the present experiments are beyond the low-field limit and Eqs. (1.5) and (1.6) are not directly applicable. Buzdin and Feinberg derived an expression for the fluctuation magnetization of 3D anisotropic materials valid for arbitrary field amplitudes and orientations [79]. However, their approach do not take into account short-wavelength effects, which may be relevant at high reduced temperatures, $\varepsilon \gg h$, here $h = H/H_{c2}(0)$ is the reduced magnetic fields and $H_{c2}(0)$ is the upper critical field for $H \perp ab$ linearly extrapolated to 0 K. In Refs. [48, 80] it was shown that the introduction of a *total-energy* cutoff in the fluctuation spectrum extends the applicability of the GGL approach to these short wavelength regimes. By combining the expression for M_{iso} in Ref. [48]

with Eqs. (1.3) and (1.4) it is obtained

$$\begin{aligned} M_{\text{fl}}^{\perp}(T,H) = -\frac{k_B T\gamma}{\pi\phi_0\xi_{ab}(0)}\int_0^{\sqrt{c-\varepsilon}} dq \Bigg[& \frac{c-\varepsilon}{2h} \\ - & \ln\Gamma\left(\frac{\varepsilon+h+q^2}{2h}\right)+\left(\frac{\varepsilon+q^2}{2h}\right)\psi\left(\frac{\varepsilon+h+q^2}{2h}\right) \\ + & \ln\Gamma\left(\frac{c+h+q^2}{2h}\right)-\left(\frac{c+q^2}{2h}\right)\psi\left(\frac{c+h+q^2}{2h}\right)\Bigg] \end{aligned} \tag{1.7}$$

and

$$M_{\text{fl}}^{\parallel}(T,H) = \frac{1}{\gamma}M_{\text{fl}}^{\perp}(T,H/\gamma). \tag{1.8}$$

Here Γ and Ψ are, respectively, the gamma and digamma functions, $\xi_{ab}(0)$ is the in-plane coherence length, and c is a cutoff constant which value is expected to be close to 0.5 [9]. In the low magnetic field limit ($h \ll \varepsilon$), in absence of cutoff ($c \to \infty$), and for isotropic materials ($\gamma = 1$), Eq. (1.7) reduces to the Schmidt result, Eq. (1.5). Equation (1.7) was successfully used to explain χ_{fl} above T_c in compounds like MgB_2 and NbSe_2 [81, 82], while their 2D and 2D-3D analogs accounted for the behavior of cuprate high-T_c compounds [65, 83–85]. It is worth noting that, in view of Eqs. (1.7) and (1.8), the ratio $M_{\text{fl}}^{\perp}/M_{\text{fl}}^{\parallel}$ decreases with h below γ^2. However, as it is illustrated in Fig. 1.5, for the h values used in the experiments, and the γ values expected after Ref. [10], such a ratio will be large enough as to determine γ with a good accuracy.

4 Analysis and discussion

4.1 Comparison with the theory

In order to compare the present measurements with the theory, we first fitted the Eq. (1.7) (normalized by the applied field) to the $\chi_{\text{fl}}^{\perp}(T,H)$ data in Fig. 1.4. The fitting region range from $T_c(H=0)$ up to $1.3T_c(H=0)$. The lower bound was chosen to avoid entering into the so-called critical region, where the Gaussian approximation

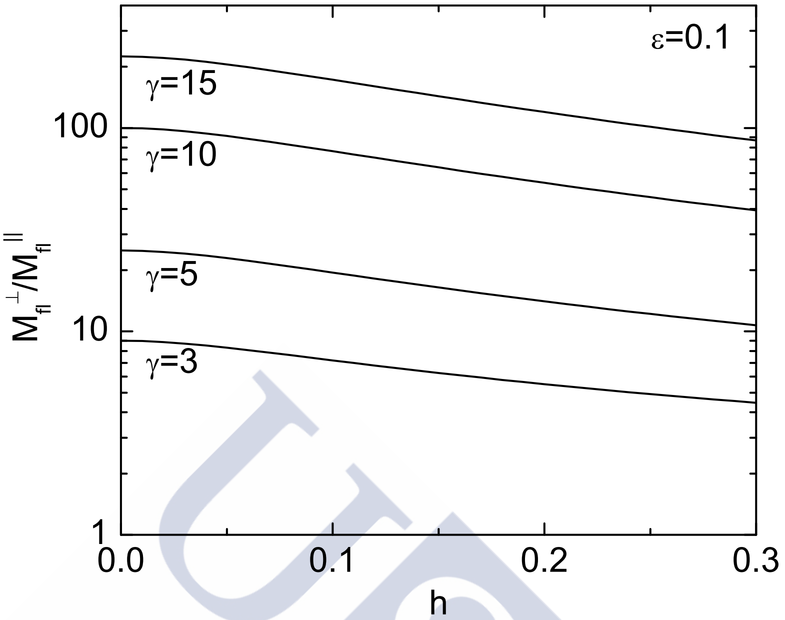

Figure 1.5: Effect of a finite applied magnetic field on the $M_{\rm fl}^{\perp}/M_{\rm fl}^{\parallel}$ ratio, according to Eqs. (1.7) and (1.8). While it is γ^2 when $h \to 0$, it is slightly reduced on increasing h.

is no longer valid.[2] In turn, the upper bound corresponds to the temperature above which fluctuation effects vanish, $T_{onset} \approx 1.3T_c$ (see Table 1). As the cutoff constant corresponds to the reduced temperature for the onset of fluctuation effects, we will use $c = \ln(T_{onset}/T_c) \approx 0.3$, a value consistent with the one found in previous works in the same material [10, 47]. For each doping level the only free parameters are $\xi_{ab}(0)$ and γ. Note that $\xi_{ab}(0)$ is present in the prefactor of Eq. (1.7) but also in the reduced magnetic field, that

---

[2] According to the field-dependent Ginzburg criterion [86] the upper bound of the critical region is given by $T_c^{\perp}(H) + T_c[4\pi k_B\mu_0 H\gamma/\Delta c\xi_{ab}(0)\phi_0]^{2/3}$ when $H \perp ab$, and by $T_c^{\parallel}(H) + T_c[4\pi k_B\mu_0 H/\Delta c\xi_{ab}(0)\phi_0]^{2/3}$ when $H \parallel ab$ (Δc is the specific heat jump at T_c) [39]. Recent measurements in a 122 iron pnictide with similar superconducting parameters ($\mathrm{Ba}_{1-x}\mathrm{K}_x\mathrm{Fe}_2\mathrm{As}_2$) revealed that, for the H amplitudes used in our experiments, the upper bound of the critical region may be approximated by $T_c(H = 0)$ for both field orientations [39].

may be expressed as $h = 2\pi\mu_0 H\xi_{ab}^2(0)/\phi_0$. As it may be seen in Figs. 1.4 (a) to (d), the agreement with the data is excellent for all field amplitudes and for all doping levels. The fluctuation magnetization for $H \parallel ab$, Eq. (1.8), depends on the same superconducting parameters. Therefore, the lines in Figs. 1.4 (e) to (h) were obtained *without free parameters*, by just using in Eq. (1.8) the $\xi_{ab}(0)$ and γ values previously determined. As it may be seen, the agreement with the data is also excellent, strongly supporting the reliability of the resulting values for $\xi_{ab}(0)$ and γ, and the applicability of the single-band 3D-aGL approach used. It has been proposed that multiband effects may be observable when there is a large difference between the coherence lengths in different bands.[11] In this case, a deviation from single-band approaches should appear at the field scale associated to the larger coherence length, ξ_1, i.e., $H_1 = \phi_0/2\pi\mu_0\xi_1^2$. Our results could suggest that in this material the coherence lengths in different bands are not too different, or that H_1 is not in the field range explored in the present work. In fact, H_1 is the field scale at which the upper critical field has upward curvature [11], and recent magnetotransport measurements in the same compounds revealed that the upper critical field presents a linear T-dependence up to well above the H values used here [45, 47].

4.2 Dependence of the superconducting parameters on the doping level

In Fig. 1.6 we present the $\xi_{ab}(0)$ and γ values resulting from the above analysis as a function of the doping level. This figure also includes the transverse coherence length amplitude, obtained as $\xi_c(0) = \xi_{ab}(0)/\gamma$. As it may be seen, $\xi_{ab}(0)$ increases moderately from 3.3 nm at optimal doping ($x = 0.05$) to 4.5 nm well inside the overdoped region ($x = 0.10$). However, γ presents a pronounced increase from ~ 3 to ~ 16 in the same interval of doping levels. We are not aware of theoretical studies about a possible dependence of the anisotropy factor with the doping level in these compounds. However, a density functional study

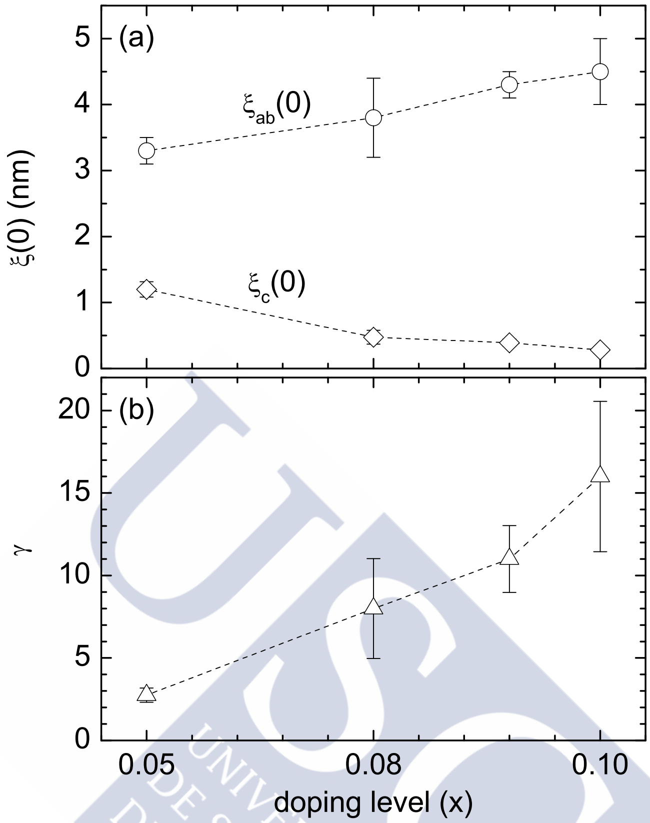

Figure 1.6: Dependence with the doping level of the coherence length amplitudes (a) and of the anisotropy factor (b), as follows from the comparison of Eqs. (1.7) and (1.8) with the data in Fig. 1.4.

by Singh and Du [14] in $\mathrm{LaFeAsO}_{1-x}\mathrm{F}_x$ shows that the Fermi-surface sheets and dimensionality strongly depend on the doping level, and that the anisotropy tends to increases when the system is doped away from the parent phase.

Associated to the increase in γ, there is a significant decrease of the transverse coherence length, from $\xi_c(0) \simeq 1.2$ nm at optimal doping to $\xi_c(0) \simeq 0.4$ nm for $x = 0.1$. This last value is even smaller than the FeAs layers interdistance, $s \simeq 0.64$ nm, which could suggest the possible presence of two-dimensional (2D) fluctuation effects.

However, according to the Lawrence-Doniach model for a system of Josephson-coupled superconducting layers, the reduced temperature at which a 3D - 2D crossover would occur is given by $\sim (2\xi_c(0)/s)^2$, which is as large as 0.77 even for the most anisotropic crystal ($x = 0.1$). This is well above the reduced temperature at which fluctuation effects are observe to vanish ($\varepsilon \simeq 0.3$), confirming the adequacy of the 3D approach used to analyze the data.

4.3 Comparison with γ values in the literature for Fe-based superconductors

The x-dependence of the superconducting parameters presented in Fig. 1.6 is consistent with the one obtained in Ref. [10] from the fluctuation-induced in-plane magnetoconductivity of single crystals of the same composition, including the large increase of the anisotropy factor in the overdoped region. The differences between these results could be attributed to the uncertainties associated with the finite size of the electrical contacts in the magnetoconductivity measurements. Other measurements of γ in $\mathrm{Ba(Fe_{1-x}Ni_x)_2As_2}$ in the literature focused in the optimal doping level [87–89]. The values found in these works ($\gamma \approx 1.7 - 3$) are close to the one observed in our optimally-doped crystal, further confirming the reliability of our analysis.

In other compounds of the 122 family, in particular in the electron-doped $\mathrm{Ba(Fe_{1-x}Co_x)_2As_2}$ and in the hole-doped $\mathrm{Ba_{1-x}K_xFe_2As_2}$, there are some studies including non optimally-doped samples. [3, 26, 88, 90–104] The corresponding γ values are plotted against x in Fig. 1.7. These values correspond to temperatures close to T_c, where no appreciable differences were observed between $\gamma_\lambda \equiv \lambda_c/\lambda_{ab}$ and $\gamma \equiv \xi_{ab}/\xi_c$, and may be directly compared to our present results. In spite of the dispersion, it seems that $\gamma(T_c)$ also tends to increase with the doping level, although the large values observed here are not observed. It is worth noting, however, that in these works the maximum studied doping level ($x_{\max}$) relative to the optimal one (x_{op}, indicated as arrows in the figures) are below the one reached in our work: in $Ba_{1-x}K_xFe_2As_2$ there are no data in the overdoped region, in $Ba(Fe_{1-x}Co_x)_2As_2$ $x_{max}/x_{op} = 1.3$, while in our present work $x_{max}/x_{op} = 2$.

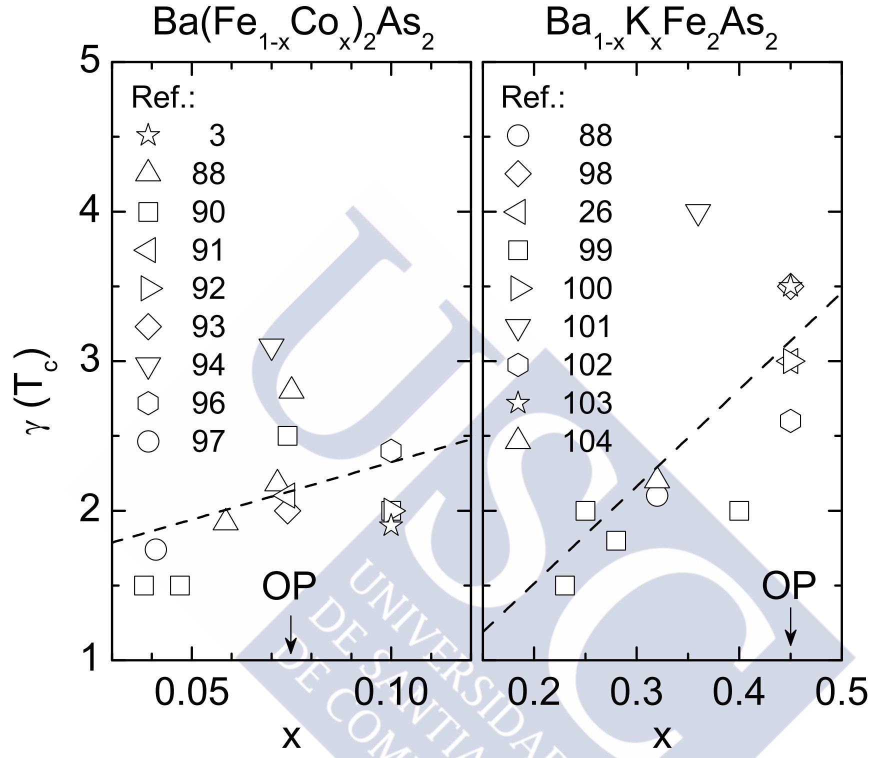

Figure 1.7: Anisotropy factor (near T_c) against the doping level in the most studied compounds of the 122 family, according to data in the literature. The optimal doping for each compound is indicated by an arrow. The lines are linear fits.

Just for completeness, in Table 1.2 we summarize the anisotropy factors found in other families of Fe-based superconductors. For these compounds no clear dependence of the anisotropy factor with the doping level is observed. 1111 compounds are more anisotropic than the ones from the 122 family (the anisotropy factor at optimal doping is about ~ 5), and they even present 2D characteristics. In spite of that, values of the anisotropy factor as large as the ones observed here

Family	Compound	x	T_c(K)	$\gamma(T_c)$	Ref.
1111	$NdFeAsO_{1-x}F_x$	0.18	47	4	[105]
		0.18	52	4.5	[106]
		0.18	46	3.9	[107]
		0.3	47.4	5	[3]
		0.35	40	3.5	[108]
	$SmFeAsO_{1-x}F_x$	0.15	49.5	8	[40]
		0.2	42	6.5	[109]
		0.2	52.3	2	[42]
	$SmFeAsO_{0.7}F_{0.25}$		49	7.5	[110]
	$PrFeAsO_{1-x}$	0.1	34	4	[111]
		0.3	45	5	[112]
	$SmFeAsO_{1-x}$	0.15	50.5	5	[109]
111	LiFeAs		17.6	2.5	[113]
11	$FeSe_{1-x}Te_x$	0.5	14.6	1.6	[114]
		0.5	14.5	$1.1-1.9$	[3]
	Fe(Se,Te)		13.6	3	[115]

Table 1.2: Summary of values in the literature for the anisotropy factor near T_c in compounds of the 1111, 111, and 11 families.

in highly overdoped $Ba(Fe_{1-x}Ni_x)_2As_2$ were still not reported.

5 Conclusions

We have presented measurements of the magnetic susceptibility just above the superconducting transition of the iron pnictide $Ba(Fe_{1-x}Ni_x)_2As_2$ with different doping levels. The measurements were performed with magnetic fields up to 7 T applied both parallel and perpendicular to the FeAs (ab) layers. The excellent structural and stoichiometric quality of the crystals studied, which show sharp diamagnetic transitions, allowed to obtain accurate data of the fluctuation effects in a wide temperature range above the superconducting transition. These experimental results were analyzed in terms of a Gaussian Ginzburg-Landau approach for 3D anisotropic superconductors valid in the finite-field (or Prange) fluctuation regime. This single-band approach was found to be in excellent agreement with the data up to the highest reduced temperatures and magnetic fields explored. This suggests that the coherence lengths in the different bands of this superconductor are not very different, or that the field scale at which multiband effects are expected to be observable is not in the field range of our experiments. The analysis allowed to determine the dependence of the in-plane $\xi_{ab}(0)$ and transverse $\xi_c(0)$ coherence lengths with the doping level. The anisotropy factor, $\gamma = \xi_{ab}(0)/\xi_c(0)$ was found to increase from ~ 3 at optimal doping ($x = 0.05$) to ~ 15 well inside the overdoped region ($x = 0.10$). These results provide a quantitative confirmation of the conclusions proposed for the same compounds in Ref. [10] from measurements of the fluctuation-induced magnetoconductivity. It would be desirable to check whether such a large increase of the anisotropy factor is also present in other Fe-based superconductors at high doping levels.

Chapter 2

Superconducting fluctuations in isovalently-substituted $\mathrm{BaFe_2(As_{1-x}P_x)_2}$: Possible observation of multiband effects

Summary of this chapter *The nature of superconducting fluctuation effects in the isovalently substituted iron pnictide* $\mathrm{BaFe_2(As_{1-x}P_x)_2}$ *at the optimal substituting level is probed through measurements of the magnetization and magnetoconductivity around the superconducting transition. The results obtained with magnetic fields up to 9 T applied in the two main crystal directions are consistent with the anisotropic Ginzburg-Landau approach for finite applied magnetic fields. The analysis allow us to determine with accuracy the transverse,* $\xi_c(0)$, *and in-plane,* $\xi_{ab}(0)$, *coherence lengths. Significant differences are found between the* $\xi_c(0)$ *values resulting from electrical transport and magnetization measurements. According to recent theoretical approaches, these differences could be interpreted in terms of the multiband nature of this material. On the other hand, the data analysis in the low-field region around the transition temperature also suggests that phase fluctuations, although possibly relevant in other Fe-based superconductors, may play a negligible role in this compound.*

1 Introduction

Superconductivity appears in iron pnictides when the antiferromagnetic phase is suppressed by chemical doping of the parent compound or by applying a pressure.[116] It is now well known that isovalent substitution (e.g., the partial replacement of As by P, or Fe by Ru)[117–119] presents notable differences with charge doping (e.g., by partially replacing O by F in ROFeAs, where R is a rare earth element,[2, 19, 120–122] or Ba by K in $BaFe_2As_2$ [25]). While isovalently-substituted compounds are closer to the clean limit,[123] charged dopants create strong scattering potentials which affect superconducting properties such as the vortex pinning, [124] the upper critical field,[5, 125, 126] and even the superconducting gap symmetry.[124, 127–129] In fact, many studies indicate that compounds with charged dopants present a fully gapped Fermi surface (see e.g., $SmFeAsO_{1-x}F_x$,[130] $PrFeAsO_{1-y}$ [131], $BaFe_{2-x}Co_xAs_2$,[132] and $BaFe_{2-x}Ni_xAs_2$ [133]), while isovalently substituted compounds such as $Ba(Fe_{1-x}Ru_x)_2As_2$ and $BaFe_2(As_{1-x}P_x)_2$ present evidences of nodes [134–138]. In spite of the interest of isovalently-substituted compounds, fluctuation effects in these materials are still unexplored. Moreover, they may also provide information about the multiband nature of these materials. In fact, it has been shown that a two-band model predicts a change in the relative amplitude of the different fluctuation observables in relation with the single-band case, mainly through a renormalization of the c-axis coherence length.[11] Among the isovalently-substituted iron pnictides, optimally-substituted $BaFe_2(As_{1-x}P_x)_2$ presents the highest critical temperature ($T_c \sim 30$ K) and thus is the best candidate to investigate thermal fluctuation effects in these materials. In this work we present a systematic study of fluctuation effects around T_c in the electrical conductivity and magnetization of several high-quality single crystals. The measurements were performed in magnetic fields up to 9 T, which close to T_c are above the so-called ghost field,[139] and allow to investigate the finite-field (or Prange) fluctuation regime.[55]

The results will allow us to probe the applicability to these materials of Ginzburg-Landau approaches for finite applied magnetic fields, and to investigate possible differences in the coherence length amplitudes associated with the multiband nature of this material. Finally, the low-field ($\sim 10^{-3}$ T) behavior of the magnetization for temperatures around T_c will be studied to check the relevance of phase fluctuations, which were claimed to be important in other iron pnictides.[42, 140]

2 Growth and characterization of the crystals

Our single crystals were grown using the Ba_2As_2/Ba_2P_3 self-flux method described in Ref. [141]. These crystals were provided by the professor Huiqian Luo (from Institute of Physics in Beijing (China)). Some details of their characterization may be seen in Ref. [142]. The crystals used in the present experiments are plate-like, with typical surfaces of several mm^2 and thicknesses up to $\sim 10^2$ μm. Their stoichiometry was checked with a scanning electron microscope (Zeiss FESEM Ultra Plus) equipped with a EDX (energy dispersive x-ray) spectroscope. A typical EDX spectrum is shown in Fig. 2.1(a). The average stoichiometry turned out to be $Ba_{1.04}Fe_{1.91}As_{1.33}P_{0.72}$, with a variation smaller than 0.4% between the different crystals and the different studied areas. The partial substitution of As by P is about 35 %, which is close to the optimal substituting level.

The crystal structure was studied in some of the crystals by x-ray diffraction (XRD) by using a Rigaku MiniFlex II diffractometer with a Cu-target. A typical example of the reflections by the ab planes is presented in Fig. 2.1(b). The absence of reflections other than the ($00l$) indicate an excellent structural quality of the crystals. An example of the rocking curve for the (004) reflection is presented in the inset of Fig. 2.1(b). It confirms that the crystal c axis presents a dispersion of only $\sim 0.11°$. Powder x-ray diffraction in some grounded crystals allowed us to determine the lattice constants of the tetragonal

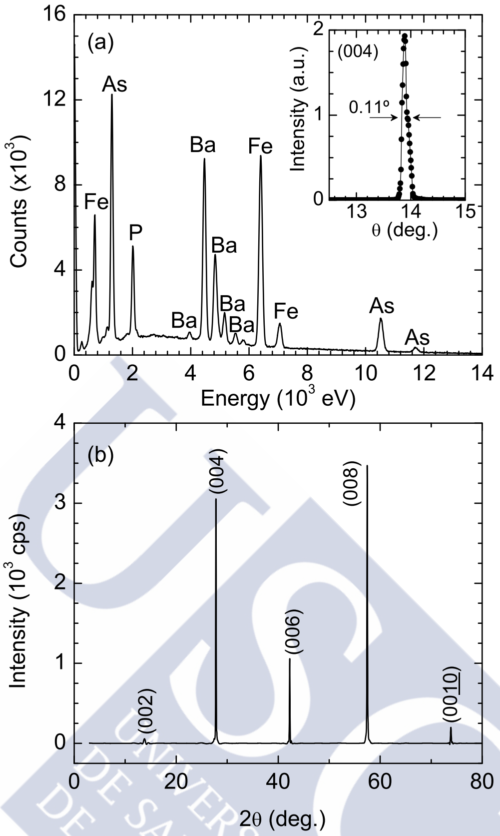

Figure 2.1: a) Example of a typical EDX spectrum. b) Example of x-ray diffraction pattern on a single crystal, obtained by using the geometry to observe the reflections in the *ab* layers. Inset: Rocking curve associated with the (004) reflection, showing that the dispersion in the orientation of the crystal *c*-axis is about 0.1°.

structure, which turned out to be $a = b = 0.39249(15)$ nm and $c = 1.2833(4)$ nm, in agreement with data in the literature.[117, 143, 144]

3 Resistivity measurements

The in-plane resistivity (along the *ab* layers), ρ_{ab}, was measured in two single crystals with a Quantum Design Physical Property

Measurement System (PPMS), by using four contacts with an in-line configuration and an excitation current of $\sim$ 1 mA at 23 Hz. The measurements were performed with magnetic fields up to $\mu_0 H = 9$ T applied both parallel and perpendicular to the *ab* layers. The size of the crystals chosen for these measurements is presented in Table 2.1. The finite size of the electrical contacts (stripes typically 0.5 mm wide) leads to an uncertainty in the ρ_{ab} amplitude of $\sim$ 25%.

crystal	surface (mm^2)	thickness (μm)	mass (mg)
R1	0.78×0.49	15	0.036
R2	1.60×1.30	18	0.234
1	5.61	58.6	2.058
2	5.86	60.4	2.216
3	3.18	96.0	1.912
4	4.89	82.8	2.536
5	6.26	88.1	3.456
6	7.38	149.8	6.920
7	4.57	80.1	2.292
8	5.84	123.1	4.500
9	3.05	75.2	1.436
10	5.35	65.3	2.188
Stack	$\sim$5.20	879.4	29.514

Table 2.1: Physical parameters of the crystals. R1 and R2 were used in the resistivity measurements; the others were used to build the stack for the magnetization measurements.

An example (corresponding to crystal 2) of the $\rho_{ab}(T)_H$ behavior around the transition is presented in Fig. 2.2. In the overview shown in the inset a linear temperature dependence up to 100 K may be seen, without the kinks associated with structural and magnetic transitions typical of undersubstituted samples.[141] In the absence of an applied field, the resistive transition in both crystals is very sharp: the transition midpoint is about $\sim$ 28 K with an uncertainty of ± 0.4 K as estimated from the 90%-10% criterion. This would allow us to investigate fluctuation effects in a wide temperature range above the transition. However, the resistivity rounding just above T_c typical of fluctuations is almost inappreciable. This is consistent with the relatively large normal-state (or background) in-plane conductivity σ_{ab}^B, as compared with the fluctuation-induced conductivity predicted by the Aslamazov-Larkin approach for 3D materials,

$$\sigma_{ab}^{\mathrm{fl}} = \frac{e^2}{32\hbar\xi_c(0)}\varepsilon^{-1/2}, \tag{2.1}$$

where $\varepsilon = \ln(T/T_c)$ is the reduced temperature, e is the electron charge, $\hbar$ the reduced Planck constant, and $\xi_c(0)$ the c-axis coherence length amplitude. By using the $\xi_c(0) = 1$ nm (see below), at $\varepsilon = 0.1$ one obtains $\sigma_{ab}^{\mathrm{fl}} \approx 2 \times 10^4$ $(\Omega\mathrm{m})^{-1}$, which is 10^2 times smaller than $\sigma_{ab}^B \approx 2.5 \times 10^6$ $(\Omega\mathrm{m})^{-1}$ just above T_c. It is worth noting, however, that a slight rounding may still be observed in the $\rho_{ab}(T)$ curves obtained under the largest H amplitudes used, which may be attributed to critical fluctuations around the $H_{c2}(T)$ line. The absence of important fluctuation effects in the resistivity allows to determine with accuracy the temperature dependence of the upper critical fields from the transition midpoints. The result for the two studied samples is presented in Fig. 2.3. For both field orientations $H_{c2}(T)$ is linear to a very good approximation, although for fields below ~ 1 T a slight positive curvature is observed. This effect occurs at temperatures within the transition width and could be due to a T_c distribution. However, it could also be attributed the multiband nature of this material, if the upper critical field of the band with the largest coherence length is about ~ 1 T (see e.g. Ref. [11]). The solid lines in Fig. 2.3 are linear fits for $H \geq 1$ T. The resulting $H_{c2}(T)$ slopes and the extrapolated T_c values are summarized in Table 2.2. From these values, the in-plane and transverse GGL coherence length amplitudes, $\xi_{ab}(0)$ and $\xi_c(0)$ respectively, were obtained through

$$\xi_{ab}(0) = \sqrt{\frac{\phi_0}{2\pi T_c\mu_0|dH_{c2}^{\perp}/dT|}} \tag{2.2}$$

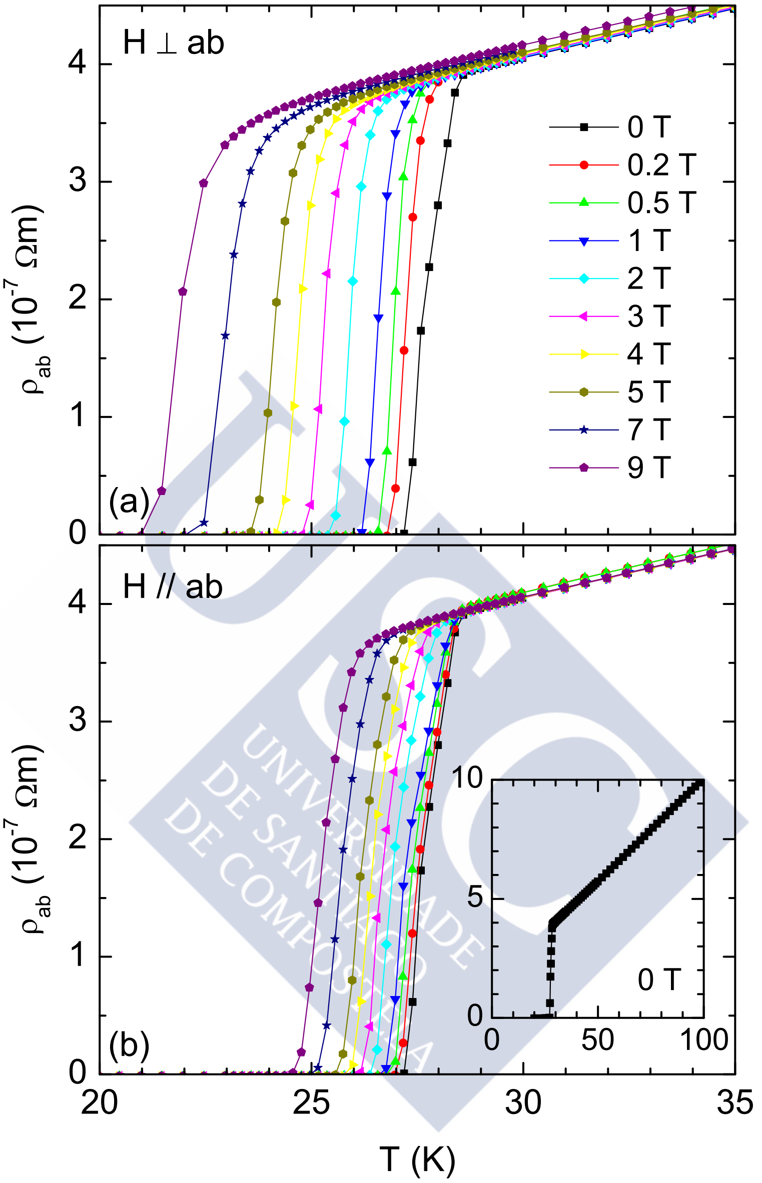

Figure 2.2: Example (corresponding to crystal 2) of the temperature dependence of the in-plane resistivity around T_c, for magnetic fields up to 9 T applied in the two main crystal directions. The inset in (b) is an overview up to 100 K.

and

$$\xi_c(0) = \xi_{ab}(0)/\gamma, \tag{2.3}$$

where

$$\gamma = \frac{dH_{c2}^{\parallel}/dT}{dH_{c2}^{\perp}/dT} \tag{2.4}$$

is the superconducting anisotropy factor. The resulting values are also compiled in Table 2.2.

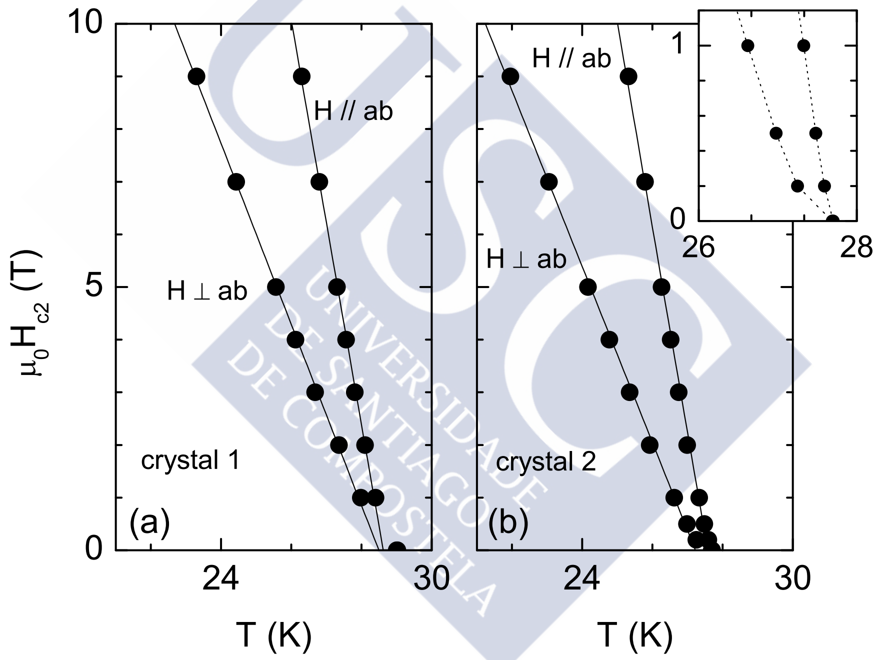

Figure 2.3: Temperature dependence of the upper critical field for $H \perp ab$ and $H \parallel ab$, and for the two crystals studied. These data were obtained from the midpoint of the corresponding resistive transitions. Straight lines indicate the linear fitting performed from 1 T up to 9 T. Inset shows the non linear behavior observed at temperature close to the critical temperature. See main text for details.

4 Magnetization measurements

The magnetization measurements were performed with a Quantum Design's SQUID magnetometer (model MPMS-XL) in a stack of ten high-quality single crystals glued with a minute amount of GE varnish, with a total mass of 29.514 mg and a volume of 4.71 mm^3 as determined from their theoretical density. A picture of the individual crystals used in the experiments and of the resulting pile may be seen in Fig. 2.4, and the sizes of the individual crystals are summarized in Table 2.1. As we will see below, such a large sample is necessary to attain the resolution needed to study the small fluctuation diamagnetism due to superconducting fluctuations.

The temperature dependence of the zero-field-cooled (ZFC) magnetic susceptibility, measured with a low field (0.2 mT) perpendicular to the *ab* layers, is presented in Fig. 2.5. These data are corrected for demagnetizing effects by using the demagnetizing factor needed to attain the ideal value of -1 at low temperatures ($D = 0.71$), which is consistent with the physical dimensions of the pile. From these curves, T_c was estimated by a linear extrapolation to $\chi = 0$ of the higher-slope $\chi(T)$ data, and the transition half-width as $\Delta T_c = T_{c0} - T_c$, where T_{c0} is the highest temperature at which a diamagnetic signal is resolved (the procedure is detailed in the inset in Fig. 2.5). In spite of the large volume of the sample, the ΔT_c value is only 0.4 K, confirming its excellent stoichiometry, and allowing to study fluctuation effects in a wide temperature region above $T_c(H)$.

To measure the weak magnetic moment due to superconducting fluctuations above T_c ($m \sim -10^{-5}$ emu, see below) we used the *Reciprocating Sample Option* (RSO). We averaged eight measurements consisting of 10 cycles at 1 Hz frequency, which lead to a resolution in the $\sim 10^{-8}$ emu range. The magnetic fields used in the experiments range from 1 to 6 T which allowed to deeply penetrate in the finite-field (or Prange) fluctuation regime (see below). The $m(T)$ data around T_c for all fields amplitudes and orientations studied are presented in Figs. 1.2(a) and (c). In the detail of Figs. 1.2(b) and (d), corresponding

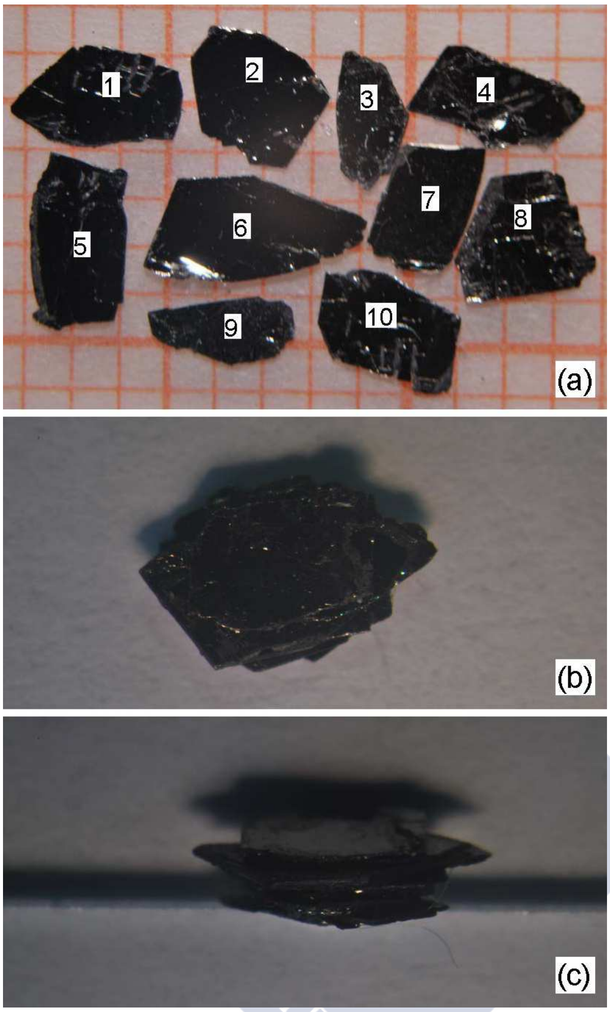

Figure 2.4: a) Single crystals used in the magnetization measurements (sizes and masses are summarized in Table 2.1). b) and c) Top view and, respectively, side view of the pile formed with the single crystals in (a).

to an applied field of 4 T, it may be appreciated a rounding extending from $T_c \approx 28.1$ K to $\sim$33 K. This interval is well beyond the transition half-width ($\sim$0.4 K), so the rounding may be attributed to superconducting fluctuations.

The fluctuation contribution to the magnetic moment was

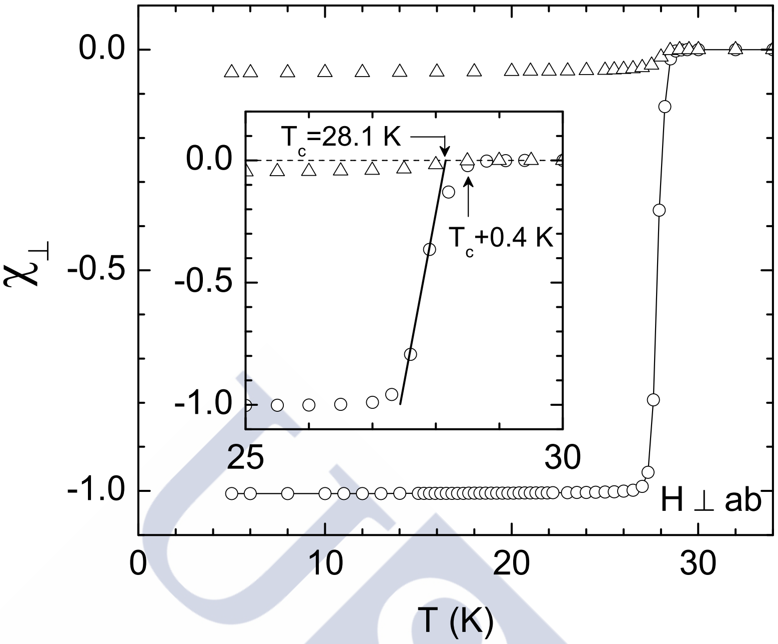

Figure 2.5: Temperature dependence of the low-field (0.2 mT) magnetic susceptibility of the pile of single crystals. These measurements were performed with $H \perp ab$ after zero-field cooling (circles) and field-cooling (triangles). The data are already corrected for demagnetizing effects. Inset: Detail around T_c showing the sharp diamagnetic transition (only 0.4 K wide). See the main text for details.

determined through

$$m_{\text{fl}}(T) = m(T) - m_B(T), \tag{2.5}$$

where $m_B(T)$ is the background contribution coming from the samples normal state and from the sample holder. It was obtained by fitting a Curie-like function

$$m_B(T) = A + BT + \frac{C}{T} \tag{2.6}$$

to the raw data in a region between 35 K up to 42 K (A, B and C are free parameters). The upper limit was chosen to avoid a small upturn (in the scale of 10^{-7} emu) observed above ∼45 K in all the measurements, and that may be attributed to an unavoidable amount of oxygen in the sample space. This upturn cannot be removed by successively pumping and venting with helium the sample space.

The resulting $m_B(T)$ contributions are presented as solid lines in Fig. 2.6. The resulting fluctuation magnetic susceptibility, $\chi_{\rm fl}(T) = m_{\rm fl}(T)/HV$ (where V is the crystals volume), is presented in Fig. 2.7. As expected, the fluctuation magnetic susceptibility is anisotropic, being significantly larger in amplitude when $H \perp ab$. Also, the $\chi_{\rm fl}$ amplitude decreases with H, which is an indicative that the fields used in the experiments are large enough as to enter in the finite field (or Prange) fluctuation regime, where $\chi_{\rm fl}$ strongly decreases with H.[78] The quantitative analysis of the data would then require using theoretical approaches valid beyond the zero-field (or Schmidt) limit.

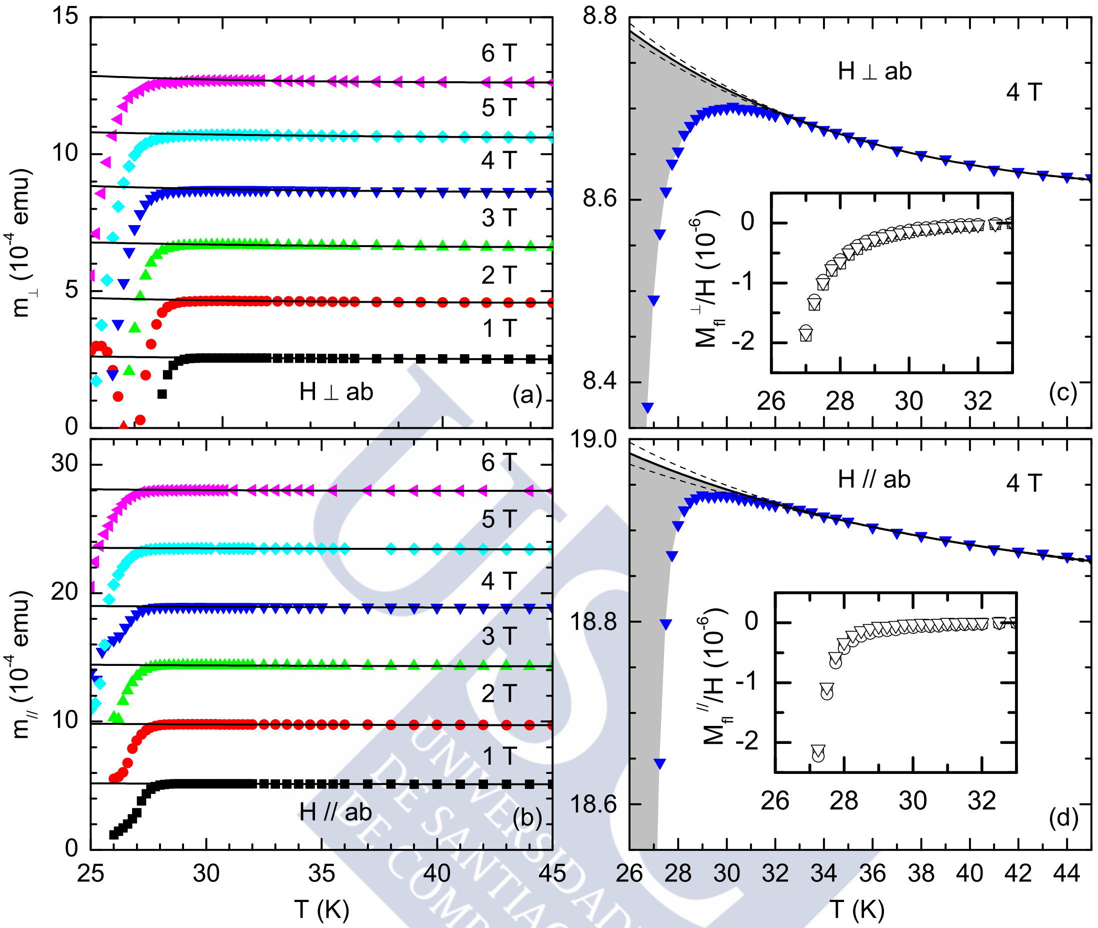

Figure 2.6: a,b) Overview of the temperature dependence of the magnetic moment above T_c for all magnetic field amplitudes and orientations investigated. The solid lines are the background contributions obtained by fitting a Curie-like function above 35 K. c,d) A detail around T_c corresponding to the measurement with $\mu_0 H = 4$ T. The shaded areas represent the fluctuation effects, extending up to 5 K above T_c and with an amplitude clearly anisotropic. The dashed lines indicate the error derived from the parameter C used in the background fitting. Insets of c,d) show the corresponding uncertainties in the fluctuation contribution to the magnetic susceptibility due to the background subtraction.

5 Analysis of fluctuation effects in the magnetization

5.1 Gaussian region above $T_c(H)$

It has been shown that the presence of several bands contributing to the superconductivity in these materials may affect the fluctuation-induced observables through a renormalization of the coherence length amplitudes, but without appreciably affecting their functional form with respect to the single band case.[11] Thus, our $\chi_{\rm fl}(T,H)$ data will be analyzed in terms of a GGL approach for single-band three-dimensional anisotropic superconductors (3D-aGL approach). The possible presence of multiband effects will be probed through differences between the resulting coherence lengths and the ones previously determined from the field dependence of the resistive transition.

In terms of the 3D-aGL approach the fluctuation magnetization $M_{\rm fl}$ of an anisotropic superconductor in presence of a finite applied magnetic field is given by [48, 69–71]

$$\begin{aligned} M_{\rm fl}^{\perp}(T,H) = &-\frac{k_BT\gamma}{\pi\phi_0\xi_{ab}(0)}\int_0^{\sqrt{c-\varepsilon}} dq \left[\frac{c-\varepsilon}{2h}\right. \\ &- \ln\Gamma\left(\frac{\varepsilon+h+q^2}{2h}\right) + \left(\frac{\varepsilon+q^2}{2h}\right)\psi\left(\frac{\varepsilon+h+q^2}{2h}\right) \\ &+ \left.\ln\Gamma\left(\frac{c+h+q^2}{2h}\right) - \left(\frac{c+q^2}{2h}\right)\psi\left(\frac{c+h+q^2}{2h}\right)\right] \end{aligned} \tag{2.7}$$

for $H \perp ab$, and

$$M_{\rm fl}^{\parallel}(T,H) = \frac{1}{\gamma}M_{\rm fl}^{\perp}(T,H/\gamma). \tag{2.8}$$

for $H \parallel ab$. Here Γ and ψ are, respectively, the gamma and digamma functions, $\varepsilon = \ln(T/T_c)$ the reduced temperature, $h = H/[\phi_0/2\pi\mu_0\xi_{ab}^2(0)]$ the reduced magnetic field, $\xi_{ab}(0)$ is the in-plane coherence length amplitude, γ the anisotropy factor, and c is a total-energy cutoff constant.[9] The cutoff was introduced to take into account short-wavelength effects, which may be relevant in particular at high reduced magnetic fields or temperatures ($h, \varepsilon \sim c$).[50] In view of Eq. (2.7), c equals the reduced temperature below which fluctuation effects appear, $T_{\text{onset}} \approx 35$ K. So, in subsequent analyses we will use $c = \ln(T_{\text{onset}}/T_c) \approx 0.16$, a value in good agreement with the one found in other Fe-based superconductors.[10, 47, 145]

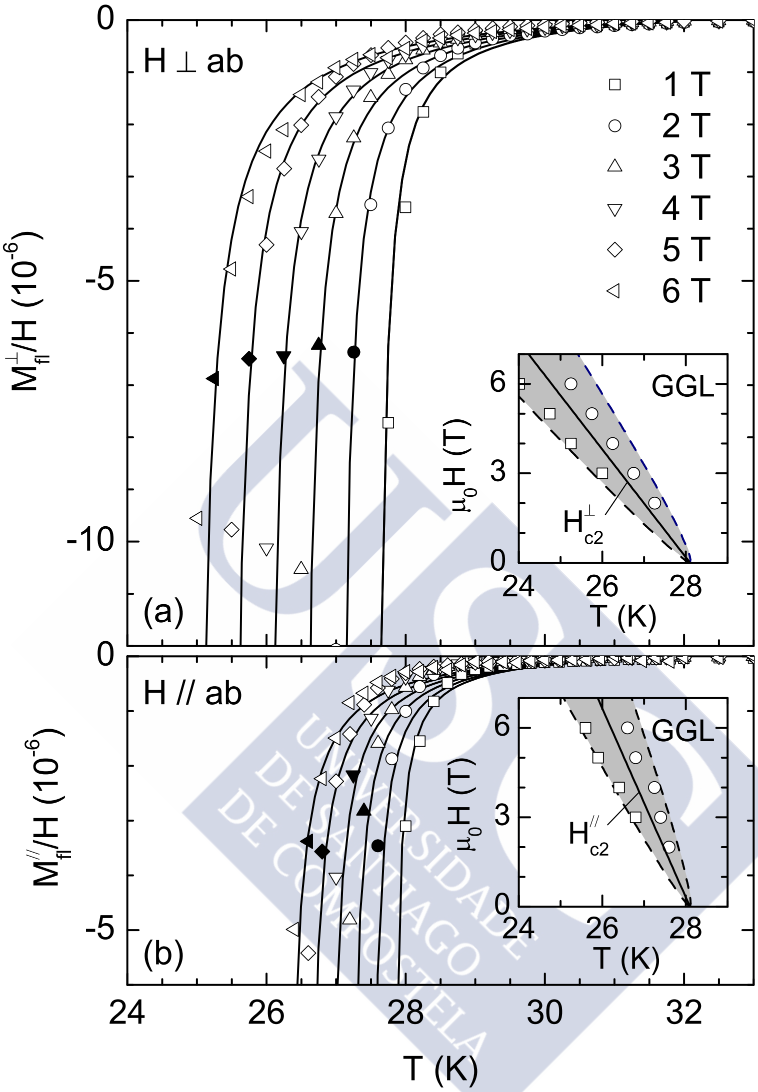

Figure 2.7: Temperature dependence of fluctuation-induced magnetic susceptibility in the Gaussian region for both $H \perp ab$ (a) and $H \parallel ab$ (b). The lines are the best fit of Eqs. (2.7) and (2.8), respectively, by using $\xi_{ab}(0)$ and γ as free parameters. The solid data points are the lower bound of the fitting region. Insets: $H-T$ phase diagrams for both field orientations. The shadowed areas represent the critical regions, as obtained from Eqs. (2.9) and (2.10). The circles (squares) represent the lower bound for the applicability of the Gaussian (critical) GL approach.

Equations (2.7) and (2.8) are expected to be applicable down to the critical fluctuation region. It is bounded by the so-called H-dependent Ginzburg criterion, which for 3D anisotropic superconductors may be written as,[146–148]

$$T_G^{\perp}(H) \approx T_c^{\perp}(H) \pm T_c \left[\frac{4\pi k_B \mu_0 H}{\Delta c \xi_c(0) \phi_0}\right]^{2/3} \tag{2.9}$$

for $H \perp ab$, and

$$T_G^{\parallel}(H) \approx T_c^{\parallel}(H) \pm T_c \left[\frac{4\pi k_B \mu_0 H}{\Delta c \xi_c(0) \gamma \phi_0}\right]^{2/3} \tag{2.10}$$

for $H \parallel ab$, where Δc is the specific-heat jump at T_c and $T_c^{\perp,\parallel}(H) = T_c(1 - \frac{H}{H_{c2}^{\perp,\parallel}(0)})$. Let us finally note that Eqs. (2.7) and (2.8) were already successfully used to explain the susceptibility rounding above T_c of iron pnictides such as $\mathrm{Ba}_{1-x}\mathrm{K}_x\mathrm{Fe}_2\mathrm{As}_2$ and $\mathrm{Ba(Fe}_{1-x}\mathrm{Ni}_x)_2\mathrm{As}_2$,[39, 145] and of other 3D anisotropic superconductors such as MgB_2 and NbSe_2.[81, 82] In turn, the 2D and 2D$-$3D (Lawrence-Doniach) versions accounted for the behavior of different high-T_c cuprates.[65, 83–85] Eqs. (2.7) and (2.8) were fitted to the set of M_{fl}/H data for both $H \perp ab$ and $H \parallel ab$ with only two free parameters, $\xi_{ab}(0)$ and γ. The best fit is represented as solid lines in Fig. 2.7. The fitting interval range from T_{onset} to the solid data points. If the fitting interval is extended to lower temperatures, the fit quality is considerably worsened. In fact, these solid data points are already close to the upper bound of the critical fluctuation region. This is better seen in the $H - T$ phase diagrams in the insets of Fig. 2.7, where the limit of applicability of the GGL approach is indicated by circles, and the shaded areas are the critical regions evaluated with Eqs. (2.9) and (2.10) by using $\Delta c/T_c \sim 0.1$ J/molK^2,[149] and the $\xi_c(0)$ and γ values in Table 2.2.

The values for the fitting parameters, $\xi_{ab}(0)$ and γ, are compiled in Table 2.2, together with the $\xi_c(0)$ value obtained as $\xi_{ab}(0)/\gamma$. The indicated uncertainties account for the range in which the fitting parameters may be changed without appreciably worsen the fitting quality. The $\xi_{ab}(0)$ value is in excellent agreement with the one determined in Section 2.3 from resistivity measurements, but the $\xi_c(0)$ value is a 30 % larger. Such a difference is beyond the experimental uncertainty, and will be discussed in Sec.2.5.3

Crystal	Observable	$\mu_0 dH_{c2}^{\perp}/dT$ (T/K)	$\mu_0 dH_{c2}^{\parallel}/dT$ (T/K)	T_c (K)	$\xi_{ab}(0)$ (nm)	$\xi_c(0)$ (nm)	γ
R1	$\rho(T)_H$	-1.72(2)	-3.84(6)	28.5(1)	2.59(2)	1.16(4)	2.23(6)
R2	$\rho(T)_H$	-1.72(2)	-4.05(9)	27.3(2)	2.65(3)	1.13(5)	2.35(8)
Stack	$M_{\rm fl}(T)_H$ (G-region)	-1.81(2)	-3.16(12)	28.1	2.54(3)	1.45(6)	1.75(5)
Stack	$M_{\rm fl}(T)_H$ (C-region)	-1.75(15)	-3.2(3)	28.2(1)	2.6(1)	1.4(3)	1.8(3)

Table 2.2: Superconducting parameters of the crystals studied, indicating the observable used to obtain them (see main text for details). Note the difference between the $\xi_c(0)$ values determined from the H-dependence of the resistive transition temperature, and from the analysis of fluctuation effects in the magnetization.

5.2 Fluctuation diamagnetism in the critical region around $T_c(H)$

As a check of consistency of the above analysis we studied the data in the critical region around the $H_{c2}(T)$ line, where the Gaussian approximation breaks down. In this region, the 3D-GL approach in the lowest-Landau-level approximation predicts that $M_{\rm fl}^{\perp}(T,H)$ and $M_{\rm fl}^{\parallel}(T,H)$ follow a scaling behavior, $m_{\perp,\parallel} = f_{\perp,\parallel}(t_{\perp,\parallel})$, the scaling variables being [150, 151]

$$m_{\perp,\parallel} \equiv \frac{M_{\perp,\parallel}}{(HT)^{2/3}} \tag{2.11}$$

and

$$t_{\perp,\parallel} \equiv \frac{T - T_c^{\perp,\parallel}(H)}{(HT)^{2/3}}. \tag{2.12}$$

As always, the indexes $\perp$ and $\parallel$ stand for $H \perp ab$ and $H \parallel ab$, respectively. The scaling functions for $H \perp ab$ and $H \parallel ab$ are related through[39]

$$f_\parallel(t_\parallel) = \frac{f_\perp(t_\parallel \gamma^{2/3})}{\gamma^{5/3}}. \tag{2.13}$$

By assuming a linear temperature dependence of the upper critical fields, the scalings for both $H \perp ab$ and $H \parallel ab$ depend on only three parameters: T_c, and the $H_{c2}^{\perp}(T)$ and $H_{c2}^{\parallel}(T)$ slopes. The best scalings, presented in Fig. 2.8, were obtained with the values for these parameters presented in the last row of Table 2.2. The indicated uncertainties represent the range of values for which the scalings are not appreciable worsened. The corresponding $\xi_{ab}(0)$ and $\xi_c(0)$ values, obtained by using Eqs. (2.2-2.4), are also compiled in Table 2.2. In spite of the larger uncertainties, these values are consistent with the ones found in the analysis of the Gaussian region. Other indications of the coherence of the present analysis are as follows: i) The scaling is acceptable down to $t_{\parallel,\perp} \sim -3 \times 10^{-6}$, a value in good agreement with the lower bound of the critical region (it leads to the squares in the $H-T$ phase diagrams in the insets of Fig. 2.7). ii) The experimental scaling functions (solid lines in Fig. 2.8) are related to each other as predicted by Eq. (2.13), see the caption in Fig. 2.8.

5.3 Discussion of the results

As shown in Table 2.2, the $\xi_{ab}(0)$ values determined from the resistivity measurements are in excellent agreement with the one derived from the fluctuation magnetization. However, there is a significant difference between the corresponding $\xi_c(0)$ values. This effect cannot be attributed to an incomplete superconducting volume fraction in the stack used for the magnetization measurements, because $\xi_{ab}(0)$ and γ (or $\xi_c(0)$) affect the amplitudes of $M_{\rm fl}^{\perp}$ and $M_{\rm fl}^{\parallel}$, but also their dependence on H. The $\xi_{ab}(0)$ and $\xi_c(0)$ values in the literature for optimally-substituted BaFe$_2$(As$_{1-x}$P$_x$)$_2$ are summarized in Table 2.3. These data were obtained from the $T_c(H)$ dependence, as probed by dc and ac electrical transport and by a static property such as the specific heat. The $\xi_{ab}(0)$ values in these works are close to each other and to the

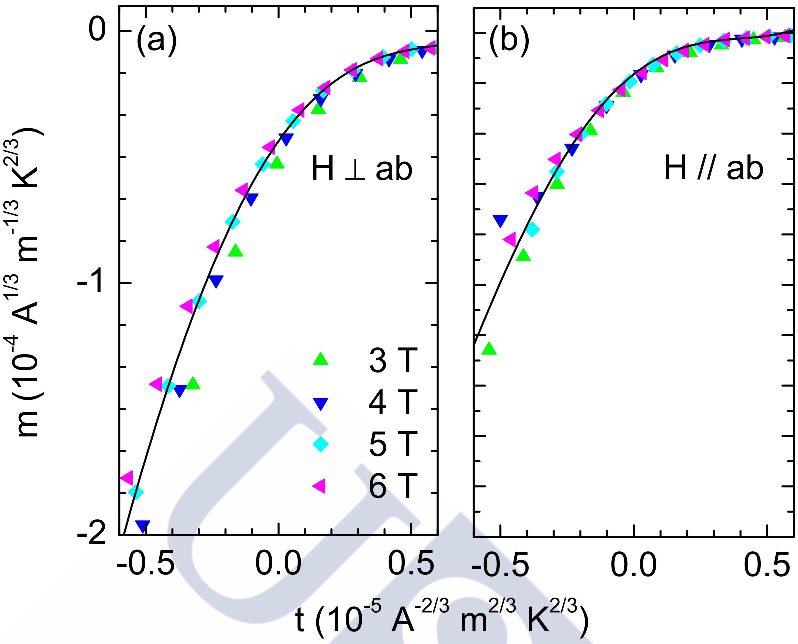

Figure 2.8: 3D-GL scaling of the magnetization in the critical region for $H \perp ab$ (a) and $H \parallel ab$ (b). The line in (a) is the experimental scaling function for $H \perp ab$, while the one in (b) for $H \parallel ab$ was calculated from the former through Eq. (2.13).

values obtained here (see Table 2.2). The $\xi_c(0)$ value obtained from dc resistivity [152] is also in excellent agreement with our data obtained from the same observable. However, a notable difference is found with the $\xi_c(0)$ values derived from other observables (0.9-1.75 nm). These results may be somewhat affected by the uncertainty associated with the use of a criterion to determine $T_c(H)$, but could confirm a possible dependence of $\xi_c(0)$ on the observable used to determine it.

Our present results could be due to the presence of several bands contributing to the superconductivity in the material under study.[5, 30, 156, 157] In fact, a recently proposed two-band model predicts that the functional forms of dominating divergences of the fluctuation-induced specific heat and electrical conductivity do

Table 2.3: Summary of the superconducting parameters of optimally-substituted $BaFe_2(As_{1-x}P_x)_2$ in the literature.

T_c (K)	$\mu_0 dH_{c2}^{\perp}/dT$ (T/K)	$\mu_0 dH_{c2}^{\parallel}/dT$ (T/K)	$\xi_{ab}(0)$ (nm)	$\xi_c(0)$ (nm)	observable	Ref.
30.6	-1.72	-3.66	2.50	1.17	$\rho(T)_H$	[152]
30.0	-2.1	–	2.30	–	$C(T)_H$	[135]
29.0	-2.1	–	2.30	–	$C(T)_H$	[153]
28.1	-2.23	-5.73	2.29	0.9	$C(T)_H$	[154]
28.4	-2.1	–	2.33	–	$C(T)_H$	[155]
30.5	-1.67	-2.41	2.54	1.75	LCR	[143]

not change with respect to the single-band case, but their relative amplitudes are affected mainly by a renormalization of the c-axis coherence length.[11] It has been suggested that this effect could be behind a dependence of the upper critical fields (for $H \parallel ab$ and $H \perp ab$) of $FeSe_{0.5}Te_{0.5}$ on the observable used to determine them. In particular, the H_{c2} values derived from measurements of the specific heat are systematically larger than the ones obtained from the electrical resistivity, and these last are in turn larger than the ones obtained from magnetic torque.[158–160] It would be then very interesting to check whether an expression for $M_{\rm fl}(T,H)$ in a two-band superconductor (still unavailable) would also quantitatively account for the differences found here with the data obtained from resistivity measurements.

5.4 Enhanced diamagnetism in the low-field region just above T_c

For completeness, we have also explored this region of the phase diagram. In contrast with the linear behavior predicted by GGL approaches under low fields ($h \ll \varepsilon$), the $M_{\rm fl}(H)$ isotherms just above T_c present an anomalous upturn at a field $\mu_0 H_{up} \approx 10^{-3}$ T for both field orientations (see Fig. 2.9). Below $H_{\rm up}$ the magnetic susceptibility is orders of magnitude larger than the one associated with Gaussian superconducting fluctuations. Above $H_{\rm up}$ the $M_{\rm fl}$ amplitude decreases and, consistently with Fig. 2.7, for fields about ~ 1 T the conventional GGL behavior is recovered.

A qualitatively similar anomalous behavior has been observed in high-T_c cuprates such as $\mathrm{La}_{2-x}\mathrm{Sr}_x\mathrm{CuO}_4$[161–163] and $\mathrm{Y}_{1-x}\mathrm{Ca}_x\mathrm{Ba}_2\mathrm{Cu}_3\mathrm{O}_y$,[164] and more recently in Fe-based superconductors like $\mathrm{SmFeAsO}_{1-x}\mathrm{F}_x$ (Sm1111) [42] and $\mathrm{Ba(Fe}_{1-x}\mathrm{Rh}_x)_2\mathrm{As}_2$ (Rh122)[140]. The similarities between our results and these previous works in iron pnictides are even quantitative. For instance, the isotherms measured a temperatures near T_c present very similar $H_{\rm up}$ and $M_{\rm up}$ values (in the case of Sm1111 one has to take into account its 2D nature and that the sample is granular). So, is it expected that the effect in optimally-substituted $\mathrm{BaFe}_2\mathrm{As}_{2-x}\mathrm{P}_x$ has the same origin as in Rh122 and Sm1111. In Refs. [42] and [12] it has been proposed that, like in the high-temperature superconductors, the anomaly is due to the presence of important phase fluctuations. Alternatively, it has been proposed that it is a consequence of a T_c distribution, which in cuprate or Fe-based superconductors would be associated with their non-stoichiometric nature.[163] Some indications incline us by this last explanation: On the one side, below $H_{\rm up}$ the magnetic susceptibility is a significant fraction of the perfect diamagnetism (indicated as a dashed line in Fig. 2.9), as if a significant volume fraction of the sample were actually in the Meissner region. On the other, the effect is limited to a range of temperatures above T_c of the order of the transition width, $2\Delta T_c$. Finally, the $H_{\rm up}$ values are consistent with the lower critical field of the higher-T_c domains, which may be approximated by $-\mu_0(\partial H_{c1}/\partial T)_{T_c}\Delta T_c$, and that is in the 10^{-3} T range.[1]

An argument supporting the phase fluctuation scenario is that in Sm1111 and Rh122, $H_{\rm up}$ increases with the temperature in some temperature interval above T_c, while the lower critical field

---

[1] By combining the Rutgers expression $\Delta c/T_c = (\mu_0/2\kappa^2)(\partial H_{c2}^{\perp}/\partial T)^2_{T_c}$ with $\Delta c = 2.8$ J/molK,[149] and $\mu_0(\partial H_{c2}^{\perp}/\partial T)_{T_c} = -1.8$ T/K (Table 2.2), one obtains $\kappa \approx 30$. Then, by using $H_{c1}^{\perp} = (\ln\kappa/\sqrt{2}\kappa^2)H_{c2}^{\perp}$ one finds $\mu_0(\partial H_{c1}^{\perp}/\partial T)_{T_c} \approx -3.4$ mT/K.

decreases.[42, 140, 165] Such an $H_{\mathrm{up}}(T)$ dependence is not observed in optimally-substituted $\mathrm{BaFe_2As_{2-x}P_x}$, in spite that the transition widths of our crystals are comparable or even smaller (in relative terms) than those in Refs. [42] and [140]. As a consequence, we may assume that phase fluctuations do not play a role in this compound, or at least they are much less relevant than in Sm1111 and Rh122.

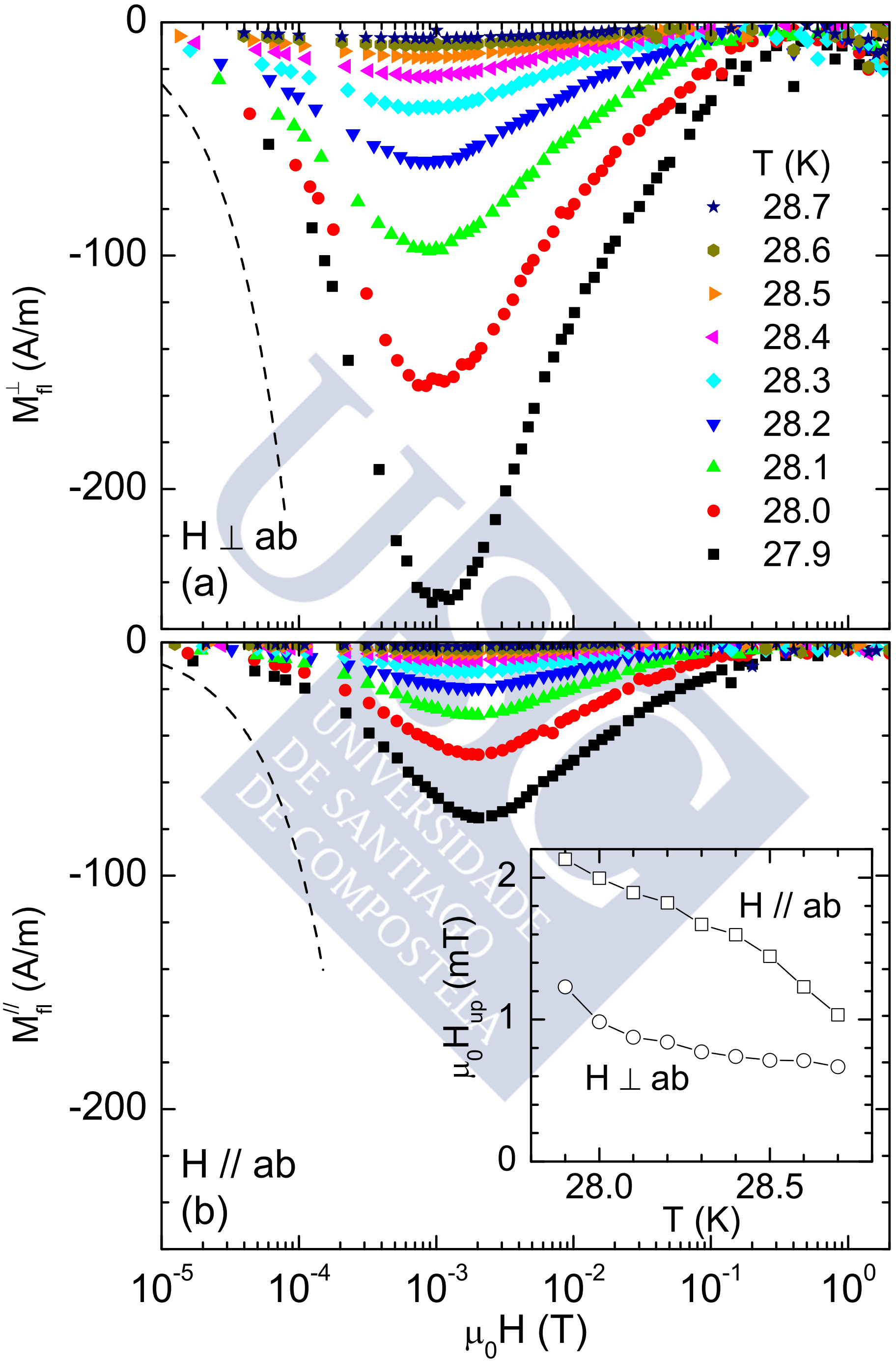

Figure 2.9: Anomalous H-dependence of the fluctuation magnetization for temperatures just above T_c and for both $H \perp ab$ (a) and $H \parallel ab$ (b). As a reference, the dashed lines represent the ideal diamagnetic response (evaluated taking into account the demagnetizing factors of the sample under study). The anomalous upturn appears at temperatures within the transition width (±0.4 K). Inset: Temperature dependence of the upturn magnetic field, H_{up}.

6 Conclusions

We have presented measurements of the magnetization and magnetoconductivity around the superconducting transition of the isovalently-substituted iron pnictide $\mathrm{BaFe_2(As_{1-x}P_x)_2}$ with a substituting level near the optimal one ($x = 0.35$). The measurements were performed with magnetic fields up to 9 T in the conductivity and 7 T in the magnetization, in both cases applied in the two main crystal directions (parallel and perpendicular to the ab layers). Due to the relatively large electrical conductivity in the normal state near T_c, the fluctuation effects in this observable are almost unobservable. As a consequence, the resistive transitions are very well defined, allowing us to determine with accuracy the temperature dependence of the parallel and perpendicular upper critical fields, and the in-plane and transverse coherence lengths. On the contrary, the magnetization presents an appreciable diamagnetic contribution above T_c that may be attributed to superconducting fluctuations. The consistent analysis in the different fluctuation regimes (Gaussian and critical) in terms of existing Ginzburg-Landau approaches, allowed to determine with accuracy the coherence length amplitudes and the anisotropy factor. The resulting $\xi_c(0)$ value presents a notable difference with the one obtained from the field dependence of the resistive transition. According to recent theoretical approaches,[11] this difference may indicate the possible presence of several bands contributing to the superconductivity in these compounds. Finally, from the analysis of the anomalous upturn in the $M(H)$ isotherms just above T_c, we find that phase fluctuations may play a negligible role in this compound, contrary to what is proposed for other Fe-based superconductors.


USC
UNIVERSIDADE
DE SANTIAGO
DE COMPOSTELA

Chapter 3

Anomalous (non GL) angular dependence of the upper critical field in optimally-substituted $\mathbf{BaFe_2(As_{1-x}P_x)_2}$

Summary of this chapter

Through the study of in-plane magnetoresistivity measurements at different orientations with respect to the c-axis (perpendicular to the FeAs layers) in $BaFe_2(As_{1-x}P_x)_2$ *(*$x \simeq 0.35$*), the angular behavior of the upper critical field,* $H_{c2}(\theta)$*, near* T_c *was determined. Two types of analysis were performed: a) A study of the superconducting fluctuation magnetoconductivity above* T_c*. b) Direct determination of* $\mu_0 H_{c2}$ *from the point which represents the 10 % of the normal resistivity in the superconducting phase transition. Both studies conclude a slight deviation from the behavior described by the anisotropic Ginzburg-Landau theory for the upper critical field when the angle between the applied field and the c-axis is close to 90°. This anomalous behavior may be associated with the multiband nature of this material.*

1 Introduction

An important aspect of the phenomenology of Fe-based superconductors is the knowledge of the angular dependence of the upper critical field, $\mu_0 H_{c2}(\theta)$. This magnitude can be used for instance, to find out the anisotropy of the order parameter, γ.[166] The theory for $\mu_0 H_{c2}(\theta)$ was developed by the mid 1960s for conventional superconductors from the anisotropic Ginzburg-Landau theory. However, since the discovery of superconductors with multiband features [81, 116, 167–169], where there is a strong link between the topology of the Fermi surface and the anisotropy of the order parameter [5, 30, 156, 157], it is not so clear that the angular dependence of the upper critical field is well described by this theory.[170] In this chapter we measured the upper critical field close to T_c with the magnetic field oriented at different angles, θ, relative to the *c*-axis (perpendicular to the FeAs layers) in the isovalently substituted $BaFe_2(As_{1-x}P_x)_2$ because this material has manifested multiband effects, some of which were presented in chapter 2. Due to its smaller coherence lengths and its higher T_c as compared with the conventional superconductors, we analyse the thermal superconducting fluctuations in the magnetoconductivity, $\Delta\sigma(T)_H$, in the Gaussian region in order to determine $H_{c2}(\theta)$. In a second part, this parameter is measured directly from the superconducting phase transition in order to verify our results by another way.

2 Measurements of the fluctuation-induced in-plane magnetoconductivity

2.1 Measurements with H parallel to the c-axis

Experimental details and results

The BaFe(As$_{1-x}$ P$_x$)$_2$ sample used in this work is a plate-like single crystal from the same batch used in the previous chapter, with dimensions of $1.60 \times 1.30 \times 0.018$ mm^3 and with the ab-layers parallel to the largest face. Their nominal P doping is $x = 0.35$, which is close to the optimal doping level (see chapter 2, where details of the characterization may be found).

The resistivity along the ab-layers, ρ, was measured with a Quantum Design's Physical Propery Measurement System (PPMS) in presence of a field, H, parallel to the c-axis up to 9 T. It was used a standard four probe method with low-contact resistance (less than 1 Ω) and an excitation current of $\sim$ 2.5mA at 112 Hz frequency (see Appendix 2). The uncertainty due to the size of the contacts implies an indetermination in the ρ amplitude of 20 %.

Several examples of $\rho(T)_H$ are shown in Fig. 3.1(a). In the inset of the same figure an overview of the behavior at zero-magnetic field of $\rho(T)$ is shown. A linear temperature dependence is appreciated up to 100 K without the kinks associated with either structural or magnetic transitions, typical of undersubstituted samples [141]. In absence of an applied field, the width of the superconducting transition in our crystal, ΔT_c, is around 0.8 K, as estimated from the difference of temperatures when in the superconducting transition the resistance reaches the 90% and the 10% of the normal resistance. A transition midpoint of 27.7 K implies that this ΔT_c will represent less than 3% of uncertainty, which allows us to investigate fluctuation effects above T_c in a wide temperature range.

Despite that the rounding due to the magnetoconductivity induced by superconducting fluctuations, $\Delta\sigma(T)_H$ above T_c is small [1], its study gives us another way to determine with accuracy several superconducting parameters such as: the out of plane anisotropy, γ, the in-plane and out of plane Ginzburg-Landau coherence lengths, ξ_{ab} and ξ_c, as well as signs of possible multiband behavior [11], phase fluctuations [42], and/or T_c inhomogeneities [85]. For each applied field, the temperature dependence of the superconducting fluctuations in the magnetoconductivity was obtained as:

$$\Delta\sigma(T)_H = \frac{1}{\rho(T)_H} - \frac{1}{\rho_B(T)_H} \tag{3.1}$$

where $\rho_B(T)_H = 1/\sigma^B(T)$ is the background contribution due to the sample in the normal state. As it is shown in Fig. 3.1(a), this contribution follows a linear temperature dependence up to the largest field used in the experiment. This allows us to parametrize the background resistivity as:

$$\rho_B(T) = \alpha + \beta\ T \tag{3.2}$$

The coefficients α and β were obtained by linear fitting to the $\rho(T)$ curves in a temperature interval between the 30% and the 50% above the midpoint of the superconducting phase transition for each magnetic field. Examples of the linear fitting of the normal-state resistivity are represented in Fig. 3.1(a) for different magnetic fields.

---

[1] According to the chapter 2, $\Delta\sigma$ is 100 times smaller compared with the normal-state (or background) in-plane conductivity σ^B. This fact allows us determine with accuracy the temperature dependence of the upper critical field from the 10 % criterion of the superconducting transition (see below for details).

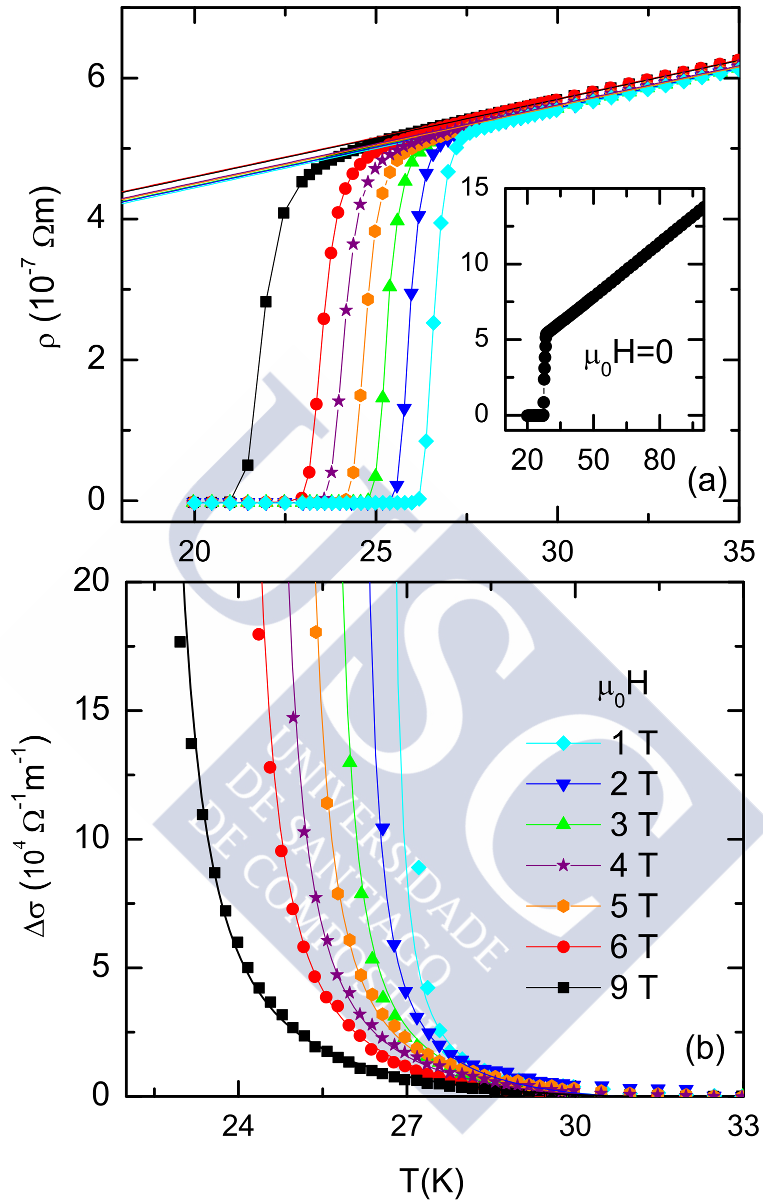

Figure 3.1: (a) Resistivity vs Temperasture curves at different magnetic fields. The linear backgrounds are indicated with the same color that the corresponding curve. *Inset* (a): Overview at null field. The absence of kink up to 100 K indicates that the composition of the sample is inside of the optimal substituting scale. (b) Experimental superconducting magnetoconductivity fluctuation at different fields (see main text for details). The solid lines show the corresponding fitting of the 3D-aGL theory.

The resulting superconducting fluctuation magnetoconductivity is presented in Fig. 3.1(b), for several fields up to 9 T. In this figure some qualitative aspects may be directly observed: i) The $\Delta\sigma$ behavior is negligible at a temperature $T_{onset} \sim 32$ K. This fact will be important in order to fix one of the parameters involved in equations that we will use in the theoretical analysis (see below). ii) As it may be observed the amplitude of $\Delta\sigma$ is clearly reduced with the applied magnetic field. This indicates that the fields used in the experiments are larger than the so-called *ghost critical field* (the symmetric above T_c of the corresponding $H_{c2}(T)$ line, [139] which implies that quantitative analysis of the data would require using theoretical approaches valid in the Prange fluctuations regime.[55]

Data analysis

As it was commented previously, iron-pnictides materials exhibit a multiband nature [116]. In spite of this behavior, previous measurements of $\Delta\sigma(T)_H$, as well as the thermal superconducting fluctuation on the magnetization above T_c, in materials like MgB_2 [81] and $NbSe_2$ [82] or in compounds of the family 122 like $Ba(Fe_{1-x}Ni_x)_2As_2$ [47, 145], or $Ba_{1-x}K_xFe_2As_2$ [39], were successfully explained in terms of the GL approach for single-band three-dimensional anisotropic superconductor (3D-aGL approach).

So, let us compare the experimental data presented in Fig. 3.1(b) with the 3DaGL-theory approach for $\Delta\sigma(T)_H$ developed in Ref. [10] (see chapter 0). This theory was developed by using a model proposed by Schmid, which is based in a combination of the standard GL-expression for the thermally average current density of the superconductor state, with the generalized Langevin equation of the order parameter.[53] The resulting expression for $\Delta\sigma$ when the magnetic field is parallel to the c-axis is given by (see chapter 0):

$$\Delta\sigma = \frac{e^2}{32\hbar\pi\xi_c(0)}\sqrt{\frac{2}{h}}\int_0^{\sqrt{\frac{c-\varepsilon}{2h}}} \mathrm{d}x \left[\psi^1\left(\frac{\varepsilon+h}{2h}+x^2\right)\right.$$
$$\left.-\psi^1\left(\frac{c+h}{2h}+x^2\right)\right] . \qquad (3.3)$$

where $h = H/H_{c2}(0^\circ)$ is the reduced magnetic field [2], and c is a cutoff constant, which is associated with the reduced temperature where the thermal fluctuations above T_c may be negligible: $c \equiv \ln(T_{onset}/T_c)$ (note that equation 3.3 leads to the $\Delta\sigma$ vanishing at $\varepsilon = c$).

In an attempt to check the applicability range of the 3D-aGL approach under an energy cutoff, the experimental data presented in Fig. 3.1(b) will be compared with Eq. 3.3. This equation is fitted to the complete set of data for $\mu_0 H \geq 3$ T, in order to avoid the strong increase of the fluctuation effects with respect to the conventional GL approach due to the possible presence of phase fluctuations and/or T_c inhomogeneities, which have been reported at lower field amplitudes. Indeed, only three free parameters are used for the fit: the out of plane GL coherence length, $\xi_c(0)$, the upper critical field perpendicular to the ab-layers, $\mu_0 H_{c2}(0^\circ) = \sqrt{\frac{\phi_0}{2\pi\xi_{ab}^2}}$, and the critical temperature T_c.

As expected, the adequacy of Eq. 3.3 extends to the temperature range represented in Fig. 3.1(b). Here the solid lines were evaluated with the resulting values of the parameters indicated above, and presented in Table 3.1. These ones are in a good agreement with those one found in the literature and with the values determined in chapter 2. However, as it has been indicated in other studies, within this figure is observed a difference between the 3D-aGL approach and the experimental data with magnetic fields below $\mu_0 H \sim 1$T. This behavior may confirm the presence of the above mentioned effects or a multiband nature.

---

[2] In this chapter $H_{c2}(0^\circ)$ is the upper magnetic field determined when $\mu_0 H$ is applied parallel to the c-axis.

Observable	T_c (K)	$\mu_0 dH_{c2}(90°)/dT$ (T/K)	$\mu_0 dH_{c2}(0°)/dT$ (T/K)	$\mu_0 H_{c2}(90°)$ (T)	$\mu_0 H_{c2}(0°)$ (T)	$\xi_{ab}(0)$ (nm)	$\xi_c(0)$ (nm)
$\Delta\sigma$	**27.2(1)**	-3.76(18)	$-1.66(8)$	102(5)	**45(2)**	2.70(6)	**1.19(4)**
10% criterion	**27.3**	**-3.84(6)**	**-1.61(2)**	103.0(1.8)	43.5(8)	2.75(3)	1.15(3)

Table 3.1: Superconducting parameters of the crystals studied, indicating the observable used to obtain them.

2.2 Measurements with H oriented at different angles with respect to the c-axis

In this section, we present experimental results of the fluctuation-induced in-plane electric conductivity for different applied fields, $\mu_0 H$, oriented with different angles, θ, relative to the crystal c-axis. Following the same procedure explained above, in Figs. 3.2 (a-c), resistivity measurements in the ab-layers are displayed, denoting the linear fitting of the normal-state resistivity $\rho_B(T)_H$. Furthermore, in Fig. 3.2 (d-f) the resulting $\Delta\sigma$ for the different angles and magnetic fields studies are shown. It may be noted that this magnitude increases with θ, reaching the highest value when $\mu_0 H$ is perpendicular to the c-axis.

As before, we will analyze these results in the context of the 3D-aGL approach: Eq. 3.3 can be generalized for magnetic fields oriented in any direction relative to the c-axis, following the scaling transformations for anisotropic materials, by just replacing h with

$$h = \frac{H}{H_{c2}(\theta)} \tag{3.4}$$

where the angular dependence at $T = 0$ K of the upper critical field, $H_{c2}(\theta)$ is described by the anisotropic Ginzburg-Landau theory [171], leading in uni-axially anisotropic crystals to

$$H_{c2}(\theta) = \frac{H_{c2}(90°)}{\sqrt{(\gamma^2 - 1)\cos^2(\theta) + 1}} \tag{3.5}$$

here γ is the anistoropy parameter defined as $\gamma \equiv H_{c2}(90°)/H_{c2}(0°)$.

In order to be sure about a possible deviation of the theory, we also estimate the boundaries of applicability of Eq. 3.3 at different θ. The lowest temperature where this one could be considered valid is given by the upper limit of the critical region [3], that in the worst case, $\theta = 90°$, this limit is given by

$$T_G^{90°}(H) \approx T_c \left(1 - \frac{H}{H_{c2}(90°)} + \left[\frac{4\pi k_B \mu_0 H}{\Delta c \xi_c(0) \gamma \phi_0} \right]^{2/3} \right) \tag{3.6}$$

where Δc is the specific-heat jump at T_c. By using $\Delta c/T_c \sim 0.1$ J/molK [149], the critical region upper limit will be $T_G^{90°} \simeq 27$, 26 and 25.5 K, for the fields, $\mu_0 H = 3,\ 6$ and 9 T respectively.

In Figs. 3.2(d-f), the same free parameter values found in the previous section are used. As it can be observed, under the condition indicated above, the fit quality of the 3D-aGL approach theory is excellent up to the largest field used in the experiments except for angles close to 90°, where the agreement with the theory worsens as the magnetic field decreases. This fact is consistent with the upturn of the $\mu_0 H_{c2}(T)$ line observed at low-field in iron-based superconductors.To check our results, in the next section, we will focus on researching this deviation from the conventional behavior, by another experimental analysis way.

---

[3] In this region, fluctuation effects are so important that the Gaussian approximation used to derive Eq. 3.3 is no longer applicable. See chapter 0 for details.

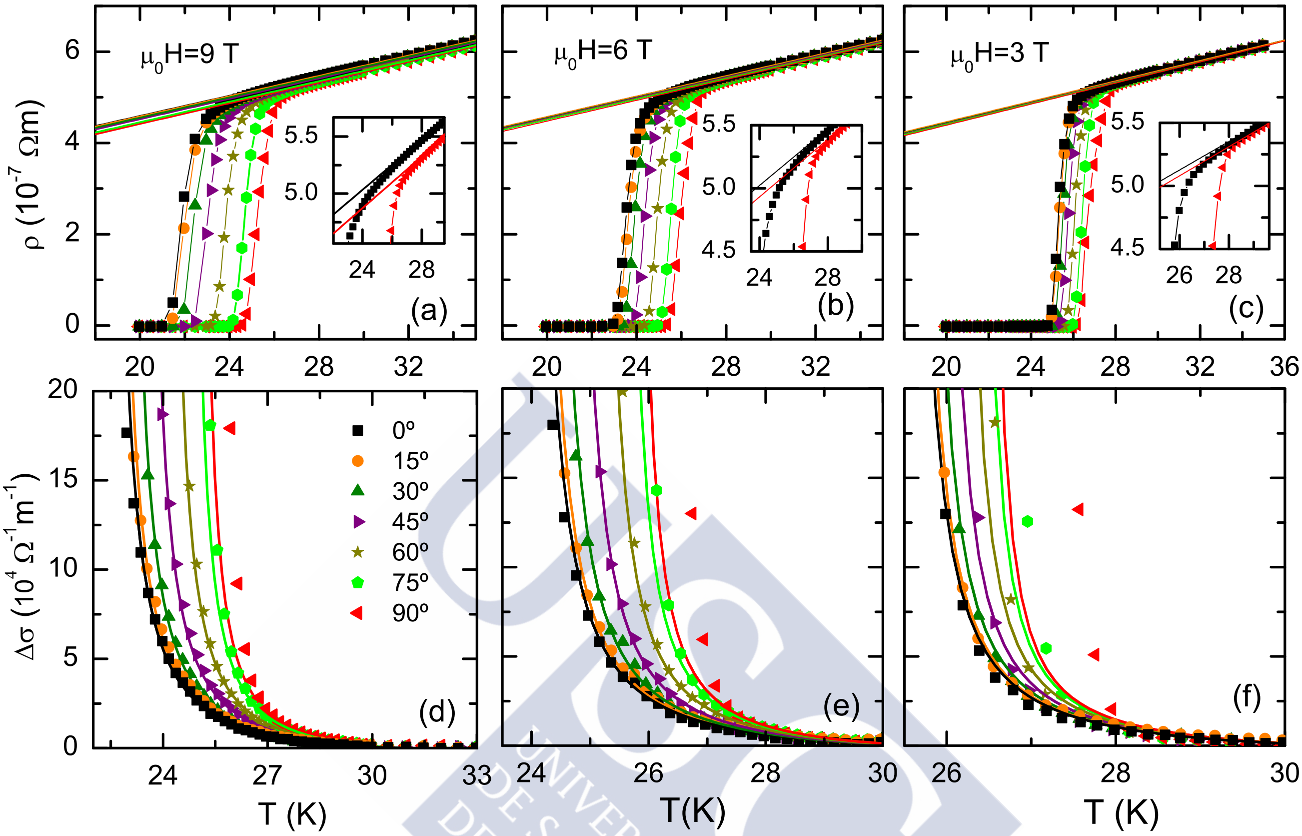

Figure 3.2: (a-c) Magnetoresistivity at different angle orientations (15° steps) with respect the c-axis. Straight lines show the linear background contributions. Insets of Fig. (a-c) represent details of the rounding with respect the linear background resistivity for 0 and 90 degrees. (c-d) Resulting magnetoconductivity fluctuations deduce from (a-c). Solid lines indicate the 3D-aGL theory fitting at different angles.

3 Direct measurement of the angular-dependent upper-critical field

For completeness, the angular-dependence of H_{c2} is measured directly from the superconducting phase transition in order to check the validity of Eq. 3.5. To this end, we represented in Figs. 3.3(a-d) several examples of $\rho(T)_H$ for different angles and magnetic fields up to 6 T. As it was explained in the previous chapter, the absence of important effect of fluctuations allows us determine with accuracy the temperature dependence of the upper critical field independently of the point chosen in the superconducting transition. However, to be consistent with the section presented above, we have chosen the superconducting transition point coinciding with the 10 % of the normal resistance ρ_B [4]. In Fig. 3.3(e), examples of the $\mu_0 H_{c2}(T)$ line are displayed for angles from 0° up to 90° with steps of 15°. As it was shown in the previous chapter: for fields below 1 T a slight deviation of the linearity appears. For this reason, the set of $\mu_0 H_{c2}(T)$ data is linearly fitted from 1.5 T up to 6 T. Then, the upper critical field extrapolated at $T = 0$ K is determined as $\mu_0 H_{c2}(\theta) = -T_c \frac{dH_{c2}(\theta)}{dT}|_{T=T_c}$. The measurements to determine $\mu_0 H_{c2}(\theta)$ at $T = 0$ K were repeated for $\mu_0 H$ =1.5 and 6 T every three degrees. The results are displayed in the inset of Fig. 3.4. To check whether this set of data accurately follows Eq. 3.5, we presented in Fig. 3.4 $(\mu_0 H_{c2}(\theta))^{-2}$ with respect to $\cos(\theta)^2$. According to Eq. 3.5 the experimental points expressed in these terms should track a linear behavior. In contrast, as seen in this last figure, a deviation from linearity is observed for angles close to 90°.

---

[4] The critical temperature determines with this criterion is in excellent agreement with that one established from the in-plane fluctuation magnetoconductivity study.

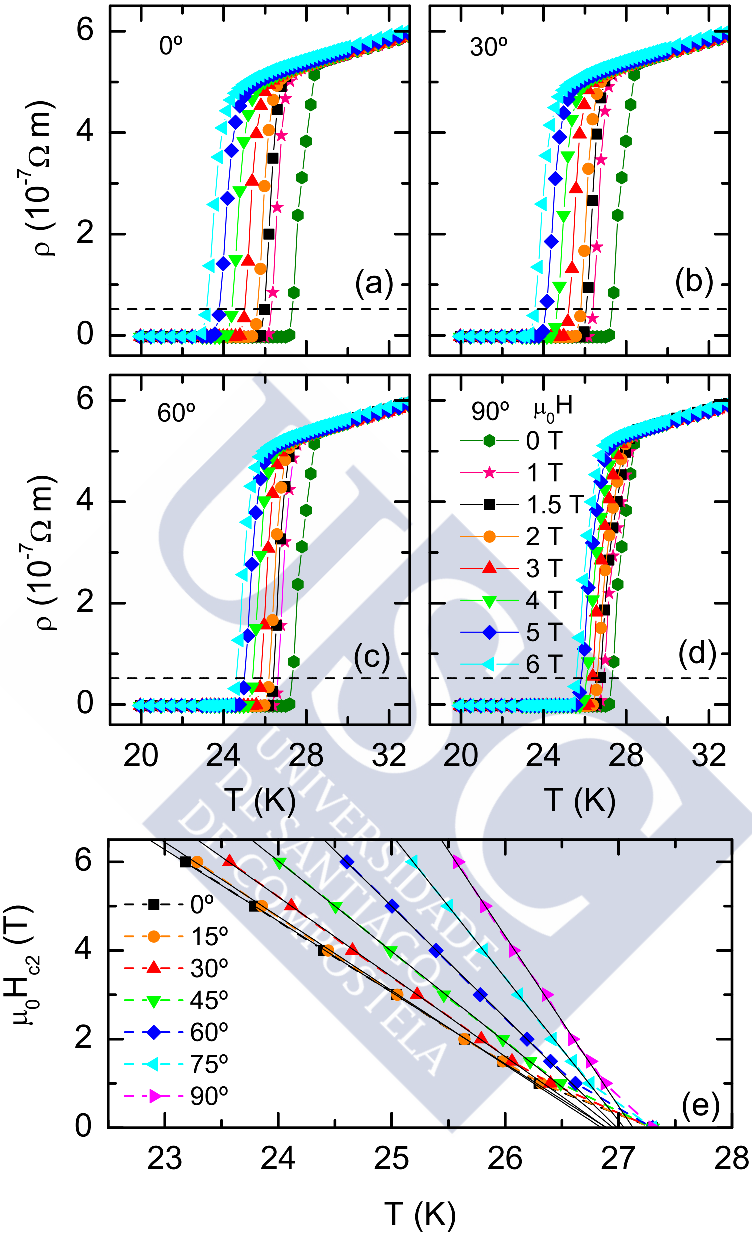

Figure 3.3: (a-d) Example of experimental resistivity measurements for different angles up to 6 T each of them. The dashed line represent the 10 % criterion. In (e) the line $\mu_0 H_{c2}$ line close to the critical temperature is represented at different angles. This one is deduced from the intersection of the resistivity curve with the line that represents the 10 % of the normal resistivity. Straight solid lines indicate the linear fit performed for $\mu_0 H_{c2}$ above 1.5 T.

4 Discussion of results and comparison with other authors

The experimental data deviation of the 3D-aGL close to 90° presented above by two different ways was observed in other materials with multiband superconducting features, as in MgB_2 [81] , $NbSe_2$ [172] and in the overdoped 122 compound $Ba(Fe_{1-x}Ni_x)_2As_2$ [170]. We note that, although the angular dependence of the upper critical field was derived for single band s-wave superconductors as a direct consequence of the linearised GL equations, in Ref. [173] is affirmed that if a factorization of the coupling potential is assumed, then a behavior as that one exposed in Eq. 3.5 will be expected independently of the Fermi surface and/or the gap symmetry. On the other hand, some authors suggest that this process is not microscopically justifiable and then, it is concluded that the coupling potential cannot be written in a separable form.[170] In addition, for iron pnictides the unusual shape of the H_{c2} was explained through important paramagnetic effects when the field is parallel to the ab-layers.[113] These facts may lead to the deviation of the behavior predicted in Eq. 3.5. Finally, note that this weird behavior has been observed from the second analysis through transport measurements, where a finite resistivity from the flux-flow regime could broaden the superconducting transition.

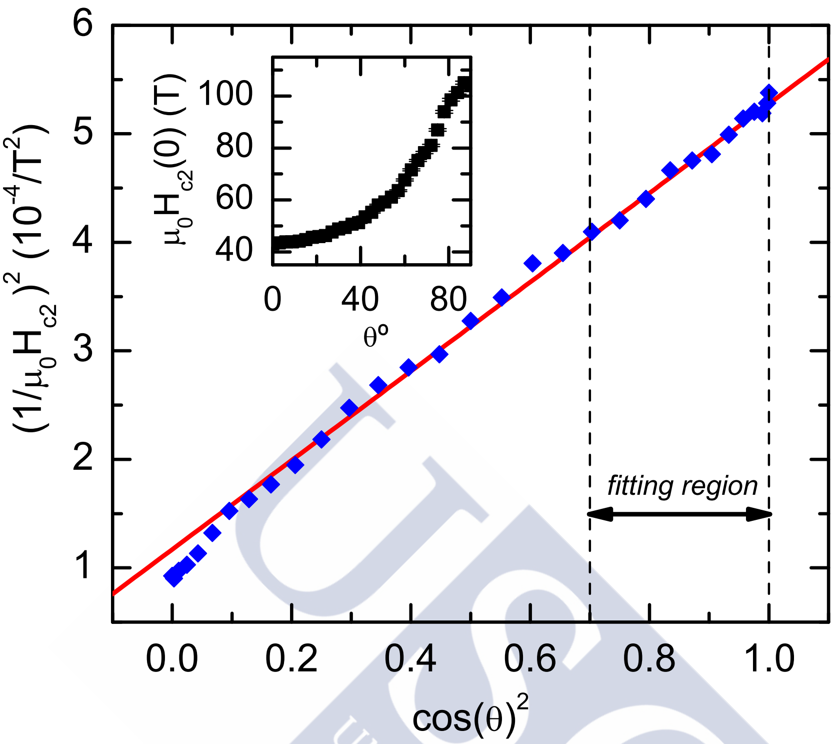

Figure 3.4: The points with diamond shape represent the experimental $(1/\mu_0 H_{c2})^2$ versus $\cos(\theta)$. Following Eq. 3.5, these ones should track a lineal behavior. A linear fit (red straight line) is performed from 0° up to 45° where is expected a good agreement with the discussed equation. The error bars are smaller than the point size. *Inset*: A overview of $\mu_0 H_{c2}$ close to T_c at different orientations is shown.

5 Conclusions

We have presented detailed measurements of the conductivity induced by superconducting fluctuations just above T_c of an optimally substituted BaFe$_2$(As$_{1-x}$P$_x$)$_2$ single crystal with H applied at different angles relative to the c-axis. These measurements were performed with different magnetic fields up to 9 T. The superconducting parameters obtained from this way are in excellent agreement with those ones found in the previous chapter from measurements of magnetic properties. On the other hand, to check our results, the $H_{c2}(T)$ line was determined from the 10 % of ρ_B criterion for different orientations with respect to the c-axis. In both cases, an anomaly in the upper critical field deduced from the anisotropic Ginzburg-Landau equations was found close to 90°. This behavior may be associated with a multiband nature and/or important intrinsic paramagnetic effects which appear in iron pnictides when the magnetic field is parallel to the Fe-As layers.


USC
UNIVERSIDADE
DE SANTIAGO
DE COMPOSTELA

Chapter 4

Importance of the "background" determination when superconducting fluctuation spectroscopy is used: Is LiFeAs a special case of iron-based superconductor?

Note: This chapter is based in a Comment published in Phys. Rev. Lett. The anomalous results found in Ref. [13] about the effective dimensionality in LiFeAs are mentioned. In this chapter, it is shown that the conclusions presented by these authors may be just a consequence of an inadequate subtraction of the normal-state behavior to determine the superconducting parameters through the study of the fluctuation spectroscopy. Such a procedure may lead to erroneous conclusions in our understanding of the nature of these materials. Data are taken directly from the graphs exposed in Ref. [13]

LiFeAs is a stoichiometric material unlike other families of iron-based superconductors. Its relatively high critical temperature, $T_c \approx$ 18 K is reached without any chemical doping [174, 175]. So, in Ref. [13] Rullier-Albenque *et al.* benefit from the reduced defect content to take accurate magnetoresistance data, $\delta\rho(H)/\rho(0)$, above the transition temperature T_c in clean LiFeAs single crystals. These samples were grown by a self-flux technique as detailed in the supplementary material of Ref. [13]. Through this study, the authors conclude that the conductivity induced by fluctuations, $\Delta\sigma$, follows a two-dimensional (2D) behavior even close to T_c, in spite that for LiFeAs the transverse coherence length $\xi_c(0) \approx 1.6$ nm is larger than the Fe-layers spacing ($s = 0.636$ nm), which would rather suggest a three-dimensional (3D) behavior [1]. This proposal would have implications in the understanding of the iron pnictides, triggering theoretical studies of superconducting fluctuations taking into account the multiband aspect and the microscopic origin of the superconductivity such as that initiated in Ref .[30]. However it also contrasts with the 3D behavior observed near T_c in the same compound [43] and in other iron pnictides with even smaller $\xi_c(0)/s$ [39]. For that, in this chapter we show that the proposal of Ref. [13] could be an artifact associated to an inadequate subtraction of the normal-state (or *background*) conductivity, σ_B.

Note first that in the clean crystals studied in Ref. [13] σ_B is orders of magnitude larger than the expected fluctuation contribution: at a reduced temperature $\varepsilon \equiv \ln(T/T_c) = 10^{-1}$ the Aslamazov-Larkin (AL) approach predicts $\Delta\sigma_{3\mathrm{D}} \sim 1.5 \times 10^4\ \Omega^{-1}\mathrm{m}^{-1}$, whereas $\sigma_B \sim 2 \times 10^7\ \Omega^{-1}\mathrm{m}^{-1}$. Thus, extracting $\Delta\rho$ in these crystals would require a highly precise procedure, in view of the fact that

$$\Delta\rho = \frac{1}{\sigma_{3\mathrm{D}}} - \frac{1}{\sigma_B}$$

---

[1] Note that we may consider a 2D behavior only if $2s > \xi_c(0)$. [8]

Above to the superconducting transition the conductivity is likely to the background conductivity, then:

$$\Delta\rho \approx \frac{1}{\sigma_B^2}\Delta\sigma \approx 10^{-10}\ \Omega\ \mathrm{m}$$

which questions the adequacy of $\Delta\sigma$ to study the superconducting fluctuations in clean LiFeAs. Secondly the procedure used in Ref. [13] to determine the background conductivity assume a strict H^2 behavior of the magnetoresistivity in the normal state [176]. For temperatures near T_c, the deviation from this behavior observed at low fields is attributed to fluctuations. However, isotherms well above T_c, where fluctuation effects are negligible, present a similar H^2 dependence. This is difficult to appreciate in Fig. 2 of Ref. [13] due to the scale, but may be clearly seen in the detailed view of the present Fig. 4.1 isotherms above 45 K present a relative rounded behavior *quite similar* to the one at 25 K, where fluctuation effects are claimed to be present. This shows that the $\delta\rho(H)/\rho(0)$ deviations from the H^2 behavior is a normal-state effect, that near T_c will be superimposed to the superconducting fluctuation effects.

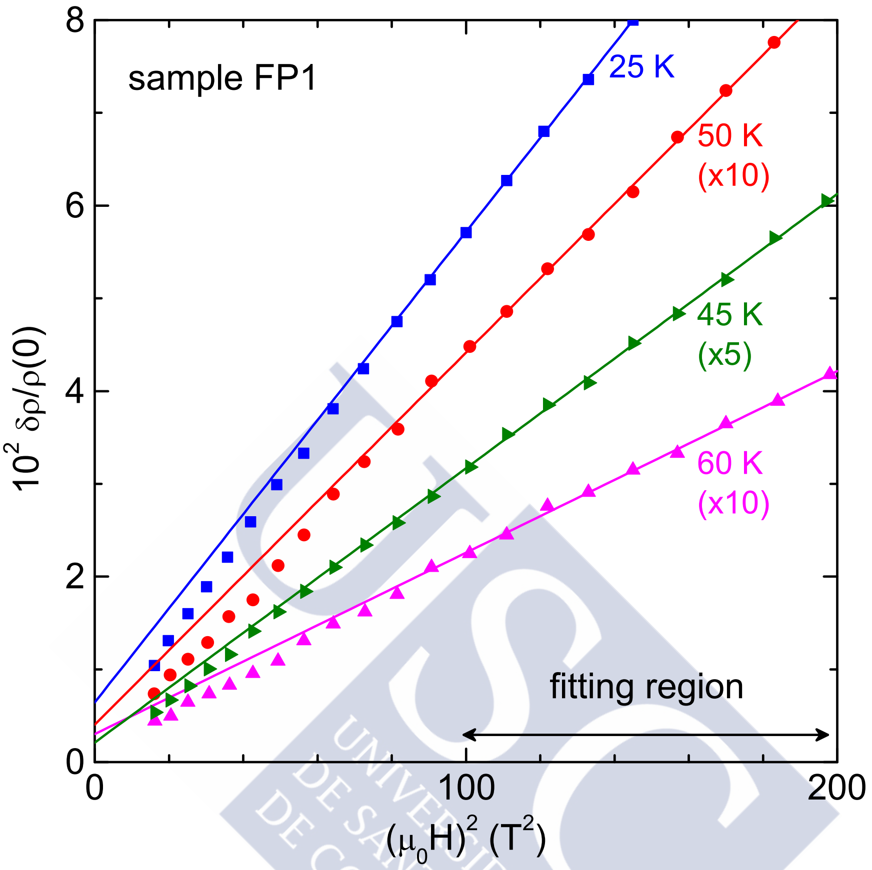

Figure 4.1: Detail of the $\mu_0 H^2$ dependence of $\delta\rho/\rho(0)$ for sample FP1 at 25, 45, 50 and 60 K (for a better comparison some isotherms are multiplied by a factor). For all isotherms the lines are fits to the data above 100 T2. These isotherms present a similar relative rounded behavior at low fields, in spite that fluctuation effects are assumed to be negligible above 45 K.

The above results suggest that the paraconductivity fluctuation data, $\Delta\sigma$ obtained in Ref. [13] which according to the authors show a 2D behavior (in the frame of Gaussian Ginzburg-Landau theory) may be strongly affected by the background contribution of the resistivity. To confirm this conclusion, note that if the shape of the different isotherms $\delta\rho/\rho(H)$ is similar (just by a multiplicative factor), the slope, "a", at any point grows in the same proportion that the extrapolation to $\mu_0 H = 0$ (See Fig. 4.2).

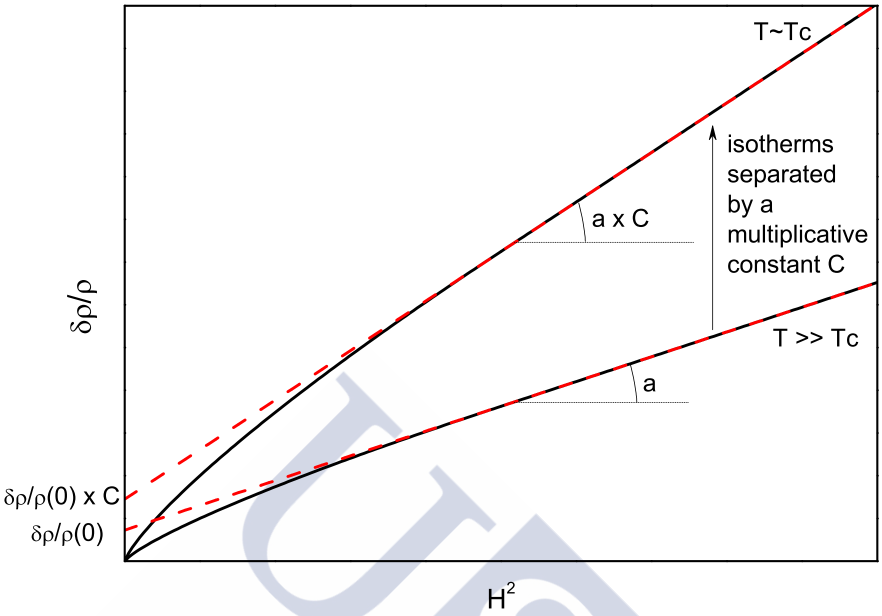

Figure 4.2: In order to clarify, here is indicated why the extrapolation at null field is proportional to the slope if the shape of the curves are proportionals.

In the mentioned article, as not too close to T_c the shape of the different isotherms is similar (the difference is roughly a multiplicative factor). Then, the quadratic extrapolation of the high-field behavior to $\mu_0 H = 0$, $\delta\rho/\rho(0)$, should be roughly proportional to "a", which is proportional to σ_B^2 obeying the Kohler's rule [177]. Taking into account these one, the paraconductivity is obtained as $\Delta\sigma = \sigma_B \delta\rho/\rho(0) \propto \sigma_B a \propto \sigma_B^3$. Therefore, this value should track the temperature dependence of σ_B^3. The scaling shown in Fig. 4.3 between σ_B^3 and $\Delta\sigma$ strongly this proporsal.

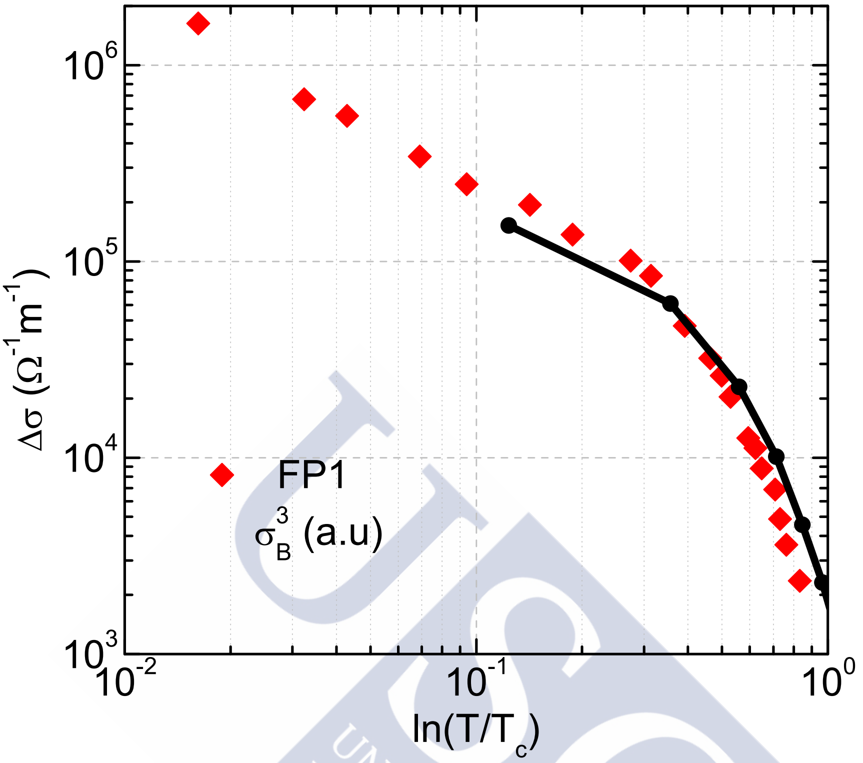

Figure 4.3: Scaling of the paraconductivity data in Ref. [13], and σ_B^3 (obtained from the data for sample FP1 in the inset in Fig. 2(a) of Ref. [13])

In conclusion, the results summarized here pose serious doubts about the 2D nature of the superconducting fluctuations in LiFeAs, and on the applicability to this material of the model proposed in Ref. [13] for $\delta\rho/\rho(0)$ in the normal state.

Conclusions

In this thesis, different unconventional effects in iron-based superconductors were studied by using the so-called *superconducting fluctuation spectroscopy*. For that, measurements of the magnetization and the magnetoconductivity were performed around T_c. A previous and complementary aim was to probe the own nature of the superconducting fluctuations in these compounds. In particular, it was probed the applicability of the so-called extended (with an energy cutoff) Gaussian-Ginzburg-Landau approach and the possible presence of superconducting phase fluctuations.

The main conclusions are summarized as follows:

In *chapter 1*, measurements of the magnetic susceptibility just above the superconducting transition on the '122' iron based superconductor $\mathrm{Ba(Fe_{1-x}Ni_x)_2As_2}$ were presented from the optimal doping to the highly overdoped region. The measurements were performed with the magnetic field applied both parallel and perpendicular to the FeAs layers. The experimental results allowed us to obtain the dependence of $\xi_{ab}(0)$ and $\xi_c(0)$ with the doping level. Well inside the overdoped region, the anisotropy factor near the critical temperature was found to be around 15 , being the highest value of anisotropy factor reported until now in these materials.

In *chapter 2*, measurements of the magnetization and magnetoconductivity around T_c on the isovalently-substituted iron pnictide $\mathrm{BaFe_2(As_{1-x}P_x)_2}$ close to the optimal substituting level were shown. The measurements were performed with the magnetic field applied perpendicular and parallel to the FeAs layers. In magnetoconductivity measurements, the absence of important fluctuation effects allowed us to determine with accuracy the temperature dependence of the upper critical fields from the H-dependence of the transition midpoint. These values are directly related with $\xi_{ab}(0)$ and $\xi_c(0)$. The diamagnetism induced by superconducting fluctuations was consistently analyzed in both the Gaussian and critical regions. This also allowed us to determine with accuracy the coherence length amplitudes. It is found that $\xi_c(0)$ determined from magnetization measurements is significantly larger than the value measured from the magnetoconductivity. According to Ref. [11], this unconventional effect may be attributed to the presence of several bands contributing to the superconductivity. Another complementary conclusion comes from the analysis of an anomalous upturn in the $M(H)$ isotherms in the low.-field region around T_c. It is found that for this compound the superconducting phase fluctuations play a negligible role, contrary to what is proposed for other Fe-based superconductors.

In *chapter 3*, detailed measurements of the magnetoconductivity induced by superconducting fluctuations just above T_c were presented for an optimally substituted $\mathrm{BaFe_2(As_{1-x}P_x)_2}$ single crystal. These measurements were performed with magnetic fields oriented at different angles, θ, with respect to the c-axis. First, the analysis of superconducting fluctuations above T_c was used to determine the upper critical fields at different orientations, $H_{c2}(\theta)$. After that, these results were checked from the direct determination of this parameter from the H-dependence of the resistive transition. In both cases, a significant difference from the $H_{c2}(\theta)$ behavior deduced from Ginzburg-Landau theory was found when θ is close to 90°. This effect may be attributed to the multiband nature of these compounds, or to the possible presence of intrinsic paramagnetic effects which appear in iron pnictides when the magnetic field is parallel to the FeAs layers.

Finally, in *chapter 4*, just as an example of how sensitive is the fluctuation spectroscopy to inadequate analysis procedures, it is shown that the anomalous 2D behavior of the superconducting fluctuations in LiFeAs observed in Ref. [13] may be attributed to an inadequate subtraction of the normal-state contribution.


USC
UNIVERSIDADE DE SANTIAGO DE COMPOSTELA

Appendix A: Magnetic property measurement system

SQUID-magnetometer

In this thesis, all measurements concerning to the magnetization properties were made using a Quantum Design's Magnetic Property Measurement System (MPMS-XL) (see Fig. A.1), which is a highly integrated instrument system to study the material's characterization tasks that require the highest detection sensitivities over a broad temperature range and in applied magnetic fields of several teslas. It is configured to detect the *magnetic moment* of a sample from which the magnetization and magnetic susceptibility can be determined.

This measurement system is based in an extremely important part of small-scale superconducting technology: the Josephson junction, a device based on a tunneling effect, theoretically proposed by B.D.Josephson [178, 179] and observed experimentally by Anderson and Rowell [180].

A more common use of the Josephson junction is in a device called SQUID (Superconducting Quantum Interference Device). A SQUID device consists of a closed superconducting loop including one or two Josephson junction in the loop's current path. Due to the quantized state of the superconducting ring, the SQUID is capable of resolving changes in the external magnetic fields that approach to 10^{-15} T.

In the MPMS-XL system there is a rf SQUID device [181] which is extraordinary sensitive to the magnetic moment of materials.

The principal components of this measurement system comprise the following [182]: *i) Temperature control system*: Precision control of the temperature in the range of 1.9 K up to 400 K. *ii) Magneto control system*: Current from a power supply is set to provide magnetic fields from zero up to 7 T. *iii) Superconducting SQUID amplifier system*: The rf SQUID detector is the heart of the magnetic moment detection system. *iv) Computer operating system*: All operating features of the MPMS are under automated computer control.

Main parts of the system:

The SQUID.

A SQUID is the most sensitive device available for measuring magnetic fields, although in the MPMS-XL system, this one does not detect directly the magnetic field from the sample. Instead, the measurement is performed by moving the sample through a system of superconducting detection coils, which are located at the center of the magnet *see fig.A.2.* As the sample moves through the coils, the magnetic moment of the sample induces an electrical current in the detection coils. Because the detection coils form with the SQUID input coil a closed superconducting loop through the connecting wires, any change of magnetic flux in the detection coil produces a change in the persistent current in the detection circuit, which is proportional to the change in magnetic flux. Thus, the SQUID functions as a highly linear current-to-voltage converter, the variations in the current detection coils produce corresponding variations in the SQUID output voltage which is proportional to the magnetic moment of the sample. Indeed, measurements of the voltage variations from the SQUID detector as a sample is moved through the detection coils provide a highly accurate measurement of the sample's magnetic moment even up to 10^{-8} emu.

On the other hand, because of the SQUID is extremely sensitive to fluctuations in magnetic fields, the sensor itself must be shielded.

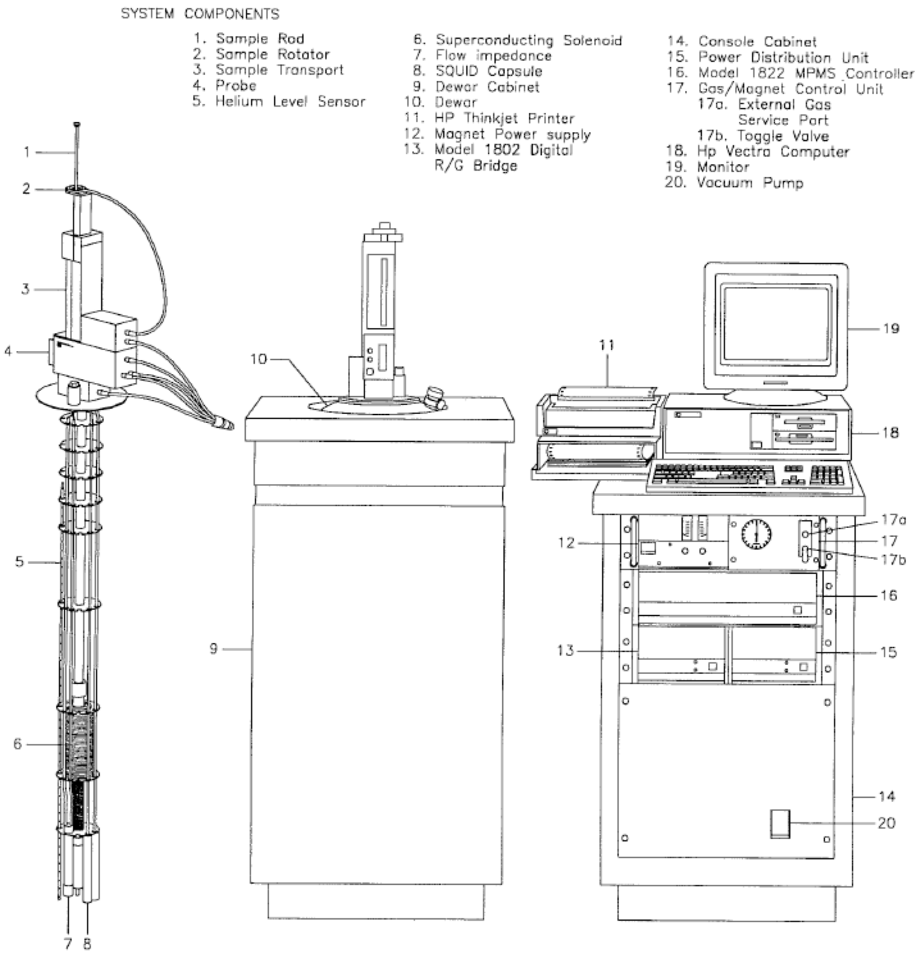

Figure A.1: MPMS system components.

The required magnetic shielding is provided by the superconducting shield which sets a volume of relatively low magnetic field where the SQUID and its coupling transformers are located.

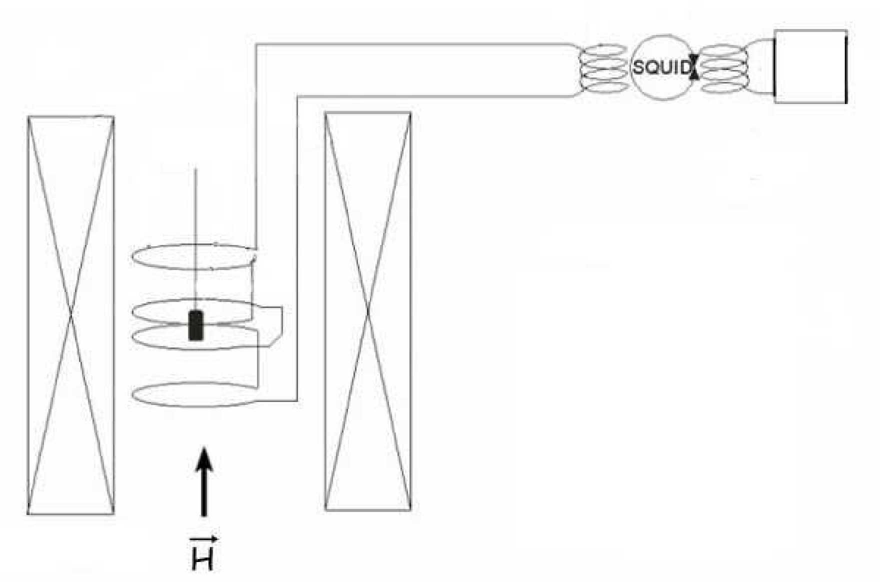

Figure A.2: The measurement is performed moving the sample through the magnets. This movement induce an electrical current in the detection coils. The variations of the current in the detection coils produce corresponding variation in the SQUID output voltage which are proportional to the magnetic moment of the sample.

The superconducting detection coils.

A SQUID inside a cryostat that is free of spurious magnetic effect can be effectively used to detect changes in the ambient magnetic field arising from a variety of sources. However, SQUID magnetometers used in this manner suffer in utility because of their extreme sensitivity to rotation. For that is used a piece of superconducting wire wound in a set of three coils configured as a gradiometer (the detection coil). This configuration is in addition to reduce noise in the detection circuit caused by fluctuations in the large magnetic field of the superconducting magnet. However, over long periods of time and many measurements, large persistent currents can build up in the detection coils, producing noise in the system when these large currents flow in the SQUID input coil. The MPMS system prevents it by heating a small section of the detection coil circuit whenever the magnetic field is being changed.

The superconducting magnet.

The MPMS employs a superconducting magnet wound in a solenoidal configuration. The magnet is constructed a completely closed superconducting loop, allowing it to be changed up to a specific current, then operated during a measurement in persistent mode without benefit of an external current source or power supply. Beside additional time may still be required before the field in the magnet becomes fully stable.

Sample space and Temperature control.

To modify the temperature of the sample and maintain the superconducting components at low temperature the MPMS system has a vacuum-insulated chamber called EverCool Dewar into which cold helium can be contained. This system reaches temperatures as low as 1.9 K with pumped helium. Furthermore MPMS system has an integrated cryocooler-dewar system that recondenses the helium directly within the EverCool Dewar. Otherwise this system contains another chamber where the sample is placed. This space is a tube of around 9 mm of diameter which is maintained at a low pressure with static helium gas. At the top of the sample space there is an airlock that can be evacuated and purged with clean helium gas (boil-off from the liquid helium bath in the dewar). Finally, two thermometers determine the sample temperature and heaters on the sample chamber can raise the temperature as high as 400 K.


USC
UNIVERSIDADE
DE SANTIAGO
DE COMPOSTELA

Appendix B: Transport property measurements

AC Transport measurement system.

The transport property measurements of this thesis were performed in a Physical Property Measurement System (PPMS) through a Quantum Design AC transport measurement system (ACT) option (see Fig.B.1). This one incorporates a precision voltmeter and a precision current source which has a resolution of 0.02μA and a maximum current of 2A [2].

---

[2] Components corresponding with the source of magnetic field, cryogenics and temperature control are essentially similar to the previous system (*appendix A*), for more information see Ref. [183]

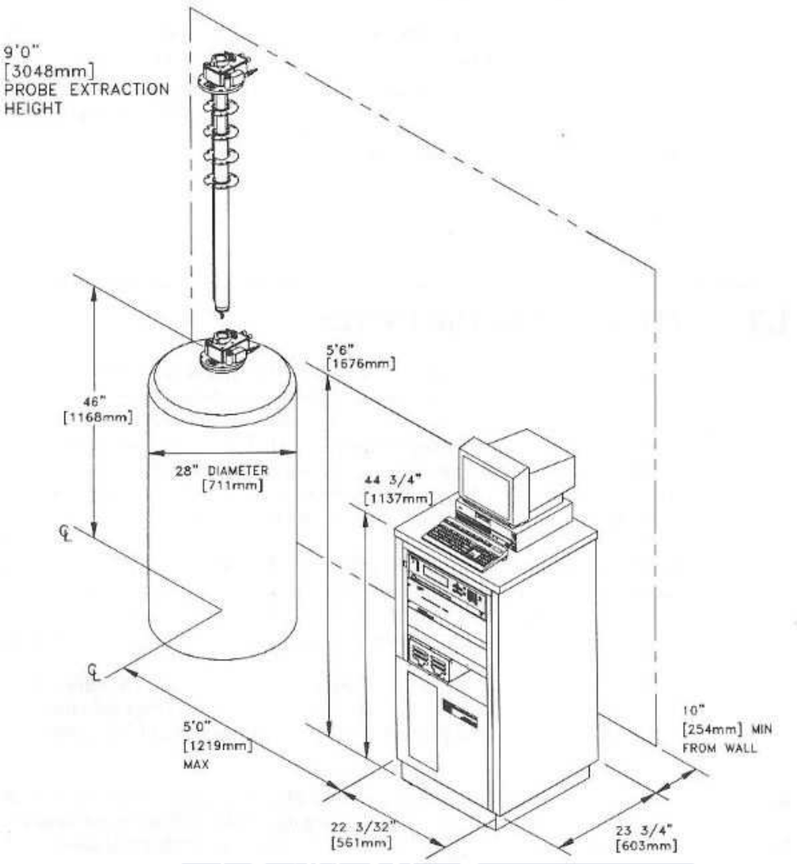

Figure B.1: PPMS system components.

Measurements were performed passing a known current through the sample and measuring the voltage drop across the sample in one direction. In this work, the ACT option was used with samples mounted on a sample rotator. This device can supply an AC bias current from 1Hz up to 1kHz and can therefore provide greater measurement sensitivity than DC instruments, because signal filtering can be employed.

Electrical resistance measurements

The ACT option supports four terminals: two leads pass a current through the sample and the others are used to measure the potential drop across the sample. Finally Ohm's law is used to calculate the sample resistance. The voltage leads do not transport electrical current, so the current through the sample and the potential drop across the sample can be known to a high degree of accuracy. This configuration virtually eliminates the effects of leads and contact resistance. In Fig.B.1 is shown that the current and voltage leads do not contact the sample at the same point: If the current and voltage leads contact the sample at the same point, the contact resistance affects the measurements. Thus it is important to perform the measurements in this way to take advantage of the instrument's sensitivity.

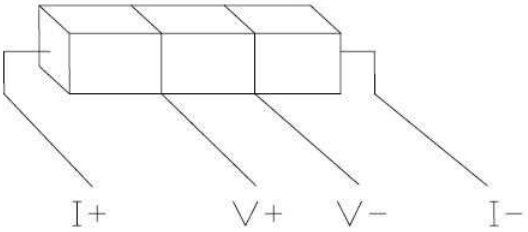

Figure B.2: Leads for Four-Wire AC resistance measurement.

During the measurements, the detected second and third harmonics are reported in dB. This information can be related to the amount of noise encountered during the measurement. The amplitude of these harmonics are usually less than -50 dB for a clean measurement and is larger when looking at very small signals or when operating at frequencies commensurate with the power line. For that it is recommended that these noisier frequencies be avoided during sensitive AC measurements.


USC
UNIVERSIDADE
DE SANTIAGO
DE COMPOSTELA

Resumen en castellano

Siguiendo el reglamento de los estudios de Tercer Ciclo de la Universidade de Santiago de Compostela, aprobado en la Junta de Gobierno el día 7 de abril de 2000 (DOG de 6 de marzo de 2001) y modificado por la Junta de Gobierno del 14 de noviembre de 2000, el Consejo de Gobierno del 22 de noviembre de 2003, del 18 de julio de 2005 (artículos 30 a 45), del 11 de noviembre de 2008 y del 14 de mayo de 2009; y, concretamente, cumpliendo las especificaciones indicadas en el capítulo 4, artículo 30, apartado 3 de dicho reglamento, mostramos a continuación un resumen en castellano de la tesis.

Breve revisión de los superconductores basados en hierro

El descubrimiento en 2006 de los superconductores basados en hierro condujo a una nueva era de la investigación en superconductividad. Estos materiales presentan un gran atractivo, debido a la coexistencia del estado superconductor junto con otras fases magnéticas, aunque su mayor interés quizás se deba a la naturaleza multibanda de su estructura electrónica. La comparación de los cupratos con estos compuestos clasificados dentro de los superconductores de alta temperatura crítica, (SAT) puede darnos la clave para entender el mecanismo de la superconductividad a altas temperaturas, y así encontrar el modo de incrementar la temperatura de transición.

A pesar de la gran variedad de compuestos, todos ellos *tienen una estructura electrónica similar, con un nivel de Fermi donde los electrones provienen principalmente de los orbitales 3d de los átomos de hierro. A pesar de su naturaleza laminar, los superconductores basados en hierro presentan una baja anisotropía cerca de la temperatura de transición, en contraste con los cupratos. Además, estos materiales tienen longitudes de coherencia pequeñas y temperaturas críticas altas comparadas con los superconductores. Estas características hacen que la dependencia con la temperatura de algunos observables presenten un importante redonde cerca de la temperatura de transición, debido al efecto de las fluctuaciones superconductoras. La topología de la superficie de Fermi está compuesta por cuatro hojas a lo largo de la dirección* k_z. *Dos de estas hojas tienen huecos como portadores y las otras dos tienen electrones. En el centro se sitúa una quinta hoja de huecos con forma de esfera ligeramente distorsionada (ver Fig. 2). En general las hojas de electrones están "anidadas" con la hoja central de huecos, lo cual promueve un ordenamiento magnético. Un incremento de la cantidad de dopantes en el sistema, irá reduciendo este "anidamiento" suprimiendo gradualmente el orden magnético, y eventualmente emergerá el estado superconductor. De esta manera, la temperatura de transición a la fase superconductora será maximizada a un cierto nivel de dopaje y decrecerá si éste sigue aumentando.*

Existen cuatro familias prototipo en los superconductores basados en hierro, las cuales son usualmente denotadas por la fracción estequiométrica de sus constituyentes químicos. Este trabajo de tesis se centra principalmente en la familia de tipo '122'. Esta familia consiste en una variedad de diferentes compuestos con un amplio rango de dopaje tanto de huecos como de electrones, donde diferentes ordenamientos magnéticos compiten o coexisten con el estado superconductor. Los compuestos base de la familia '122' son AFe_2As_2 *(A= Ca, Sr, Ba), que aunque en ellos no emerge la superconductividad tienen comportamientos de tipo metálico cuando se mide el comportamiento de la resistividad con la temperatura.[25, 26] Sin embargo, la resistencia eléctrica a temperatura ambiente es dos órdenes de magnitud mayor que en metales puros, por esta razón estos elementos son denominados "malos conductores". Dichas propiedades metálicas contrastan con los cupratos, para los cuales los compuestos* *base son aislantes tipo Mott.[27] Los materiales más estudiados de este grupo provienen del compuesto base* $BaFe_2As_2$*, el cual es un metal compensado (o lo que es lo mismo, el volumen de las hojas de electrones es el mismo que el de las hojas de huecos).[28] Existen diferentes modos de dopar los compuestos base y conseguir que la fase superconductora emerja en este tipo de materiales como se muestra en la Tabla 1.*

Podemos resaltar las similitudes y diferencias que existen entre los superconductores basados en hierro y los conocidos cupratos. En primer lugar, ambos compuestos comparten una estructura cristalina laminar, lo cual juega un importante papel en la mayoría de las propiedades físicas. Los dos poseen un orden antiferromagnético, así como una estructura ortorrómbica en el estado normal. En los dos, la superconductividad emerge bajo un cierto nivel de dopaje electrónico. Por otro lado existen diferencias fundamentales, como el hecho de que los compuestos base de los cupratos son aislantes Mott, mientras que en los superconductores basados en hierro se presentan características metálicas en medidas de resistencia eléctrica. Además se puede conseguir el estado superconductor si una presión es aplicada en estos nuevos materiales, a diferencia de los cupratos, en lso que sólo aumenta la temperatura crítica superconductora si este estado fue alcanzado previamente.

En esta tesis trataremos de caracterizar algunos de estos novedosos materiales a través del estudio de fluctuaciones superconductoras, las cuales han sido usadas en un número considerable de trabajos para caracterizar propiedades a través de observables como la conductividad eléctrica, la magnetización o el calor específico. [3, 10, 13, 29–47]

Capítulo 1: Incremento del factor de anisotropía en la región sobredopada de $\mathrm{Ba(Fe_{1-x}Ni_x)_2As_2}$ medido a través de espectroscopía de fluctuaciones

Las propiedades de los superconductores basados en hierro en sistemas óptimamente dopados son actualmente bien conocidas. Sin embargo, el comportamiento del material en niveles de dopaje fuera del óptimo es menos investigado, y algunos aspectos relacionados con su caracteriazación permanecen aún en un debate abierto. Un ejemplo es el incremento del factor de anisotropía, γ*, en* $\mathrm{Ba(Fe_{1-x}Ni_x)_2As_2}$ *determinado a través del estudio de las fluctuaciones superconductoras en la magnetoconductividad, cuando la corriente es aplicada paralela a los planos de hierro y arsénico. En este compuesto, este valor incrementa desde* $\gamma = 2$ *en el nivel de dopado óptimo (*$x = 0.05$*) hasta alrededor de* $\gamma = 15$ *para* $x = 0.10$*.[10] Este factor de anisotropía es el mayor reportado hasta el momento en pinicturos de la familia 122 y es incluso mayor que el observado para algunos cupratos. Sin embargo, las medidas de resistividad presentadas para determinar* γ *podrían estar afectadas por incertidumbres en la geometría del cristal y los contactos eléctricos, por tanto es necesario una verificación de tales resultados experimentales a través de otro observable como la susceptibilidad magnética. Para dicho cometido, usaremos un conjunto de monocristales con los planos ab paralelos a las caras con mayores dimensiones (ver Tabla 1.1), los cuales fueron crecidos a través del método " self-flux " en el Instituto de física y laboratorio nacional para la materia condensada, en China (ver la Ref. [76] donde todos los detalles sobre el crecimiento de los cristales pueden ser encontrados). Sus niveles nominales de dopaje fueron x = 0.05, 0.075, 0.09, 0.10. Consistentemente nosotros comprobamos su excelente esteiquiometría y calidad estructural a través del estudio de difracción de rayos X, estimándose una dispersión del nivel de dopaje de* $\Delta x = 0.01$ *.*

Las medidas de magnetización se realizaron con un magnetómetro SQUID comercial de Quantum Design, modelo MPMS-XL, el cual puede llegar a proporcionar campos magnéticos de hasta 7 T. Para *realizar las medidas con el campo paralelo a los planos cristalográficos ab, uno de los cristales fue pegado con un barniz "General Electric" a una varilla de cuarzo y se comprobó a través del microscopio un desalineamiento máximo de 0.1°. Para medir con el campo magnético perpendicular a la muestra se realizó una pequeña hendidura en la varilla de cuarzo. En este caso el alineamiento tuvo un error de 5°. Esto permitió determinar el factor de anisotropía con una incertidumbre de* 0.5%. *En Fig. 1.2 se presenta la dependencia con la temperature de la susceptibilidad magnética a muy bajo campo . Esta medida es realizada pasando previamente la muestra al estado superconductor y luego midiendo con un campo perpendicular a los planos ab de 0.5 mT. Los efectos demangetizantes son corregidos para obtener un valor ideal en la susceptibilidad magnética de -1 a bajas temperaturas. Desde estas curvas, la temperatura crítica T_c es determinada por la extrapolación lineal a $\chi = 0$ de los datos con mayor pendiente. El ancho de la transición estará por debajo de 1 K en la mayoría de los cristales, lo cual permitirá estudiar el efecto de las fluctuaciones en una amplia región de temperaturas.*

Para medir las fluctuaciones superconductoras en la magnetización por encima de la temperatura crítica, se han usado campos magnéticos por encima de 3T, lo cual nos permitió analizar los datos con la teoría convencional de Ginzburg Landau (a bajos campos fue reportado que el efecto de las fluctuaciones en estos materiales está fuertemente afectada por posibles efectos de fluctuaciones de fase [42] o incluso inhomogeneidades [10]). Algunos ejemplos de estas medidas son presentados en la Fig. 1.3, donde el redondeo debido a fluctuaciones ya puede ser apreciado. Para cada campo aplicado la dependencia de las fluctuaciones con la temperatura fue obtenida según la ecuación 1.1. En ella $m_B(T)$ es la contribución "background" debido al estado normal de la muestra y a la pequeña contribución magnética que pudiera tener la varilla de cuarzo. Dicha contribución será ajustada a una función como la presentada en la Eq.1.2 (donde se aprecia un término de tipo Curie) en un intervalo de temperatura que irá desde $\sim 1.3T_c$ *hasta* $\sim 1.8T_c$. *El límite inferior del ajuste corresponde con la temperatura a partir de la cual el efecto de las fluctuaciones es despreciable, como ya se vio en otros artículos (véase Ref. [10, 47]). El resultado del ajuste de "background" es presentado por líneas sólidas* en la Fig. 1.3.

Las fluctuaciones en susceptibilidad magnética son presentadas en la Fig. 1.4 para todos los dopajes estudiados y para ambas orientaciones del campo magnético aplicado. A pesar de la naturaleza multibanda del compuesto, previas medidas en conductividad eléctrica fueron analizadas a través de la teoría convencional de Ginzburg-Landau con cutoff en energía (3D-aGL). En este capítulo usaremos por tanto las mismas teorías para analizar nuestros datos experimentales.

En términos de la 3D-aGL las fluctuaciones en magnetización de un superconductor anisotrópico pueden estar relacionadas con las de uno isotrópico a través de la Eq. 1.3 (sacada de la referencias [69–71]) , para campos aplicados perpendiculares a los planos principales y Eq. 1.4, para campos magnéticos paralelos a los planos. Así pues, combinando esto con las expresiones dadas para campos isotrópicos en la referencia [48] con las ecuaciones 1.3 y 1.4, obtendremos las ecuaciones 1.7 y 1.8 que usaremos para analizar nuestros datos experimentales. En estas ecuaciones Γ y Ψ son respectivamente las funciones gamma y digamma. Por otra para ξ_{ab} es la longitud de coherencia en los planos y c es una constante llamada “cutoff”, la cual indica. la temperatura reducida, $\varepsilon = \ln(T/T_c)$, a la cual las fluctuaciones son despreciables.

Con el objetivo de comparar la teoría expuesta arriba con los datos experimentales, nosotros ajustamos la ecuación 1.7 (normalizada por el campo aplicado) a los datos experimentales de la Fig. 1.4. Para cada muestra con distinto nivel de dopaje, los únicos parámetros ajustables son $\xi_{ab}(0)$ y γ.

Como puede comprobarse, el acuerdo de la teoría con los datos experimentales es excelente. Por otro lado, fue propuesto que efectos multibanda podrían ser observados cuando hay una gran diferencia entre las longitudes de coherencia de las diferentes bandas.[11] Si ese fuera el caso, una desviación desde la aproximación monobanda debería de aparecer a un campo cercano al asociado a la longitud de coherencia alta. Nuestros resultados podrían sugerir que en este material, las longitudes de coherencia entre las diferentes bandas no son muy diferentes, o que el campo crítico superior asociado a la banda de mayor longitud de coherencia no es cercano a los campos magnéticos, que han sido explorados en nuestro experimento.

En la Fig. 1.6 los valores de $\xi_{ab}(0)$ y γ resultantes del análisis *anterior como función del nivel de dopaje son representados. Esta figura también incluye la longitud de coherencia transversal,* $\xi_c(0)$. *Como puede verse* γ *presenta un incremento con el nivel de dopaje desde* ~ 3 *hasta* ~ 16.

En otros compuestos de la familia 122, en particular en compuestos dopados con electrones $Ba(Fe_{1-x}Co_x)_2As_2$ *y dopados con huecos* $Ba_{1-x}K_xFe_2As_2$ *hay algunos estudios que incluyen rangos de dopado fuera del óptimo. [3, 26, 88, 90–104] En Tabla 1.2 se presenta un resumen de los valores de* γ *reportados en otras familias de superconductores basados en hierro, como puede verse el mayor valor de anisotropía reportado hasta la fecha es presentado en este trabajo. Sería por tanto deseable comprobar si tal incremento del factor de anisotropía en la región sobredopada está también presente en otros superconductores basados en hierro.*

Capítulo 2: Fluctuaciones superconductoras en el compuesto isovalentemente sustituido $\mathrm{BaFe_2(As_{1-x}P_x)_2}$: Posible observación de efectos multibanda

Es bien conocido que los superconductores isovalentemente sustituidos [117–119] presentan notables diferencias con aquellos que se dopan con carga eléctrica [2, 19, 25, 120–122]. Mientras que los compuestos isovalentemente sustituidos son cercanos al límite "limpio",[123] los superconductores dopados eléctricamente crean fuertes potenciales de dispersión que afectan a las propiedades superconductoras, tal y como la fijación de los vórtices,[124] el campo crítico superior,[5, 125, 126], o incluso las simetrías del gap superconductor.[124, 127–129] A pesar del interés de los compuestos isovalentemente sustituidos, los efectos de fluctuaciones estÃ¡n aún sin explorados. En este capítulo se comprobarán experimentalmente algunas propuestas teóricas que predicen una diferencia en la amplitud de las fluctuaciones cuando se miden con diferentes observables.[11] Los resultados presentados aquí, también probarán la aplicabilidad de las aproximaciones de Ginzburg-Landau en estos materiales, *como medio para investigar los posibles efectos relacionados con la naturaleza multibanda de estos compuestos. Finalmente, el comportamiento a muy bajos campos magnéticos cerca de la transición superconductora será estudiado con el fin de comprobar la relevancia de las fluctuaciones de fase, las cuales han sido marcadas como de gran importancia en otros superconductores basados en hierro.[42, 140]*

Los cristales usados aquí, fueron crecidos a través del método "self-flux", provistos por el grupo del profesor Huiqian Luo. Algunos detalles sobre su caracterización pueden ser encontrados en la Ref. [142]. La superficie de los cristales es de varios mm^2 *y sus espesores* $\sim 10^2\ \mu m$. *Su estequiometría fue comprobada con un microscopio electrónico de barrido equipado con un espectroscopio EDX. En la Fig. 2.1(a) se muestra un espectro EDX típico de estas muestras. La estequiometría media resultó ser* $Ba_{1.04}Fe_{1.91}As_{1.33}P_{0.72}$ *con una variación más pequeña del 0.4% entre los diferentes cristales y áreas estudiadas. La sustitución parcial de As por P fue del* 35 %, *lo cual es cercano al nivel óptimo de dopaje (donde se alcanza la máxima temperatura de transición de fase).*

La estructura cristalina fue estudiada a través de un difractómetro de rayos X cuyo patrón se muestra en la Fig. 2.1(b). La ausencia de reflexiones más que por los planos (00l) indica una excelente calidad estructural de los cristales. Un ejemplo del resultado de una curva de balanceo correspondiennte al pico (004) es presentado en el inset de la Fig. 2.1(b).

La resistividad dentro de los planos ab fue medida en dos monocristales en el PPMS usando la técnica de cuatro contactos (dos para introducir la intensidad y otros dos para medir la caída de potencial). Los tamaños de los cristales usados en esta medida se presentan en la Tabla 2.1. Un ejemplo del comportamiento de la magnetoresistividad en los planos ab es presentado en la Fig. 2.2. Aquí puede visualizarse en el inset una dependencia lineal hasta 100 K, sin los saltos asociados a transiciones magnéticas o estructurales típicas de los superconductores dopados por debajo del nivel óptimo.[141] El punto medio de la transición se estimó entorno a 28 K con un error de ±0.4 *K. El redondeo producido por las fluctuaciones es casi inapreciable y solo será tenido en cuenta en el siguiente capítulo como una corrección mayor del segundo orden. La práctica ausencia del* *efecto de las fluctuaciones nos va a permitir determinar con precisión la dependencia con la temperatura del campo crítico superior desde la determinación del punto medio de la transición superconductora. Los resultados son presentados en la Fig. 2.3 para las dos muestras estudiadas, y para ambas orientaciones, donde podemos comprobar un comportamiento lineal en buena aproximación, aunque en campos por debajo de* ~ 1 *T una pequeña curvatura positiva es observada (este efecto ocurre dentro del ancho de la transición así que puede deberse a efecto de las inhomogeneidades, o en otro escenario a efectos multibanda). Los resultados de las pendientes del campo crítico superior y la temperatura crítica pueden verse en resumidos en la Tabla 2.2. Desde esta tabla los valores de las longitudes de coherencia pueden ser derivados.*

Las medidas de magnetización han sido realizadas en un magnetómetro SQUID, sobre un apilamiento de 10 muestras de alta calidad para obtener mayor señal magnética. La pila de cristales fue encapsulada en una resina epoxy para evitar la señal magnética debida al oxígeno dentro de la cámara de medida. Una imagen de los cristales individuales usados en el experimento y de la pila resultante puede ser vista en la Fig. 2.4. Las dimensiones de cada uno de los cristales son resumidas en la Tabla 2.1. La dependencia con la temperatura de la susceptibilidad magnética cuando el superconductor se ha enfriado por debado de la temperatura crítica sin la aplicación de campo es presentado en la Fig. 2.5. Estos datos fueron corregidos de efectos demagnetizantes, usando el factor necesario para que la susceptibilidad extrapolara al valor ideal -1 a temperaturas muy por debajo de T_c*. De estas curvas la temperatura crítica ha sido determinada por de la extrapolación lineal a* $\chi = 0$ *de la máxima pendiente de los datos de* $\chi(T)$*, y el ancho medio de la transición es:* $\Delta T_c = T_{c0} - T_c$*, donde* T_{c0} *es la temperatura más alta en la cual una señal diamagnética es resuelta (el procedimiento se detalla en la Fig. 2.5). El valor de* ΔT_c *es sólo 0.4 K, confirmando su excelente estequiometría y permitiendo el estudio de las fluctuaciones superconductoras en un amplio rango de temperatura.*

Los datos del momento magnético frente a la temperatura para diferentes campos son mostrado en las Figs. 1.2(a) y (b). En detalle puede verse en las Fig. 1.2(c) y (d), correspondientes a un campo *magnético aplicado de 4 T. Como puede apreciarse, existe un redondeo que va desde T_c hasta 33 K (esta última temperatura será usada como aquella donde las fluctuaciones son despreciables para una de las constantes implícitas en las ecuaciones).*

La contribución de las fluctuaciones al momento magnético puede ser determinada substrayendo el "background". Como en el capítulo anterior éste se determina ajustando la ecuación 2.6 en una región de temperatura por encima de aquella donde las fluctuaciones son despreciables. El resultado de la contribución de este "background" es presentado a través de líneas continuas en la Fig. 2.7. Como era de esperar, las fluctuaciones de la susceptibilidad magnética decrecen con el campo aplicado, lo cual indica que los campos usados en el experimento son suficientemente altos como para entrar en el rango de Prange o de campo finito (aquí la amplitud de las fluctuaciones en la magnetización decrecen rápidamente con el campo aplicado) [78].

El diamagnetismo inducido por fluctuaciones superconductoras se modelará teóricamente como en el capítulo anterior a través de las ecuaciones 2.7 y 2.8. En estas ecuaciones aparece la constante de corte en energía definida anteriormente, la cual indica la temperatura a partir de la cual las fluctuaciones son despreciables, por lo que no será tratado como un parámetro de ajuste, los únicos dos parámetros de ajuste serán $\xi_{ab}(0)$ y γ. El mejor ajuste de estas ecuaciones a los datos experimentales es presentado a través de líneas sólidas en la Fig. 2.7. En dicha figura los puntos sólidos representan la frontera que separa la región gausiana de la región crítica (allí donde las fluctuaciones son suficientemente grandes como para que deban de tenerse en cuenta términos por encima del segundo orden en la expansión del funcional de GL). Los valores del ajuste son compilados en la Tabla 3.1, junto con aquellos deducidos de estos. Como puede comprobarse los valores de $\xi_{ab}(0)$ están en un excelente acuerdo con los determinados en previamente a través de medidas de resistividad. Sin embargo los valores de $\xi_c(0)$ son un 30 % más grandes y tal diferencia no es atribuible a errores experimentales.

Podemos comprobar el análisis previo a través del estudio de las fluctuaciones dentro de la región crítica. En esta región existen ecuaciones de escala, es decir, los datos experimentales expresados a través de ciertas variables deben escalar independientemente del *campo aplicado. Dichas ecuaciones de escalas fueron desarrolladas en las referencias [150, 151], y se muestran en las ecuaciones 2.11 y 2.12. Las funciones de escala están relacionadas como se indica en la ecuación 2.13 (lo cual se muestra por primera vez en [39]).*

Asumiendo un comportamiento lineal del campo magnético superior con la temperatura, las ecuaciones de escala dependen únicamente de la temperatura crítica y de las longitudes de coherencia dentro y fuera de los planos, $\xi_{ab}(0)$ *y* $\xi_c(0)$. *El mejor escalamiento determinado es presentado en la Fig. 2.8 el cual fue obtenido con los parámetros presentados en la Tabla 3.1. Las incertidumbres indicadas aquí representan el rango de valores para los cuales el escalamiento no empeora apreciablemente. Como se comprueba estos valores son consistentes con aquellos encontrados desde el estudio de las fluctuaciones superconductoras en la región gausiana.*

Los valores de las longitudes de coherencia $\xi_{ab}(0)$ *obtenidos desde los dos observables (magnetización y resistividad) están en excelente acuerdo entre ellos. Sin embargo hay notables diferencias entre los correspondientes valores de* $\xi_c(0)$. *Esta diferencia tampoco puede ser atribuida a un incompleto volumen superconductor en la pila de cristales usados para la magnetización, ya que* γ *y* $\xi_c(0)$ *afectan a las amplitudes de la magnetización pero también a su dependencia con el campo magnético.*

Estas diferencias obsevadas entre las longitudes de coherencia $\xi_c(0)$ *dependiendo del observable medido puede deberse a la presencia de varias bandas electrónicas contribuyendo a la superconductividad en el material bajo estudio. [5, 30, 156, 157] De hecho una reciente propuesta de un modelo de dos bandas predice que la forma funcional entre las fluctuaciones derivadas del calor específico, y la conductividad eléctrica no cambian con respecto al caso monobanda, aunque existe una renormalización de la longitud de coherencia del eje c entre ellas. Esto ya fue observado en otros superconductores como se muestra en las referencias [158–160].*

Por último, para completar nuestro estudio exploraremos la región del diagrama de fase de bajos campos magnéticos muy cerca de la temperatura crítica. En contraste con el comportamiento lineal que predicen las teorías de Ginzburg-Landau, las isotermas justo por encima de la temperatura crítica presentan una anómala curvatura *a campos del orden de mT como se muestra en la Fig. 2.9. Este comportamiento ha sido observado también en cupratos [161–164] y recientemente en otros superconductores basados en hierro [42, 140]. Las similitudes entre nuestros resultados, y trabajos previos son cuantitativas. En las referencias [12, 42] fue propuesto que la anomalía es debida a importantes efectos de fluctuaciones de fase, alternativamente esto puede ser explicado a través de una distribución de* T_c *debido a inhomogeneidades, asociados a la naturaleza no estequiométrica de estos materiales, al igual que en los cupratos.[163] En este trabajo nos inclinamos por el segundo escenario debido a que: por debajo del* H_{up} *(campo donde aparece la máxima amplitud de la respuesta magnética en cada una de las isotermas) puede interpretarse que hay una fracción de la muestra que se encuentra en la región Meissner (como se indica en las líneas punteadas), lo cual es consistente con el hecho de que el efecto sea limitado al ancho de la transición superconductora por encima de la temperatura crítica. Por último los valores de* H_{up} *están en buen acuerdo con el campo crítico inferior debido a los dominios de mayor temperatura crítica, el cual puede ser aproximado por* $-(\mu_0\partial H_{c1}/\partial T)_{T_c}\Delta T_c$ *(que está en el orden de mT). Un argumento que soporta el escenario de las fluctuaciones de fase es que* H_{up} *incrementa con la temperatura, en un intervalo por encima de la temperatura crítica, mientras que el campo crítico inferior decrece.[42, 140, 165] Sin embargo dicho comportamiento no es observado en este estudio, a pesar de que el ancho de la transición es menor que el observado en las referencias [42, 140] donde se aceptan las fluctuaciones de fase. Como consecuencia nosotros asumiremos que este último escenario no juega un papel importante en nuestro compuesto, o al menos es mucho menos relevante que en las referencias propuestas.*

Capítulo 3: Dependencia anómala angular del campo crítico superior en el superconductor isovalentemente sustituido $BaFe_2(As_{1-x}P_x)_2$

Determinar la forma funcional del campo crítico superior en los superconductores basados en hierro es un aspecto debatido. Las teorías para $H_{c2}(\theta)$ fueron diseñadas en los años 60, para superconductores convencionales desde las ecuaciones de Ginzburg-Landau generalizadas para materiales anisotrópicos. Sin embargo, desde el descubrimiento de los superconductores con características multibanda, [81, 116, 167–169] donde hay una fuerte correlación entre la topología de la superficie de Fermi y la anisotropía del parámetro de orden no es tan claro que la dependencia angular de H_{c2} sea bien descrita por las ecuaciones anteriores.En este sentido, algunos autores afirman que existe una desviación del comportamiento convencional (no GL) del campo crítico superior.[170] En este capítulo, tal comportamiento será determinado desde el estudio de las fluctuaciones superconductoras por encima de la temperatura crítica, en medidas de magnetorresistividad con el campo aplicado en diferentes orientaciones con respecto al eje c.

La muestra de $BaFe_2(As_{1-x}P_x)_2$ usada en este trabajo pertenece al mismo lote de cristales usados en el capítulo anterior. Las dimensiones del cristal son $1.60 \times 1.30 \times 0.018$ mm^3, y su nivel nominal de dopaje es $x = 0.35$ lo cual es cercano al nivel óptimo.

La resistividad se midió en un PPMS (ver apéndice 2) en primer lugar, para determinar la temperatura crítica, con el campo magnético aplicado paralelo al eje c de la muestra. Varios ejemplos de $\rho(T)_H$ son mostrados en Fig. 3.1(a). En el inset de la misma figura podemos ver el comportamiento del campo magnético a campo nulo. Un comportamiento lineal con la temperatura es apreciado hasta 100 K. *En ausencia de campo, el ancho de la transición superconductora es de* 0.8 K, *estimado desde la diferencia de temperaturas cuando la transición superconductora alcanza el* 90% *y el* 10% *de la resistividad en estado normal. Un punto medio de la transición superconductora* *de* 27.7 K *implica que el ancho de la misma representa menos del* 3% *de incertidumbre, lo cual permitirá investigar el efecto de las fluctuaciones superconductoras en un amplio rango de temperaturas.*

A pesar de que el redondeo debido a las fluctuaciones en la conductividad por encima de la temperatura crítica es pequeño (ver capítulo anterior), su estudio nos da otro modo de determinar con precisión las longitudes de coherencia y posibles efectos multibanda. Para cada campo aplicado, la dependencia con la temperatura con las fluctuaciones en magnetoconductividad viene dado por la ecuación 3.1. El "background" fue determinado de forma similar a capítulos anteriores, a través de un ajuste lineal desde 1.3 hasta 1.5 veces la temperatura crítica. Ejemplos de los ajustes son presentados en Fig. 3.1 (a). El resultado de las fluctuaciones se muestra en Fig. 3.1(b) para varios campos magnéticos hasta 9 T. Como se observa en esta última figura, la amplitud de las fluctuaciones se reduce con el campo aplicado, lo cual indica que debemos usar las ecuaciones de Ginzburg-Landau en el régimen de Prange.[55]

Los resultados serán comparados con la ecuación 3.3, la cual es ajustada al conjunto de datos experimentales con parámetros libres de, $\xi_c(0)$, $\mu_0 H_{c2}(0°)$ *y* T_c. *Los resultados de los ajustes son presentados en 3.1, los cuales están en muy buen acuerdo con los mostrados en el capítulo anterior. Aquí se observa una diferencia con la aproximación de las ecuaciones de Ginzburg-Landau a campos magnéticos por debajo de 1 T, lo cual confirma la presencia de efectos multibanda.*

Siguiendo el mismo procedimiento, en Figs. 3.2 (a-c) se presentan medidas de la resistividad para distintos ángulos entre el campo magnético aplicado y el eje c del cristal. Además en las Figs. 3.2 (d-f) se muestra el resultado de las fluctuaciones superconductoras en la magnetocoductividad dependientes del ángulo. Puede notarse que esta magnitud incrementa con el ángulo, alcanzando los valores más altos cuando los planos cristalográficos son paralelos al campo magnético.

Los resultados se analizan usando la forma generalizada de las fluctuaciones superconductoras en magnetoconductividad para materiales anisotrópicos dadas por la ecuación 3.3, y haciendo el cambio que se muestra en la ecuación 3.4. En Figs. 3.2(d-f) los mismos valores de los parámetros de ajuste derivados anteriormente *son usados. Como se observa el acuerdo es excelente, excepto para ángulos cercanos a 90° donde el acuerdo de la teoría empeora conforme el campo magnético decrece. Por ello, para comprobar nuestro resultado, podemos estudiar esta desviación de la teoría convencional desde otro punto de vista de análisis experimental.*

En las Figs. 3.3(a-d) varios ejemplos de la magnetorresistividad para diferentes ángulos son mostrados. Como fue explicado antes, la ausencia de importantes efectos de redondeo debido a fluctuaciones nos permitirá determinar con precisión la dependencia con la temperatura del campo magnético superior, independientemente del punto elegido en la transición superconductora. Sin embargo, para ser consistentes con el resultado elegido el la sección previa tomaremos el punto que coincida con el 10% de la resistividad normal (medida cerca de la transición de fase).

En la Fig. 3.3(e), mostramos varios ejemplos de las líneas de $\mu_0 H_{c2}(T)$ *para ángulos desde 0° hasta 90° con pasos de 15°. Al igual que en el capítulo anterior, aparece una ligera desviación para campos por debajo de 1 T. Por ello, los datos son ajustados linealmente desde 1.5 hasta 6 T. El campo crítico superior será el resultado de la extrapolación a* $T = 0$ *K. Las medidas fueron repetidas cada tres grados. El resultado es mostrado en el inset de la Fig. 3.4. Para comprobar con precisión si este conjunto de datos experimentales sigue la curva predicha por la ecuación 3.5, en la Fig. 3.4 se presentan las variables* $(\mu_0 H_{c2}(\theta))^{-2}$ *con respecto a* $\cos(\theta)^2$*. De acuerdo con la ecuación señalada, los puntos experimentales expresados en estas variables deberían de seguir un comportamiento lineal. En contraste, como puede ser visto en dicha figura, una desviación de la linealidad es observada para ángulos cercanos a 90°.*

La desviación de las ecuaciones de Ginzburg-Landau para ángulos cercanos a 90° ya fue observada en otros materiales con características multibanda (ver por ejemplo las Refs.[81, 170, 172]). Hay que notar que aunque $\mu_0 H_{c2}(0)$ *fue derivado en términos de teorías monobandas, en la Ref. [173] se afirma que si una factorización del potencial de apareamiento entre los pares de Cooper es asumida, entonces el comportamiento expuesto en la ecuación 3.5 será esperado independientemente de la superficie de Fermi o de la simetría del gap superconductor. Por otra parte, algunos autores apuntan que este* *proceso no es justificable microscópicamente, y por tanto es necesario otros modelos teóricos que describan el comportamiento del campo crítico superior en función del ángulo.*

Capítulo 4: Importancia de la determinación del estado normal cuando se usa la espectroscopía de fluctuaciones ¿Es LiFeAs un caso especial dentro de los superconductores basados en hierro?

LiFeAs es un material esteiquiométrico con una temperatura crítica de aproximadamente 18 K. Dicha temperatura es alcanzada sin ningún dopaje químico [174, 175]. Por ello, en la referencia [13], los autores usan el poco contenido de defectos para medir con precisión la magnetoresistencia de monocristales de este compuesto. En esta referencia los autores concluyen que la conductividad inducida por fluctuaciones superconductoras, $\Delta\sigma$*, sigue un comportamiento 2D, (incluso muy cerca de la temperatura crítica, donde la longitud de coherencia diverge con la temperatura), a pesar de que para LiFeAs, la longitud de coherencia transversal es mayor que la distancia entre los planos superconductores. Esta propuesta ha tenido implicaciones en el comprendimiento de los superconductores basados en hierro.[30] En contraste, hay estudios de comportamientos de 3D observados para el mismo material (véase [43]). En este capítulo se indica que la propuesta llevada en la referencia [13] podría ser un artefacto debido a una inadecuada substracción del estado normal,* σ_B*.*

En primer lugar, hay que notar que σ_B *es órdenes de magnitud mayor que la contribución de las fluctuaciones esperadas. Este hecho questiona ya el estudio de* $\Delta\sigma$ *para determinar parámetros superconductores. Por otro lado, el procedimiento usado en [13] para determinar la conductividad en el esado normal, asume un comportamiento cuadrático del campo magnético. Para temperaturas cerca de la temperatura crítica, una desviación de este comportamiento es* *atribuída al efecto de las fluctuaciones. Sin embargo, para isotermas bien por encima de la temperatura crítica donde el efecto de las fluctuaciones debería de ser despreciable, se presenta una dependencia similar con el campo magnético. En la Fig. 4.1 esto es apreciado, donde isotermas por encima de 45 K presentan el mismo redondeo que aquella a 25 K.*

La propuesta mencionada indica que el resultado sugerido en Ref. [13], puede estar afectado fuertemente por la contribución del "background". Para confirmar esta conclusión hay que notar que la forma de las isotermas $\delta\rho/\rho(H)$ *son similares (sólo se distinguen por un factor multiplicativo), por tanto, la pendiente de las curvas crece en la misma proporción que la extrapolación a campo nulo (ver Fig. 4.2). Siguiendo este razonamiento, puede comprobarse que los valores de las fluctuaciones siguen la dependencia con la temperatura de* σ_B^3 *(ya que la pendiente es proporcional a* σ_B^2 *obedeciendo la regla de Kohler [177]).*

Por todo ello, en este capítulo se cuestiona la naturaleza bidimensional de las fluctuaciones superconductoras determinada en la referencia [13].


USC
UNIVERSIDADE
DE SANTIAGO
DE COMPOSTELA

Bibliography

[1] Kamihara Y, Hiramatsu H, Hirano M, Kawamura R, Yanagi H, Kamiya T and Hosono H 2006 *J. Am. Chem. Soc.* **128** 10012

[2] Kamihara Y, Watanabe T, Hirano M and Hosono H 2008 *J. Am. Chem. Soc.* **130** 3296

[3] Putti M, Pallecchi I, Bellingeri E, Cimberle M R, Tropeano M, Ferdeghini C, Palenzona A, Tarantini C, Yamamoto A, Jiang J, Jaroszynski J, Kametani F, Abraimov D, Polyanskii A, Weiss J D, Hellstrom E E, Gurevich A, Larbalestier D C, Jin R, Sales B C, Sefat A S, McGuire M A, Mandrus D, Cheng P, Jia Y, Wen H H, Lee S and Eom C B 2010 *Supercond. Sci. Technol.* **23** 034003

[4] Moll P J W, Puzniak R, Balakirev F, Rogacki K, Karpinski J, Zhigadlo N D and Batlogg B 2010 *Nat. Mater.* **9** 628

[5] Gurevich A 2010 *Phys. Rev. B* **82** 184504

[6] Si W, Zhou J, Jie Q, Dimitrov I, Solovyov V, Johnson P D, Jaroszynski J, Matias V, Sheehan C and Li Q 2011 *Applied Physics Letters* **98** 262509

[7] Vidal F, Torrón C, Viña J and Mosqueira J 2000 *Physica C* **332** 166

[8] For reviews on the theoretical and experimental aspects of the superconducting fluctuations see, e.g., M. Tinkham, *Introduction to Superconductivity* (McGraw-Hill, New York, 1996), Chap. 8 F. Vidal, M.V. Ramallo, *The Gap Symmetry and*

Fluctuations in High-T_c Superconductors (Plenum, New York, 1998), vol. 371, p. 443. A. Larkin, A. Varlamov, *Theory of Fluctuations in Superconductors* (Oxford University Press, 2005)

[9] Vidal F, Carballeira C, Currás S R, Mosqueira J, Ramallo M V, Veira J A and Viña J 2002 *Europhys. Lett.* **59** 754

[10] Rey R I, Carballeira C, Mosqueira J, Jr S S S, Alvarenga A D, Luo H Q, Lu X Y, Chen Y C and Vidal F 2013 *Supercond. Sci. Technol.* **26** 055004

[11] Koshelev A E and Varlamov A A 2014 *Supercond. Sci. Technol.* **27** 124001

[12] Rigamonti A, Lascialfari A, Romanó L, Varlamov A and Zucca I 2005 *J. Supercond. Nov. Magn.* **18** 763

[13] Rullier-Albenque F, Colson D, Forget A and Alloul H 2012 *Phys. Rev. Lett.* **109** 187005

[14] Singh D J and Du M H 2008 *Phys. Rev. Lett.* **100** 237003

[15] Zhu X, Han F, Mu G, Cheng P, Shen B, Zeng B and Wen H H 2009 *Phys. Rev. B* **79** 220512

[16] Lee K W and Pickett W E 2010 *Euro. Phys. Lett.* **89** 57008

[17] Zhang Y, Yang L X, Xu M, Ye Z R, andC He F C, Xu H C, Jiang J, Xie B P, Ying J J, Wang X F, Chen X H, Hu J P, Matsunami M, Kimura S and Feng D L 2011 *Nature Mater.* **10** 273

[18] Mou D, Liu S, Jia X, He J, Peng Y, Zhao L, Yu L, Liu G, He S, Dong X, Zhang J, Wang H, Dong C, Fang M, Wang X, Peng Q, Wang Z, Zhang S, Yang F, Xu Z, Chen C and Zhou X J 2011 *Phys. Rev. Lett.* **106** 107001

[19] Hiroki T, Kazumi I, Kazunobu A, Yoichi K, Masahiro H and Hideo H 2008 *Nature (London)* **453** 376

[20] Miyazawa K, Kihou K, Shirage P M, Lee C H, Kito H, Eisaki H and Iyo A 2009 *J. Phys. Soc. Jpn.* **78** 034712

[21] Wang X, Liu Q, Lv Y, Gao W, Yang L, Yu R, Li F and Jin C 2008 *Solid State Commun.* **148** 538

[22] Tanatar M A, Spyrison N, Cho K, Blomberg E C, Tan G, Dai P, Zhang C and Prozorov R 2012 *Phys. Rev. B* **85** 014510

[23] Hsu F C, Luo J Y, Yeh K W, Chen T K, Huang T W, Wu P M, Lee Y C, Huang Y L, Chu Y Y, Yan D C, and Wu M K 2008 *Proc. Natl. Acad. Sci. U.S.A.* **105** 14262

[24] Sales B C, Sefat A S, McGuire M A, Jin R Y, Mandrus D and Mozharivskyj Y 2009 *Phys. Rev. B* **79** 094521

[25] Rotter M, Tegel M and Johrendt D 2008 *Phys. Rev. Lett.* **101** 107006

[26] Ni N, Bud'ko S L, Kreyssig A, Nandi S, Rustan G E, Goldman A I, Gupta S, Corbett J D, Kracher A and Canfield P C 2008 *Phys. Rev. B* **78** 014507

[27] Lee P A, Nagaosa N and Wen X G 2006 *Rev. Mod. Phys.* **78** 17

[28] Kondo T, Fernandes R M, Khasanov R, Liu C, Palczewski A D, Ni N, Shi M, Bostwick A, Rotenberg E, Schmalian J, Bud'ko S L, Canfield P C and Kaminski A 2010 *Phys. Rev. B* **81** 060507

[29] Pallecchi I, Fanciulli C, Tropeano M, Palenzona A, Ferretti M, Malagoli A, Martinelli A, Sheikin I, Putti M and Ferdeghini C 2009 *Phys. Rev. B* **79** 104515

[30] Fanfarillo L, Benfatto L, Caprara S, Castellani C and Grilli M 2009 *Phys. Rev. B* **79** 172508

[31] Salem-Sugui S, Ghivelder L, Alvarenga A D, Pimentel J L, Luo H, Wang Z and Wen H H 2009 *Phys. Rev. B* **80** 014518

[32] Choi C, Kim S H, Choi K Y, Jung M H, Lee S I, Wang X F, Chen X H and Wang X L 2009 *Supercond. Sci. Technol.* **22** 105016

[33] Liu S L, Haiyun W and Gang B 2010 *Phys. Lett. A* **374** 3529

[34] Murray J M and Tešanović Z 2010 *Phys. Rev. Lett.* **105** 037006

[35] Pandya S, Sherif S, Chandra L S S and Ganesan V 2010 *Supercond. Sci. Technol.* **23** 075015

[36] Kim S H, Choi C H, Jung M H, Yoon J B, Jo Y H, Wang X F, Chen X H, Wang X L, Lee S I and Choi K Y 2010 *J. Appl. Phys.* **108**

[37] Liu S, Haiyun W and Gang B 2011 *Solid State Commun.* **151** 1

[38] Pandya S, Sherif S, Chandra L S S and Ganesan V 2011 *Supercond. Sci. Technol.* **24** 045011

[39] Mosqueira J, Dancausa J D, Vidal F, Salem-Sugui S, Alvarenga A D, Luo H Q, Wang Z S and Wen H H 2011 *Phys. Rev. B* **83** 094519

[40] Welp U, Chaparro C, Koshelev A E, Kwok W K, Rydh A, Zhigadlo N D, Karpinski J and Weyeneth S 2011 *Phys. Rev. B* **83** 100513

[41] Liu S L, Longyan G, Gang B, Haiyun W and Yongtao L 2011 *Supercond. Sci. Technol.* **24** 075005

[42] Prando G, Lascialfari A, Rigamonti A, Romanó L, Sanna S, Putti M and Tropeano M 2011 *Phys. Rev. B* **84** 064507

[43] Song Y J, Kang B, Rhee J S and Kwon Y S 2012 *Europhys. Lett.* **97** 47003

[44] Marra P, Nigro A, Li Z, Chen G, Wang N, Luo J and Noce C 2012 *New J. Phys.* **14** 043001

[45] Jr S S S, Alvarenga A D, Rey R I, Mosqueira J, Luo H Q and Lu X Y 2013 *Supercond. Sci. Technol.* **26** 125019

[46] Mosqueira J, Dancausa J D, Carballeira C, Salem-Sugui J S, Alvarenga A D, Luo H Q, Wang Z S, Wen H H and Vidal F 2013 *J. Supercond. Nov. Magn.* **26** 1217

[47] Rey R I, Ramos-Álvarez A, Carballeira C, Mosqueira J, Vidal F, Jr S S S, Alvarenga A D, Zhang R and Luo H 2014 *Supercond. Sci.Technol.* **27** 075001

[48] Carballeira C, Mosqueira J, Ramallo M V, Veira J A and Vidal F 2001 *J. Phys. Condens. Matter* **13** 9271

[49] Ginzburg V and Landau L 1950 *Zh Eksperim. Teor. Fiz.* **20**

[50] Tinkham M 1996 *Introduction to Superconductivity* Chapt. 8

[51] Skocpol W J and Tinkham M 1975 *Rep. Prog. Phys.* **38** 1049

[52] Landau L and Lifchitz E 1978 vol 2 (Oxford-Pergamon Press)

[53] Schmid A 1969 *Phys. Rev.* **180** 527

[54] Schmidt H 1968 *Z.Phys.* **43** 336

[55] Prange R E 1970 *Phys. Rev. B* **1** 2349

[56] APLevanyuk 1959 *Soviet Phys. JETP* **36**

[57] Ginzburg V 1960 *Soviet Phys. -Solid State* **2**

[58] Tinkham M 1996 *Introduction to Superconductivity* Chapt. 3

[59] Johnson W L and Tsuei C C 1976 *Phys. Rev. B* **13** 4827

[60] Johnson W L, Tsuei C C and Chaudhari P 1978 *Phys. Rev. B* **17** 2884

[61] Freitas P P, Tsuei C C and Plaskett T S 1987 *Phys. Rev. B* **36** 833

[62] Hopfengärtner R, Hensel B and Saemann-Ischenko G 1991 *Phys. Rev. B* **44** 741

[63] Gauzzi A and Pavuna D 1995 *Phys. Rev. B* **51** 15420

[64] Carballeira C, Currás S R, Viña J, Veira J A, Ramallo M V and Vidal F 2001 *Phys. Rev. B* **63** 144515

[65] Mosqueira J, Carballeira C, Ramallo M V, Torrón C, Veira J A and Vidal F 2001 *Europhys. Lett.* **53** 632

[66] Viña J, Campá J A, Carballeira C, Currás S R, Maignan A, Ramallo M V, Rasines I, Veira J A, Wagner P and Vidal F 2002 *Phys. Rev. B* **65** 212509

[67] Mosqueira J, Carballeira C and Vidal F 2001 *Phys. Rev. Lett.* **87** 167009

[68] Carballeira C, Ramallo M V and Vidal F 2001 *J. Phys.: Condens. Matter* **13** 2573

[69] Klemm R A and Clem J R 1980 *Phys. Rev. B* **21** 1868

[70] Blatter G, Geshkenbein V B and Larkin A I 1992 *Phys. Rev. Lett.* **68** 875

[71] Hao Z and Clem J R 1992 *Phys. Rev. B* **46** 5853

[72] Tinkham M 1996 *Introduction to Superconductivity* Chapt. 10

[73] For a review on different theoretical and experimental aspects of τ in low-temperature superconductors, see Skocpol W. J. and Tinkham M., *Rep. Prog. Phys.*, **38** (1975) 1049

[74] Carballeira C, Mosqueira J, Revcolevschi A and Vidal F 2003 *Physica C* **384** 185

[75] Aslamazov L and Larkin A 1968 *Phys. Lett. A* **26** 238

[76] Chen Y, Lu X, Wang M, Luo H and Li S 2011 *Supercond. Sci. Technol.* **24** 065004

[77] Mosqueira J, Ramallo M V, Revcolevschi A, Torrón C and Vidal F 1999 *Phys. Rev. B* **59** 4394

[78] Soto F, Carballeira C, Mosqueira J, Ramallo M V, Ruibal M, Veira J A and Vidal F 2004 *Phys. Rev. B* **70** 060501

[79] Buzdin A and Feinberg D 1994 *Physica C* **220** 74

[80] Mosqueira J, Carballeira C and Vidal F 2001 *Phys. Rev. Lett.* **87** 167009

[81] Mosqueira J, Ramallo M V, Currás S R, Torrón C and Vidal F 2002 *Phys. Rev. B* **65** 174522

[82] Soto F, Berger H, Cabo L, Carballeira C, Mosqueira J, Pavuna D and Vidal F 2007 *Phys. Rev. B* **75** 094509

[83] Mosqueira J, Cabo L and Vidal F 2007 *Phys. Rev. B* **76** 064521

[84] Mosqueira J and Vidal F 2008 *Phys. Rev. B* **77** 052507

[85] Mosqueira J, Cabo L and Vidal F 2009 *Phys. Rev. B* **80** 214527

[86] Ikeda R, Ohmi T and Tsuneto T 1989 *J. Phys. Soc. Jpn.* **58** 1377
Ikeda R, Ohmi T and Tsuneto T 1990 *J. Phys. Soc. Jpn.* **59** 1397
Kim D H, Gray K E and Trochet M D 1992 *Phys. Rev. B* **45** 10801

[87] Tao Q, Shen J Q, Li L J, Lin X, Luo Y K, Cao G H and Xu Z A 2009 *Chin. Phys. Lett.* **26** 097401

[88] Sun D L, Liu Y and Lin C T 2009 *Phys. Rev. B* **80** 144515

[89] Shahbazi M, Wang X L, Lin Z W, Zhu J G, Dou S X and Choi K Y 2011 *J. Appl. Phys.* **109** 07E151

[90] Ni N, Tillman M E, Yan J Q, Kracher A, Hannahs S T, Bud'ko S L and Canfield P C 2008 *Phys. Rev. B* **78** 214515

[91] Tanatar M A, Ni N, Martin C, Gordon R T, Kim H, Kogan V G, Samolyuk G D, Bud'ko S L, Canfield P C and Prozorov R 2009 *Phys. Rev. B* **79** 094507

[92] Yamamoto A, Jaroszynski J, Tarantini C, Balicas L, Jiang J, Gurevich A, Larbalestier D C, Jin R, Sefat A S, McGuire M A, Sales B C, Christen D K and Mandrus D 2009 *Appl. Phys. Lett.* **94**

[93] Prozorov R, Tanatar M A, Gordon R T, Martin C, Kim H, Kogan V G, Ni N, Tillman M E, Bud'ko S L and Canfield P C 2009 *Physica C* **469** 582

[94] Nojima T, Honda Y, Nakajima Y and Tamegai T 2010 *Physica C* **470** 813

[95] Maiorov B, Katase T, Baily S A, Hiramatsu H, Holesinger T G, Hosono H and Civale L 2011 *Supercond. Sci. Technol.* **24** 055007

[96] Hänisch J, Iida K, Haindl S, Kurth F, Kauffmann A, Kidszun M, Thersleff T, Freudenberger J, Schultz L and Holzapfel B 2011 *IEEE Trans. Appl. Supercond.* **21** 2887

[97] Vinod K, Satya A T, Sharma S, Sundar C S and Bharathi A 2011 *Phys. Rev. B* **84** 012502

[98] Altarawneh M M, Collar K, Mielke C H, Ni N, Bud'ko S L and Canfield P C 2008 *Phys. Rev. B* **78** 220505

[99] Wang Z S, Luo H Q, Ren C and Wen H H 2008 *Phys. Rev. B* **78** 140501

[100] Martin C, Gordon R T, Tanatar M A, Kim H, Ni N, Bud'ko S L, Canfield P C, Luo H, Wen H H, Wang Z, Vorontsov A B, Kogan V G and Prozorov R 2009 *Phys. Rev. B* **80** 020501

[101] Kim H J, Liu Y, Oh Y S, Khim S, Kim I, Stewart G R and Kim K H 2009 *Phys. Rev. B* **79** 014514

[102] Welp U, Xie R, Koshelev A E, Kwok W K, Luo H Q, Wang Z S, Mu G and Wen H H 2009 *Phys. Rev. B* **79** 094505

[103] Jiao L, Zhang J L, Balakirev F F, Chen G F, Luo J L, Wang N L and Yuan H Q 2011 *J. Phys. Chem. Solids* **72** 423

[104] Gasparov V A, Wolff-Fabris F, Sun D L, Lin C T and Wosnitza J 2011 *JETP Lett.* **93**

[105] Welp U, Xie R, Koshelev A E, Kwok W K, Cheng P, Fang L and Wen H H 2008 *Phys. Rev. B* **78** 140510

[106] Jia Y, Cheng P, Fang L, Luo H, Yang H, Ren C, Shan L, Gu C and Wen H H 2008 *Appl. Phys. Lett.* **93** 032503

[107] Wang X, Ghorbani S R, Peleckis G and Dou S 2009 *Adv. Mater.* **21** 236

[108] Eisterer M, Mishev V, Zehetmayer M, Zhigadlo N D, Katrych S and Karpinski J 2014 *Supercond. Sci. Technol.* **27** 044009

[109] Lee H S, Bartkowiak M, Park J H, Lee J Y, Kim J Y, Sung N H, Cho B K, Jung C U, Kim J S and Lee H J 2009 *Phys. Rev. B* **80** 144512

[110] Karpinski J, Zhigadlo N, Katrych S, Bukowski Z, Moll P, Weyeneth S, Keller H, Puzniak R, Tortello M, Daghero D, Gonnelli R, Maggio-Aprile I, Fasano Y, Fischer, Rogacki K and Batlogg B 2009 *Physica C* **469** 370

[111] Okazaki R, Konczykowski M, van der Beek C J, Kato T, Hashimoto K, Shimozawa M, Shishido H, Yamashita M, Ishikado M, Kito H, Iyo A, Eisaki H, Shamoto S, Shibauchi T and Matsuda Y 2009 *Phys. Rev. B* **79** 064520

[112] Shirage P M, Miyazawa K, Ishikado M, Kihou K, Lee C H, Takeshita N, Matsuhata H, Tomioka R K Y, Ito T, Kito H, Eisaki H, Shamoto S and Iyo A 2009 *Physica C* **469** 355

[113] Cho K, Kim H, Tanatar M A, Song Y J, Kwon Y S, Coniglio W A, Agosta C C, Gurevich A and Prozorov R 2011 *Phys. Rev. B* **83** 060502

[114] Bendele M, Weyeneth S, Puzniak R, Maisuradze A, Pomjakushina E, Conder K, Pomjakushin V, Luetkens H, Katrych S, Wisniewski A, Khasanov R and Keller H 2010 *Phys. Rev. B* **81** 224520

[115] Iida K, Hänisch J, Reich E, Kurth F, Hühne R, Schultz L, Holzapfel B, Ichinose A, Hanawa M, Tsukada I, Schulze M, Aswartham S, Wurmehl S and Büchner B 2013 *Phys. Rev. B* **87** 104510

[116] For reviews on the properties of Fe-based superconductors See e.g. Johnston D C 2010 *Adv. Phys.* **59** 803. Mazin I I 2010 *Nature*

464 183. Paglione J and Greene R 2010 *Nat. Phys.* **6** 645. Wang F and Lee D -H 2011 *Science* **332** 200. Stewart G R 2011 *Rev. Mod. Phys.* **83** 1589.

[117] Jiang S, Xing H, Xuan G, Wang C, Ren Z, Feng C, Dai J, Xu Z and Cao G 2009 *J. Phys.: Condens. Matter* **21** 382203

[118] Shishido H, Bangura A F, Coldea A I, Tonegawa S, Hashimoto K, Kasahara S, Rourke P M C, Ikeda H, Terashima T, Settai R, Ōnuki Y, Vignolles D, Proust C, Vignolle B, McCollam A, Matsuda Y, Shibauchi T and Carrington A 2010 *Phys. Rev. Lett.* **104** 057008

[119] Sharma S, Bharathi A, Chandra S, Reddy V R, Paulraj S, Satya A T, Sastry V S, Gupta A and Sundar C S 2010 *Phys. Rev. B* **81** 174512

[120] Kito H, Eisaki H and Iyo A 2008 *J. Phys. Soc. Jpn* **77** 063707

[121] Ren Z A, Yang J, Lu W, Yi W, Che G, Dong X, Sun L and Zhao Z 2008 *Mater. Res. Innovations* **12** 105

[122] Chen G F, Li Z, Wu D, Li G, Hu W Z, Dong J, Zheng P, Luo J L and Wang N L 2008 *Phys. Rev. Lett.* **100** 247002

[123] Demirdiş S, Fasano Y, Kasahara S, Terashima T, Shibauchi T, Matsuda Y, Konczykowski M, Pastoriza H and van der Beek C J 2013 *Phys. Rev. B* **87** 094506

[124] van der Beek C J, Konczykowski M, Kasahara S, Terashima T, Okazaki R, Shibauchi T and Matsuda Y 2010 *Phys. Rev. Lett.* **105** 267002

[125] Jaroszynski J, Hunte F, Balicas L, Jo Y j, Raičević I, Gurevich A, Larbalestier D C, Balakirev F F, Fang L, Cheng P, Jia Y and Wen H H 2008 *Phys. Rev. B* **78** 174523

[126] Golubov A A and Koshelev A E 2003 *Phys. Rev. B* **68** 104503

[127] Glatz A and Koshelev A E 2010 *Phys. Rev. B* **82** 012507

[128] Onari S and Kontani H 2009 *Phys. Rev. Lett.* **103** 177001

[129] Kontani H and Onari S 2010 *Phys. Rev. Lett.* **104** 157001

[130] Malone L, Fletcher J D, Serafin A, Carrington A, Zhigadlo N D, Bukowski Z, Katrych S and Karpinski J 2009 *Phys. Rev. B* **79** 140501

[131] Hashimoto K, Shibauchi T, Kato T, Ikada K, Okazaki R, Shishido H, Ishikado M, Kito H, Iyo A, Eisaki H, Shamoto S and Matsuda Y 2009 *Phys. Rev. Lett.* **102** 017002

[132] Barannik A, Cherpak N T, Tanatar M A, Vitusevich S, Skresanov V, Canfield P C and Prozorov R 2013 *Phys. Rev. B* **87** 014506

[133] Rey R I, Ramos-Álvarez A, Mosqueira J, Salem-Sugui S, Alvarenga A D, Luo H Q, Lu X Y, Zhang R and Vidal F 2014 *Supercond. Sci. Technol.* **27** 055015

[134] Yamashita M, Nakata N, Senshu Y, Tonegawa S, Ikada K, Hashimoto K, Sugawara H, Shibauchi T and Matsuda Y 2009 *Phys. Rev. B* **80** 220509

[135] Hashimoto K, Yamashita M, Kasahara S, Senshu Y, Nakata N, Tonegawa S, Ikada K, Serafin A, Carrington A, Terashima T, Ikeda H, Shibauchi T and Matsuda Y 2010 *Phys. Rev. B* **81** 220501

[136] Kim J S, Hirschfeld P J, Stewart G R, Kasahara S, Shibauchi T, Terashima T and Matsuda Y 2010 *Phys. Rev. B* **81** 214507

[137] Suzuki K, Usui H and Kuroki K 2011 *J. Phys. Soc. Jpn.* **80** 013710

[138] Qiu X, Zhou S Y, Zhang H, Pan B Y, Hong X C, Dai Y F, Eom M J, Kim J S, Ye Z R, Zhang Y, Feng D L and Li S Y 2012 *Phys. Rev. X* **2** 011010

[139] Kapitulnik A, Palevski A and Deutscher G 1985 *J. Phys. C* **18** 1305

[140] Bossoni L, Romanó L, Canfield P C and Lascialfari A 2014 *J. Phys.: Condens. Matter* **26** 405703

[141] Nakajima M, Uchida S, Kihou K, Lee C H, Iyo A and Eisaki H 2012 *J. Phys. Soc. Jpn.* **81** 104710

[142] Hu D, Lu X, Zhang W, Luo H, Li S, Wang P, Chen G, Han F, Banjara S R, Sapkota A, Kreyssig A, Goldman A, Yamani Z, Niedermayer C, Skoulatos M, Georgii R, Keller T, Wang P, Yu W and Dai P 2015 *Phys. Rev. Lett.* **114** 157002

[143] Goh S K, Nakai Y, Ishida K, Klintberg L E, Ihara Y, Kasahara S, Shibauchi T, Matsuda Y and Terashima T 2010 *Phys. Rev. B* **82** 094502

[144] Ishikado M, Kodama K, Kajimoto R, Nakamura M, Inamura Y, Wakimoto S, Iyo A, Eisaki H, Arai M and Shamoto S 2011 *Physica C* **471** 643

[145] Ramos-Álvarez A, Mosqueira J, Vidal F, Lu X and Luo H 2015 *Supercond. Sci. Technol.* **28** 075004

[146] Ikeda R, TOhmi and Tsuneto T 1989 *J. Phys. Soc. Jpn.* **58** 1377

[147] Ohmi R I I and Tsuneto T 1990 *J. Phys. Soc. Jpn.* **59** 1397

[148] Kim D H, Gray K E and Trochet M D 1992 *Phys. Rev. B* **45** 10801

[149] Zaanen J 2009 *Phys. Rev. B* **80** 212502

[150] Ullah S and Dorsey A T 1990 *Phys. Rev. Lett.* **65** 2066

[151] Ullah S and Dorsey A T 1991 *Phys. Rev. B* **44** 262

[152] Chong S, Hashimoto S and Kadowaki K 2010 *Solid State Communications* **150** 1178

[153] Putzke C, Walmsley P, Fletcher J D, Malone L, Vignolles D, Proust C, Badoux S, See P, Beere H E, Ritchie D A, Kasahara S, Mizukami Y, Shibauchi T, Matsuda Y and Carrington A 2014 *Nat. Commun.* **5** 5679

[154] Chaparro C, Fang L, Claus H, Rydh A, Crabtree G W, Stanev V, Kwok W K and Welp U 2012 *Phys. Rev. B* **85** 184525

[155] Diao Z, Campanini D, Fang L, Kwok W K, Welp U and Rydh A *arXiv:1503.04088*

[156] Orlova N V, Shanenko A A, Milošević M V, Peeters F M, Vagov A V and Axt V M 2013 *Phys. Rev. B* **87** 134510

[157] Marciani M, Fanfarillo L, Castellani C and Benfatto L 2013 *Phys. Rev. B* **88** 214508

[158] Klein T, Braithwaite D, Demuer A, Knafo W, Lapertot G, Marcenat C, Rodière P, Sheikin I, Strobel P, Sulpice A and Toulemonde P 2010 *Phys. Rev. B* **82** 184506

[159] Serafin A, Coldea A I, Ganin A Y, Rosseinsky M J, Prassides K, Vignolles D and Carrington A 2010 *Phys. Rev. B* **82** 104514

[160] Braithwaite D, Lapertot G, Knafo W and Sheikin I 2010 *J. Phys. Soc. Jpn.* **79** 053703

[161] Lascialfari A, Rigamonti A, Romano' L, Varlamov A A and Zucca I 2003 *Phys. Rev. B* **68** 100505

[162] Cabo L, Soto F, Ruibal M, Mosqueira J and Vidal F 2006 *Phys. Rev. B* **73** 184520

[163] Mosqueira J, Dancausa J D and Vidal F 2011 *Phys. Rev. B* **84** 174518

[164] Lascialfari A, Rigamonti A, Romano' L, Tedesco P, Varlamov A and Embriaco D 2002 *Phys. Rev. B* **65** 144523

[165] Bernardi E, Lascialfari A, Rigamonti A, Romanò L, Scavini M and Oliva C 2010 *Phys. Rev. B* **81** 064502

[166] P G L 1984 *JETP Lett.* **40** 1155

[167] Nagamatsu J, Nakagawa N, Muranaka T, Zenitani Y and Akimitsu J 2001 *Nature (London)* **410** 63

[168] Bud'ko S L, Kogan V G and Canfield P C 2001 *Phys. Rev. B* **64** 180506

[169] Bouquet F, Fisher R A, Phillips N E, Hinks D G and Jorgensen J D 2001 *Phys. Rev. Lett.* **87** 047001

[170] Murphy J, Tanatar M A, Graf D, Brooks J S, Bud'ko S L, Canfield P C, Kogan V G and Prozorov R 2013 *Phys. Rev. B* **87** 094505

[171] See Tinkham M 1996 , *Introduction to Superconductivity* (McGraw-Hill, New York, 1996), p 321.

[172] Morris R C, Coleman R V and Bhandari R 1972 *Phys. Rev. B* **5** 895

[173] Kogan V G and Prozorov R 2012 *Rep. Prog. Phys.* **75** 114502

[174] Tapp J H, Tang Z, Lv B, Sasmal K, Lorenz B, Chu P C W and Guloy A M 2008 *Phys. Rev. B* **78** 060505

[175] Pitcher M J, Parker D, Adamson P, Herkelrath S J C, Boothroyd A T and Clarke S J 2008 *Chem. Commun. (Cambridge)* **41** 5918

[176] This is intended to be justified in the Supplementary Ma- terial for ref. [13]. Unfortunately, the claimed measurements of the Hall effect up to 14 T are not shown.

[177] A. B. Pippard, *Magnetoresistance in Metals* (Cambridge University Press, Cambridge, England, 1989).

[178] Josephson B 1962 *Phys. Lett.* **1** 251

[179] Josephson B *Rev. Mod. Phys.* **46** 251

[180] Anderson P W and Rowell J M 1963 *Phys. Rev. Lett.* **10** 230

[181] J. Clarke and A. I. Braginski 2004 The SQUID handbook 1. Wiley-Vch.

[182] Magnetic Property Measurement System Harware *Manual Quantum Design*

[183] Physical Property Measurement System Harware *Manual Quantum Design* Chapter 2-3


USC
UNIVERSIDADE
DE SANTIAGO
DE COMPOSTELA

List of Figures


USC
UNIVERSIDADE
DE SANTIAGO
DE COMPOSTELA

List of Tables


USC
UNIVERSIDADE
DE SANTIAGO
DE COMPOSTELA

List of A. Ramos-Álvarez publications

- Ramos-Álvarez A, Mosqueira J and Vidal F "*Comment on Multiorbital effects on the transport and the superconducting Fluctuations in LiFeAs*" 2015 *Phys. Rev. Lett.* **115** 139701

- Ramos-Álvarez A, Mosqueira J and Vidal F "*Superconducting fluctuations in isovalently substituted* $BaFe_2(As_{1-x}P_x)_2$*: Possible observation of multiband effects*" 2015 *Phys. Rev. B* **92** 094508

- Ramos-Álvarez A, Mosqueira J, Vidal F, Lu X-Y and Luo H-Q "*Large increase of the anisotropy factor in the overdoped region of* $Ba(Fe_{1-x}Ni_x)_2As_2$ *as probed by fluctuation spectroscopy*" 2015 *Supercond. Sci. Technol.* **28** 075004

- Soto F, Carballeira C, Doval J M, Mosqueira J, Ramallo M V, Ramos-Álvarez A, Sóñora D, Verde J C and Vidal F "*Magnetic field dependence of the precursor diamagnetism in La superconductors with magnetic Pr impurities*" 2015 *Supercond. Sci. Technol.* **28** 065015

- Rey R I, Ramos-Álvarez A, Mosqueira J, Salem-Sugui Jr, Alvarenga A D, Luo H-Q, Lu X-Y, Zhang R and Vidal F "*Direct measurement of the temperature dependence of the magnetic penetration depth in* $Ba(Fe_{1-x}Ni_x)_2As_2$ *superconductors*" 2014 *Supercond. Sci. Technol.* **27** 055015

- Rey R I, Ramos-Álvarez A, Caraballeira C, Mosqueira J, Vidal F, Salem-Sugui S, Alvarenga A D, Zhang R and Luo H-Q "*Measurements of the superconducting fluctuations in optimally doped* $BaFe_{2-x}Ni_xAs_2$ *under high magnetic fields: probing the 3D anisotropic Ginzburg Landau approach*" 2014 *Supercond. Sci. Technol.* **27** 075001

- Soto F, Cotón N, Dancausa J D, Doval J M, Ramos-Álvarez A, Rey R I, Rodríquez L, Carballeira C, Mosqueira J, Ramallo M V and Vidal F "*Precursor superconducting diamagnetism in* $YBa_2Cu_3O_7$ *with in-plane or intercalated magnetic impurities*" 2013 *Supercond. Sci. Technol.* **26** 045007

- Rey R I, Ramos-Álvarez A, Mosqueria J, Ramallo M V and Vidal F "*Comment on Diamagnetism and cooper pairing above* T_c *in cuprates*" 2013 *Phys. Rev. B* **87** 056501

- Cotón N, Dancausa J D, Doval J M, Ramallo M V, Ramos-Álvarez A, Rey R I and Vidal F "*Finite element and effective medium calculations of the electrical behaviour near the vortex antivortex binding transition of planar superconductors with critical temperature inhomogeneities*" 2012 *J. Supercond. Nov. Magn.* **26** 3065

- Rey R I, Mosqueira J, Cotón N, Dancausa J D, Doval J M, Ramos-Álvarez A, Wahl A, Tello M and Vidal F "*Angular dependence of the fluctuation magnetization vector above the superconducting transition of a highly anisotropic high-*T_c *cuprate*" 2012 *J. Supercond. Nov. Magn.* **26** 1119

- Dancausa J D, Cotón N, Doval J M, Mosqueira J, Ramallo M V, Ramos-Álvarez A, Rey R I and Vidal F "*New results on the anomalous precursor diamagnetism in the underdoped* $La_1.9Sr_0.1CuO_4$ *superconductor*" 2012 *J. Supercond. Nov. Magn.* **26** 1115